Doklady Physics, Vol. 46, No. 4, 2001, pp. 219–222. Translated from Doklady Akademii Nauk, Vol. 377, No. 4, 2001, pp. 464–467.

PHYSICS

Equilibrium and Nonequilibrium Impurity Atmospheres

N. M. Vlasov

Presented by Academician V.V. Osiko November 20, 2000

Received August 4, 2000

In this paper, formation kinetics of equilibrium and nonequilibrium impurity atmospheres in the vicinity of triple junctions of grain boundaries is considered.

Equilibrium impurity atmospheres are formed in the vicinity of structural imperfections of a crystal free of external loads. Thus, an inhomogeneity related to impurity atoms appears near the triple junctions of the boundary grains with a positive dilatation, increasing the crystal lattice parameter. This entails the appearance of concentration compressive stresses which retard the diffusion of the impurity atoms. In other words, the impurity atmosphere hinders its own development. Nonequilibrium impurity atmospheres are formed in the vicinity of crystal structural imperfections under irradiation. Interstitial atoms of radiative origin form complexes with impurities of small atomic radius and transfer them to sinks with a positive dilatation. The interstitial atoms are absorbed by sinks, and the remaining impurities produce nonequilibrium impurity atmospheres [1]. In the vicinity of a sink, concentration tensile stresses appear which accelerate the migration of impurity atoms in the complex structure. A nonequilibrium impurity atmosphere facilitates its own formation. This is the fundamental difference in the formation processes for equilibrium and nonequilibrium impurity atmospheres. The aim of this report is to compare the kinetics of both processes using as an example formation of the corresponding impurity atmospheres in the vicinity of grain-boundary triple junctions. A disclination model of this structural defect allows one to obtain an exact analytical solution to the diffusion equation in the field of forces, thereby setting off the characteristic features of the formation of equilibrium and nonequilibrium impurity atmospheres [2, 3].

The effect of concentration stresses on diffusion is determined, in general, by an accepted model of a point defect. Thus, in the model of dilatation centers, these stresses do not affect the migration of the impurity atoms [4]. Physically, this is due to the fact that the redistribution of dilatation centers does not change the energy of a system [5]. However, the model of dilatation centers, as a rule, is unacceptable for the description of actual systems, where the determining role is found to belong to the interaction between the impurity atoms. Therefore, we will use the experimental dependence of the lattice parameter on the concentration of impurity atoms c (Vegard's rule) [6]:

$$\frac{a}{a_1} = 1 + \frac{a_2 - a_1}{a_1}c, \tag{1}$$

where a_1 and a_2 are the lattice parameters of the solvent and the dissolved component, respectively; $\frac{a_2 - a_1}{a_1}$ is the relative change in the lattice parameter per unit concentration; and $\frac{a}{a_1}$ is the relative change in the lattice parameter depending on the impurity atom concentration. If $(a_2 - a_1) > 0$, the lattice parameter increases in accordance with the concentration profile. The neighboring regions with lower impurity concentration impede free concentration expansion. Therefore, in the places with the highest concentration of impurity atoms, compression stresses appear which retard the diffusion of large impurity atoms. If $(a_2 - a_1) < 0$, the lattice parameter is reduced. The neighboring regions with a lower impurity concentration impede free concentration compression and tensile stresses arise. These stresses aid the migration of impurities of small atomic radius into the structure of the complex with interstitial atoms.

Now, we consider the formation of an equilibrium impurity atmosphere in the vicinity of a triple junction of grain boundaries in the case of initial concentration inhomogeneity. The diffusion of impurity atoms is described by the unsteady diffusion equation in a field of forces with corresponding initial and boundary conditions:

$$\frac{1}{D}\frac{\partial c}{\partial t} = \nabla c + \frac{\nabla(c\nabla V)}{kT}, \tag{2}$$
$$c(r, 0) = c_0, \quad c(R, t) = c_0, \quad c(r_0, t) = c_p.$$

Here, D is the diffusivity of the impurity atoms, k is the Boltzmann constant, T is the absolute temperature, c_0 is

State Research Institute, Scientific and Industrial Company "Luch," Podol'sk, Moscow oblast, Russia

1028-3358/01/4604-0219$21.00

the mean concentration of impurity atoms, c_p is the equilibrium concentration of impurity atoms in the vicinity of the triple junction line with characteristic size r_0, R is the outer radius of the triple junction, and V is the potential of the interaction of the impurity atom with the structural defect with allowance for the concentration inhomogeneity. At the initial instant, the concentration of the impurity atom is equal to the mean concentration c_0. The same concentration is also retained for $r = R$. This physically means that, as the impurities escape toward the triple junction line, the impurities from the triple junctions go to the boundary $r = R$ with the opposite dilatation field. The boundary condition for $r = r_0$ implies that an equilibrium concentration of impurity atoms is established there instantaneously and, further on, is retained during the whole time of their diffusive migration.

Wedge disclination is considered the commonly accepted model of the triple junction of grain boundaries. In this case, r_0 represents a disclination core radius and R is its outer radius. The potential of the interaction of the impurity atom with the wedge disclination is defined by the relationship

$$V_1 = A_1 \ln\frac{r}{R}, \quad A_1 = \frac{\mu\omega(1+\nu)}{3\pi(1-\nu)}\Delta\upsilon, \tag{3}$$

where μ is the shear modulus, ν is Poisson's ratio, ω is the disclination rotation vector, and $\Delta\upsilon$ is the crystal-volume change due to the disposition of the impurity atom. The finite values of r_0 and R enable us to avoid logarithmic divergence of the potential V_1 for $r \longrightarrow 0$ and $R \longrightarrow \infty$. Then, without loss of generality, we introduce a steady-state concentration inhomogeneity under the problem boundary conditions presented in (2). The tensor trace for concentration stresses in the region $r_0 \le r \le R$ for the boundaries free from radial stresses is defined by a known expression similar to that for temperature stresses [7]:

$$\sigma_{ll} = \frac{2\beta\mu(1+\nu)(c_p - c_0)}{1-\nu}\left\{\frac{1 + 2\ln\frac{r}{R}}{\ln\frac{R}{r_0}} + \frac{2r_0^2}{R^2 - r_0^2}\right\}, \tag{4}$$

where $\beta = \dfrac{a_2 - a_1}{a_1}$ is the change of the lattice parameter per unit impurity concentration. The remaining notations correspond to those accepted earlier. The constants in relation (4) play no role, as the diffusion process depends on the quantity $\dfrac{\Delta\upsilon}{3}\nabla\sigma_{ll}$. The potential of the interaction of the impurity atom with the steady-state concentration inhomogeneity coincides with that for a wedge disclination to within a constant factor:

$$V_2 = A_2 \ln\frac{r}{R}, \quad A_2 = \frac{4\beta\mu(1+\nu)(c_p - c_0)}{3(1-\nu)\ln\frac{R}{r_0}}\Delta\upsilon. \tag{5}$$

The logarithmic coordinate dependences of V_1 and V_2 essentially simplify the diffusion equation in the field of forces:

$$\frac{1}{D}\frac{\partial c}{\partial t} = \frac{\partial^2 c}{\partial r^2} + \frac{1 + \alpha_1 + \alpha_2}{r}\frac{\partial c}{\partial r},$$

$$\alpha_1 = \frac{A_1}{kT}, \quad \alpha_2 = \frac{A_2}{kT}, \tag{6}$$

$$c(r, 0) = c_0, \quad c(R, t) = c_0, \quad c(r_0, t) = c_p.$$

The dimensionless parameters α_1 and α_2 determine the contribution of structural stresses and concentration stresses to the kinetics of the formation of the equilibrium impurity atmosphere. For the wedge disclination with a positive dilatation, $\alpha_1 < 0$, because $\omega < 0$ in relation (3). Therefore, the rate of the impurity atmosphere formation increases. On the other hand, the concentration inhomogeneity reduces the rate of arrival of impurity atoms, since $\alpha_2 > 0$ for $\beta > 0$. This immediately follows from the form of Eq. (6). In fact, for $\dfrac{\partial c}{\partial r} < 0$, the impurity accumulation rate $\dfrac{\partial c}{\partial t}$ increases for $\alpha_1 < 0$ and decreases for $\alpha_2 > 0$. Thus, to elucidate the role of the concentration stresses in the formation of the equilibrium impurity atmosphere, the following model is suggested. The diffusion of impurity atoms in the stress field of the wedge disclination is analyzed for the case of a steady-state concentration inhomogeneity. Such a "frozen" inhomogeneity should be considered a certain structural defect whose stress field also affects the diffusion of impurity atoms. Certainly, the physical simplicity of the model is achieved at the expense of its mathematical simplification. In a rigorous statement, the concentration stresses depend on the current value of the concentration and the equation becomes nonlinear.

The formation of the nonequilibrium impurity atmosphere in the vicinity of the wedge disclination is also described by Eq. (6). However, some constants acquire another physical meaning. Thus, coefficient D characterizes the diffusion of impurities of small atomic radius in the structure of complexes with interstitial atoms. The value of c_p defines the limiting concentration of impurity atoms near a sink. The gradient of their concentration is directed opposite to the flux of interstitial atoms, and all the complexes decompose in the vicinity of the sink. For a wedge disclination with a positive dilatation, $\alpha_1 < 0$, since the impurities of small

atomic radius are transferred by the interstitial atoms. However, $\alpha_2 < 0$, since $\beta < 0$ in relation (5). This implies that the concentration inhomogeneity of small impurity atoms increases the rate of formation of the nonequilibrium impurity atmosphere. In this case, we consider $\Delta\upsilon$ in relation (5) to be the change in crystal volume caused by the disposition of the interstitial atom–impurity complex.

Finally, we outline a case which is more easily perceived, when the structural stresses are taken into account only in the boundary condition. Then, the kinetics of the diffusion process depends only on the parameter α_2:

$$\frac{1}{D}\frac{\partial c}{\partial t} = \frac{\partial^2 c}{\partial r^2} + \frac{1+\alpha_2}{r}\frac{\partial c}{\partial r}, \quad (7)$$
$$c(r, 0) = c_0, \quad c(R, t) = c_0, \quad c(r_0, t) = c_p.$$

When $|\alpha_2| \gg 1$, the concentration stresses greatly contribute to the kinetics of the diffusion process. For $|\alpha_2| \ll 1$, the formation of the impurity atmosphere is caused by the gradient of the impurity concentration. When $|\alpha_2| \approx 1$, the diffusion fluxes of the impurity atoms due to concentration gradients and concentration stresses are comparable. The estimates show that for actual systems, within the framework of the adopted model, $|\alpha_2| \approx 1$. Actually, for the Cu–Au system, for $\beta = 0.13$, $c_p - c_0 = 50$ at. %, $\mu = 4.2 \times 10^{10}$ Pa, $\nu = 0.35$, $\frac{R}{r_0} = 10^2$, $\Delta\upsilon = 4.9 \times 10^{-30}$ m^3, and $kT = 10^{-20}$ J, we have $\alpha_2 = 0.8$. Therefore, we consider the following cases: (i) $\alpha_2 = -1$ (nonequilibrium atmospheres); (ii) $\alpha_2 = 1$ (equilibrium atmospheres); (iii) $\alpha_2 = 0$ (absence of the concentration inhomogeneity). For the accepted values of the α_2 parameter, we obtain from Eq. (7), correspondingly,

$$\frac{1}{D}\frac{\partial c}{\partial t} = \frac{\partial^2 c}{\partial r^2}, \quad (8a)$$

$$\frac{1}{D}\frac{\partial c}{\partial t} = \frac{\partial^2 c}{\partial r^2} + \frac{2}{r}\frac{\partial c}{\partial r}, \quad (8b)$$

$$\frac{1}{D}\frac{\partial c}{\partial t} = \frac{\partial^2 c}{\partial r^2} + \frac{1}{r}\frac{\partial c}{\partial r}. \quad (8c)$$

The solution to these equations for similar initial and boundary conditions determines the contribution of the concentration inhomogeneities to the kinetics of the formation process of the impurity atmospheres in isolated (a crystal without external loads) and open (a crystal being irradiated) systems. A cylindrically symmetric impurity atmosphere is formed for $\alpha_2 = 0$. The initial concentration inhomogeneity in the isolated system ($\alpha_2 = 1$) changes the diffusion equation: the cylindrically symmetric atmosphere is formed according to the spherical-symmetry law. This retards the accumulation rate for the impurity atoms. In fact, for $\frac{\partial c}{\partial r} < 0$, it follows from Eq. (8b) that $\frac{\partial c}{\partial t}$ is smaller than the corresponding value from Eq. (8c). The concentration inhomogeneity in open systems ($\alpha_2 = -1$) also changes the diffusion equation: now, the cylindrically symmetric atmosphere is formed according to the plane symmetry law. This results in an increase in the accumulation rate of impurity atoms. For $\frac{\partial c}{\partial r} < 0$, it follows from Eq. (8a) that $\frac{\partial c}{\partial t}$ is larger than the corresponding value in Eq. (8c). A mathematically clear comparison of the kinetics of the two processes is possible due to the logarithmic coordinate dependence of the potential of the interaction of impurity atoms with an initial concentration inhomogeneity. Other coordinate dependences of the interaction potential complicate the diffusion equation, with a corresponding loss of mathematical clearness. The physical meaning of this result is evident. The additional term $\frac{1}{r}\frac{\partial c}{\partial r}$ $\left(\frac{\partial c}{\partial r} < 0\right)$ in the right-hand side of Eq. (8b), as compared to Eq. (8c), reflects the presence of sinks for impurity atoms. Therefore, the rate of formation of the equilibrium impurity atmosphere is retarded. The formation of the nonequilibrium impurity atmosphere leads to the disappearance of the term $\frac{1}{r}\frac{\partial c}{\partial r}$ $\left(\frac{\partial c}{\partial r} < 0\right)$ in Eq. (8c). This corresponds to the appearance of sources of impurity atoms in Eq. (8a), and the rate of formation of the nonequilibrium impurity atmosphere increases.

The solution to Eq. (8) under similar initial and boundary conditions is well known:

$$\frac{c - c_0}{c_p - c_0} = \frac{R - r}{R - r_0} - \frac{2}{\pi}\sum_{n=0}^{\infty}\frac{\sin\frac{\pi n(r - r_0)}{R - r_0}}{n}\exp\left[-\frac{\pi^2 n^2 Dt}{(R - r_0)^2}\right], \quad (9a)$$

$$\frac{c - c_0}{c_p - c_0} = \frac{r_0}{r}\left\{\frac{R - r}{R - r_0} - \frac{2}{\pi}\sum_{n=0}^{\infty}\frac{\sin\frac{\pi n(r - r_0)}{R - r_0}}{n}\exp\left[-\frac{\pi^2 n^2 Dt}{(R - r_0)^2}\right]\right\}, \quad (9b)$$

$$\frac{c-c_0}{c_p-c_0} = \frac{\ln\frac{R}{r}}{\ln\frac{R}{r_0}} + \pi\sum_{n=1}^{\infty}\frac{J_0\left(\frac{\mu_n R}{r_0}\right)J_0(\mu_n)Z_0\left(\frac{\mu_n r}{r_0}\right)}{J_0^2(\mu_n)-J_0^2\left(\frac{\mu_n R}{r_0}\right)}\exp\left(-\frac{\mu_n^2 Dt}{r_0^2}\right). \quad (9c)$$

Here,

$$Z_0\left(\frac{\mu_n r}{r_0}\right) = N_0\left(\frac{\mu_n R}{r_0}\right)J_0\left(\frac{\mu_n R}{r_0}\right) - J_0\left(\frac{\mu_n R}{r_0}\right)N_n\left(\frac{\mu_n R}{r_0}\right),$$

μ_n are the roots of the equation

$$J_0(\mu)N_0\left(\frac{\mu R}{r_0}\right) - J_0\left(\frac{\mu R}{r_0}\right)N_0(\mu) = 0,$$

and $J_0(\mu)$ and $N_0(\mu)$ are the Bessel functions of the first and second kind, respectively. It is seen that, for a similar period of time, the dimensionless concentration of the impurity atoms takes different values. Thus, for steady-state values of $\frac{c-c_0}{c_p-c_0}$ in the region $r_0 < r < R$, we have

$$\frac{r_0}{r}\frac{R-r}{R-r_0} < \frac{\ln(R/r)}{\ln(R/r_0)} < \frac{R-r}{R-r_0}. \quad (10)$$

This testifies to the different rates of accumulation of the impurity atoms. The nonequilibrium impurity atmosphere (9a) is characterized by the highest rate of formation, while the formation rate of the equilibrium impurity atmosphere (9b) is naturally lower.

Thus, the equilibrium impurity atmosphere in isolated systems (a crystal in the absence of external loads) impedes its own formation. The nonequilibrium impurity atmosphere in open systems (a crystal being irradiated) helps its own formation. The result obtained is of general physical meaning. It is well known, for example, that nonequilibrium states are enhanced in open systems [8]. Under external actions, any system tends, as fast as possible, to free itself from this action at the cost of the enhancement of the nonequilibrium state.

REFERENCES

1. *Phase Transformations under Irradiation*, Ed. by F. V. Nolfi, Jr. (Applied Science Publ., London, 1983; Metallurgiya, Chelyabinsk, 1989).
2. N. M. Vlasov and V. A. Zaznoba, Dokl. Akad. Nauk **363** (4), 472 (1998) [Phys. Dokl. **43**, 761 (1998)].
3. N. M. Vlasov and V. A. Zaznoba, Fiz. Tverd. Tela (St. Petersburg) **41** (1), 64 (1999) [Phys. Solid State **41**, 55 (1999)].
4. B. Ya. Lyubov, *Diffusion Processes in Inhomogeneous Solid Media* (Nauka, Moscow, 1981).
5. A. G. Khachaturyan, *The Theory of Phase Transformations and the Structure of Solids Solutions* (Nauka, Moscow, 1974).
6. Ya. S. Umanskiĭ and Yu. A. Skakov, *Physics of Metals* (Atomizdat, Moscow, 1978).
7. S. P. Timoshenko and J. N. Goodier, *Theory of Elasticity* (McGraw-Hill, New York, 1970; Nauka, Moscow, 1979).
8. G. Nicolis and I. Prigogine, *Exploring Complexity* (Freeman, New York, 1989; Mir, Moscow, 1990).

Translated by T. Galkina

Doklady Physics, Vol. 46, No. 4, 2001, pp. 223–226. Translated from Doklady Akademii Nauk, Vol. 377, No. 4, 2001, pp. 468–471.

PHYSICS

Interrelation between Diamagnetic and Thermodynamic Properties of Materials

A. F. Korolev*, S. S. Krotov*, N. N. Sysoev*, and P. V. Lebedev-Stepanov**

Presented by Academician Yu.A. Osip'yan October 25, 2000

Received November 13, 2000

In this paper, we show that introducing the zeroth component of a toroidal moment, which is normalized to the scalar electric potential (scalar moment), is an efficient method of ascertaining the relation between diamagnetic and thermodynamic properties of continua. This allows thermodynamic characteristics to be used for estimating the diamagnetic properties of materials in the case when direct magnetic measurements are incapable of providing such information (e.g., in the case of atoms having intrinsic magnetic moments). On the other hand, this makes it possible to predict certain thermodynamic parameters (such as the specific surface energy or the evaporation heat) using known diamagnetic properties. In this case, the scalar moment of a chemical element is treated as an additive characteristic similar to the parachor, which allows us to pass from the properties of simple materials to characteristics of complex molecules.

Since the character of interaction of atoms or molecules (van der Waals forces) is determined by the charge distributions in them, the diamagnetic susceptibility χ (with $\mathbf{M} = \chi\mathbf{B}$, where $\mathbf{M}$ and $\mathbf{B}$ are the magnetization vector and the magnetic-induction vector, respectively) can be considered one of the intermolecular-interaction parameters and can be related to the thermodynamic properties of the material (see [1, pp. 577–579]):[1]

$$\chi = \frac{\mu_0 e n}{6m}\int \rho r^2 dV. \tag{1}$$

Here, m is the electron mass, e is the elementary charge, n is the density of atoms (or molecules), ρ is the atomic-charge density, and r is the radius vector in the atom center-of-mass system. The integration in (1) is performed over the entire atomic volume. The presence of the factor r^2 leads to an exclusively predominate contribution of the electron cloud to the integrand. Therefore, the above integral, as expression (1), has a negative sign (i.e., the diamagnetic susceptibility is negative). Here, under the assumption of random orientation of molecules, there appears a factor 1/6 having a statistical nature. As follows from (1), the quantity χ is a measure of the mean radius squared for the electric-charge distribution in an atom.

The integral entering into (1),

$$a = -\frac{1}{6}\int \rho r^2 dV, \tag{2}$$

arises also in the expansion (over irreducible tensor representations) for the energy corresponding to the charge density ρ in the external potential φ (see [2, p. 1206]):

$$\int \rho\varphi dV = q\varphi + (q\mathbf{r}\nabla)\varphi + Q_{ij}\nabla_i\nabla_j\varphi + \frac{\nabla^2\varphi}{6}\int \rho r^2 dV + \ldots \tag{3}$$

Here, Q_{ij} is the quadrupole moment and the last term can be rewritten in the form

$$\frac{\nabla^2\varphi}{6}\int \rho r^2 dV = a\rho_e, \tag{4}$$

where $\rho_e = -\nabla^2\varphi$ is the external-charge density. The quantity a introduced in this manner is a characteristic of the system's (atom) response to this external-charge density. For definiteness, we refer to the quantity a as a scalar moment. A spherical charged capacitor is a simple model for an electrically neutral system possessing a scalar moment.

For an electrically neutral atom, its scalar moment calculated in the center-of-mass system of the atom can be proven to be an additive quantity. Indeed, the scalar moment for a group of atoms is the sum of their scalar moments, provided that the interaction disturbing the charge distribution is ignored.

[1] Here, the SI system of units is used; for simplification of the formulas, it is sometimes assumed that $\varepsilon_0 = 1$ and $c = 1$.

* *Moscow State University, Vorob'evy gory, Moscow, 119899 Russia*

** *Moscow Institute of Aviation, Volokolamskoe sh. 4, Moscow, 125080 Russia*

1028-3358/01/4604-0223$21.00

Scalar moments of compounds

	H	Li	Na	K	Hg	Cu	Ag	Au	–
H	3.72	5.97	–	–	–	–	–	–	1.9
Cl	21.07	22.72	28.36	36.53	55.25	37.38	45.90	63.07	19
I	44.71	46.80	53.81	60.17	78.34	59.5	75.43	85.64	43
Br	31.12	32.85	38.89	46.39	54.11	46.9	56.44	57.53	29
F	8.12	9.55	15.19	22.23	50.05	–	37.25	–	6
OH	12.20	11.69	22.29	20.68	–	–	–	–	10
–	1.9	4	10	17	36	17	27	43	–

For the density n of atoms, each having the scalar moment a, the energy density corresponding to formula (4) is

$$\omega = na\rho_e. \tag{5}$$

In electrostatics, the energy density has the form $\varphi\rho_e$; therefore, the quantity na entering into (5) is proportional to the scalar potential of substantial (i.e., depending on the substance properties) nature,

$$\varphi = na, \tag{6}$$

or, with regard to expression (1), to the diamagnetic susceptibility,

$$\varphi = -\frac{m\chi}{e\varepsilon_0}. \tag{7}$$

For materials in the condensed state, this potential is usually on the order of several volts [2].

The dipole toroidal moment is known to determine the matter response to the substantial manifestation of the vector potential [3, 4]. The electromagnetic potential is a four-dimensional vector. Therefore, scalar moment (2) enters into the zeroth component (time component) of the toroidal-moment vector.

With an accuracy to the first-order terms in the expansion over the velocity of the point charge q, the operator of the toroidal-moment zeroth component, which is consistent with the definition of the toroidal-moment operator [3], takes the form

$$T_0 = -\frac{1}{5}qr^2 + \frac{1}{5}\left\{\mathbf{r}\times\left(g_l\mathbf{L} + \frac{5}{2}g_\sigma\boldsymbol{\sigma}\right)\cdot\mathbf{v}\right\}. \tag{8}$$

Here, $\mathbf{v}$ is the particle-velocity operator, $\mathbf{L} = \mathbf{r}\times m\mathbf{v}$ is the angular-momentum operator, and $g_\sigma\boldsymbol{\sigma} = \mathbf{p}_m$ is the intrinsic magnetic moment. In this formula, all the terms, except for the first, are relativistic in character. Hence, the first term in the right-hand side of (8) is, generally, a reliable estimate for the scalar toroidal moment:

$$T_0 = -\frac{1}{5}qr^2. \tag{9}$$

The difference in the numerical factors [1/5 in (9) instead of 1/6 in (2)] is associated with the fact that the toroidal-moment vector was defined in [3] in terms of a three-dimensional multipole expansion, which ignores the normalization of its density to the four-dimensional vector potential.

Based on formulas (1) and (2) for the scalar moment of an atom or a molecule in a material with diamagnetic susceptibility χ, we have

$$a = -\frac{\chi m}{\mu_0 en}. \tag{10}$$

Introducing the conventional magnetic susceptibility related to the unit mass density χ_m, we rewrite (10) as

$$a = -\frac{\chi_m mM}{\mu_0 e}, \tag{11}$$

where M is the mass of an atom or a molecule of the material under consideration.

In the table, we present the values of the scalar moment $a\times10^{40}$ C m^2 for hydrogen and additive compounds of certain univalent metals with hydrogen, chlorine, iodine, bromine, fluorine, and hydroxide-ion. The scalar moments of compounds were evaluated by Eq. (11) on the basis of data of [5] (these values are given at the intersection of the corresponding column and row).

We can see that the gradual increase in the atomic mass from H to K affects the scalar moments for the compounds of these chemical elements with Cl, I, etc. Moreover, in each of the rows, the passage from a column to a neighboring one leads to approximately the same increment in the scalar moment. This fact allows the increment to be related to the scalar-moment differences for adjacent chemical elements in the series H, Li, Na, and K. The compounds of these chemical elements with the hydroxide-ion seem to be an exception.

This might be due to the bivalent (composite) nature of this ion or to certain experimental errors associated with the formation of molecules of alkalis and water in a dissociated solution and with effects of other distorting agents. Similar arguments are basically valid for the other metals listed in the first row of the table.

The scalar moments of hydrogen and the metals are represented in the bottom row of the table. They were evaluated by analyzing the differences between the scalar moments listed in the columns, with the error not exceeding 5% for hydrogen and alkaline metals (for other metals, the errors may be slightly larger).

The scalar moments of the elements listed in the left column are presented in the right column. They were evaluated on the basis of the arguments indicated above. A value standing at an intersection is approximately equal to the sum of the scalar moments of the elements in the headings of the corresponding column and row.

When evaluating the partial moments, we use the additivity principle for the scalar moment of a compound while ignoring distortions caused by the formation of chemical bonds. This procedure is the main source of errors in the estimates made above. The additivity principle can be markedly violated in more complex compounds. This is associated with the strong distortions of partial moments by chemical bonds, so that the scalar moments of chemical bonds should also be taken into account.

The scalar-moment density in a liquid is, in accordance with (6), a scalar electric potential of substantial nature which describes the resulting action of the van der Waals forces. This density can be related to the thermodynamic parameters of the liquid, such as the specific surface energy, the evaporation heat, the specific heat, etc. This implies that the measurements of the characteristics mentioned above allow us to evaluate the diamagnetic susceptibility of the liquid by formula (10). In this case, we avoid magnetic measurements or complicated calculations involving wave functions. The method for determining the mean-square radius of the charge distribution in an atom or a molecule may be the only experimental method of indirectly studying diamagnetic properties of paramagnetic materials.

Formulas (6) and (7) describe the scalar potential averaging manifestations of intermolecular or interatomic forces; this allows us to ascertain the relation between the scalar moment (and also diamagnetic susceptibility) and thermodynamic parameters.

We now consider an interface (between two different solids, a solid and a liquid, a solid and a gas, or a gas and a liquid). Let the contacting phases be characterized by the diamagnetic constants χ_1 and χ_2, respectively. (In particular, for vacuum $\chi_2 = 0$.) With regard to (7), the potential difference at the interface is

$$\Delta\varphi_{1-2} = \frac{m}{e\varepsilon_0}(\chi_1 - \chi_2). \tag{12}$$

In the case of dielectric phases, we can disregard the effect of conduction electrons (equalizing the potential difference by varying their density in the near-boundary layer). Let δ_{1-2} be the thickness of the interfacial boundary layer. Then, potential difference (12) of the dielectric phases corresponds to an electric-field with intensity

$$E = \frac{\Delta\varphi_{1-2}}{\delta_{1-2}}. \tag{13}$$

Hence, the volume energy density is

$$\omega = \frac{\varepsilon_0 E^2}{2}, \tag{14}$$

while the surface energy density in the interfacial layer is given by

$$\sigma = \omega\delta_{1-2} = \frac{\varepsilon_0\varphi_{1-2}^2}{2\delta_{1-2}} = \frac{(a_1 n_1 - a_2 n_2)^2}{2\varepsilon_0\delta_{1-2}}. \tag{15}$$

In the case of an interface between a liquid and vacuum or two liquids, quantity (15) is, respectively, the absolute or relative surface tension. It is convenient to choose the effective thickness of the interfacial layer in the form

$$\delta = Kn^{-1/3}, \tag{16}$$

where K is a certain number. The values of K evaluated by formulas (15) and (16) according to the experimental data for a variety of organic liquids and water are close to 4 (e.g., at room temperature, $K \simeq 4.2$ and 4.3 for H_2O and D_2O, respectively) [2].

The magnitude of K is mainly determined by the polarization of molecules of the liquid in the near-surface electric field (13).

The decrease in the electric-field intensity is determined by the permittivity ε_{hf} in the high-frequency region, since the essentially short-range near-surface field is subjected to high-frequency oscillations corresponding to the thermal motion of molecules. Thus, the effective mean electric-field intensity is lower by a factor of ε_{hf} than that given by expression (13). The corresponding energy decrease is inversely proportional to ε_{hf} squared or to the fourth power of the refractive index. For example, the refractive index for water is about 1.3, and its fourth power is about 3. This number is close to the values of K with a correction for the density decrease in the near-surface layer. For the other dielectric liquids under consideration, the refractive index is approximately the same.

When studying the surface tension of complex liquids, the scalar moment might be used as an additive characteristic instead of the parachor (sometimes used in these cases), because the latter is a purely empirical quantity having no clear physical meaning and providing no acceptable accuracy of description.

The relation between the surface tension and the evaporation heat can be found on the basis of analysis of the interaction energy for an isolated molecule and the entire continuum. Within the framework of a simplified model for spherically symmetric molecules, the formula

$$\alpha_m \simeq \frac{2\pi N_A a^2 K n^{5/3}}{\varepsilon_0} \quad (17)$$

was derived in [2], which relates the molar evaporation heat α_m and the scalar moment [or, with regard to (10), the diamagnetic susceptibility]. Here, N_A is the Avogadro's number and $K \simeq \varepsilon_{hf}^{-2}$ [see (16)]. Far from the liquid–gas critical point, this formula is in satisfactory agreement (within 10%) with the experimental data for water and organic liquids [2] and allows both the molar scalar moment a and diamagnetic properties of a liquid to be related to its evaporation heat.

Similarly, it is possible to ascertain the relation between the scalar moment of a molecule and other thermodynamic and thermal characteristics of its corresponding material. This makes it possible to study the dielectric properties of materials by both thermodynamic and thermal-physics experimental methods.

REFERENCES

1. D. I. Blokhintsev, *Quantum Mechanics* (Nauka, Moscow, 1976; Reidel, Dordrecht, 1964).
2. P. V. Lebedev-Stepanov, Available from VINITI, No. 1537 (Moscow, 2000).
3. V. M. Dubovik and L. A. Tosunyan, Fiz. Élem. Chastits At. Yadra **14**, 1193 (1983) [Sov. J. Part. Nucl. **14**, 504 (1983)].
4. V. M. Dubovik, S. S. Krotov, and V. V. Tugushev, Preprint JINR-E17-86-499, OIYaI (Joint Institute for Nuclear Research, Dubna, 1986).
5. *Physical Quantities. Handbook*, Ed. by I. S. Grigor'ev and E. Z. Meĭlikhov (Énergoatomizdat, Moscow, 1991).

Translated by V. Chechin

Doklady Physics, Vol. 46, No. 4, 2001, pp. 227–231. Translated from Doklady Akademii Nauk, Vol. 377, No. 4, 2001, pp. 472–476.

PHYSICS

Parameters of the Spinodal in Metastable Phases: Correlation with the Characteristics of Homogeneous Nucleation

O. F. Shlenskiĭ

Presented by Academician V.V. Osiko November 3, 2000

Received September 26, 2000

The parameters of spinodals are related to the work needed for the formation of homogeneous nuclei of the new phase and to their maximum number per unit volume at accessible levels of overheating or supercooling in metastable systems. Several examples illustrating the implementation of the obtained relationships are considered.

In the thermodynamics of metastable systems, the position of the limiting temperature that characterizes the boundary of phase states (spinodal) is determined by setting the second variation of a certain thermodynamic potential equal to zero, for example, $\delta^2 G = 0$, where G is the Gibbs free energy [1, 2]. According to this definition, the parameters characterizing the boundary of phase states can be found with the help of the equation of state by setting the derivatives $\partial T/\partial V$ or $\partial p/\partial V$ equal to zero.

Along with the thermodynamic definition of the phase state boundary, its "kinetic" definition is often used for practical purposes. The latter definition relates the vicinity of this boundary to the steep growth in the homogeneous nucleation rate (by 3–9 orders of magnitude as temperature increases by one degree of centigrade) [2]. The sharpening of the nucleation regime near the phase state boundary is observed in experiments as spontaneous (fluctuation-driven) boiling of liquids [2, 3] upon their intense heating in the absence of heterogeneous nucleation centers.

The aforementioned definitions of the phase state boundary are formally not related to each other, while they do lead to similar results in calculations of parameters that characterize this boundary. The purpose of the present paper is to reveal the relationship between the parameters of the spinodal and the characteristics of nucleation. The existence of such a relationship stems from the fact that both the spinodal and the nucleation are the manifestations of the same phenomenon, namely, the breakdown of stability in metastable systems under the effect of thermal disturbances. This is the case both for overheated and supercooled systems.

In the absence of centers of homogeneous nucleation, overheating above the temperature T_∞ of equilibrium phase transformation is accompanied by the formation of homogeneous nuclei. The work needed for this formation is [2]

$$W_* = \frac{16\pi\sigma^3}{3(p_s - p')^2(1 - v'/v'')^2}, \quad (1)$$

where σ is the surface tension, p_s is the pressure of saturation, and p' is the applied pressure; v' and v'' are the specific volumes of the condensed and gaseous phases, respectively.

The probability of formation of a homogeneous nucleus in a unit volume per unit time is proportional to the nucleation rate. The latter is given by the following relationship at the stage of the steady-state flow of nuclei [2]:

$$J = N_0 B \exp(-W_*/kT), \quad (2)$$

where k is the Boltzmann constant, N_0 is the number of molecules per unit volume, and B is the frequency factor, $B = 10^{10}$ 1/s.

Relationship (2) is found under the assumption that the arising nuclei do not produce any effect on each other. In fact, their mutual influence does not exist at the initial stage of nucleation, when the number of nuclei is small. However, as soon as the positions for the formation of nuclei become exhausted, the effect of "overcrowding" manifests itself and the rate J decreases. At a certain moment, it vanishes. If the neighboring nuclei are located close to each other and the amount of the condensed phase is insufficient for the formation of a new nucleus, then the phase transi-

Mendeleev University of Chemical Technology, Miusskaya pl. 9, Moscow, 125190 Russia

1028-3358/01/4604-0227$21.00

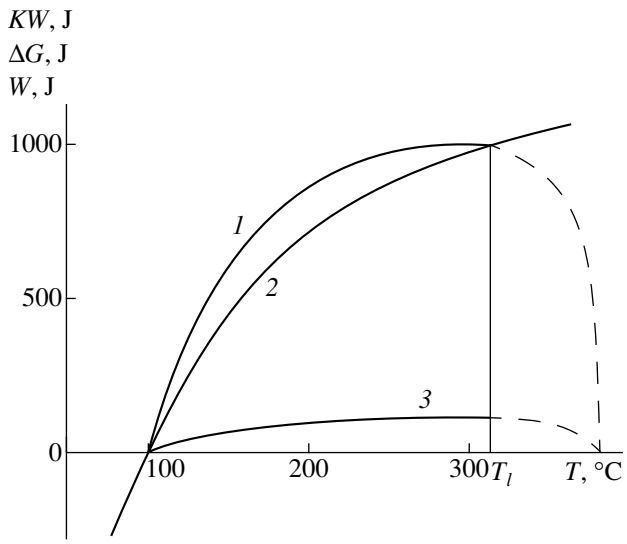

Fig. 1. Graphical solution of Eq. (4) determining the coefficient K: (*1*) KW; (*2*) ΔG; (*3*) W. Dashed lines denote the behavior of the corresponding plots above T_l according to Eq. (3).

tion terminates. A similar situation is observed upon cooling.

The relation under discussion allows us to give the following definitions for the upper and lower bounds of metastable states. The upper bound is determined by the temperature set $T_l(p)$, above which nucleation is impossible because the potential nucleation centers are exhausted as a result of the complete transformation of the material into another phase. Correspondingly, the lower bound defines the temperature level below which nucleation becomes impossible owing to the same mechanism. Nucleation occurs only when the corresponding Gibbs free energy ΔG is available; therefore, overheating (or supercooling) of the substance can be done up (down) to the limiting temperature T_l, below (above) which the excess energy ΔG is sufficient for the formation of the maximum number n_m of homogeneous nuclei per unit mass.

We now find the relationship between the excess energy ΔG and n_m. To create n homogeneous nuclei of critical size, we need to expend the work $W'' = nW_*$. Assuming that the entire mass M of the material was spent in forming the highest number of nuclei, we find that their number n_m is $M/\rho''V_*$, where $\rho'' = 1/v''$ is the density of a nucleus and $V_* = 4\pi r_*^3/3$ is its volume. The radius of a critical nucleus is [2]

$$r_* = \frac{2\sigma}{p_s - p'}\left(1 - \frac{v'}{v''}\right).$$

Bearing relationship (2) in mind for W_*, we find the total work W'' required for the formation of nuclei:

$$W'' = n_m W_* = (p_s - p')(1 - v'/v'')/2\rho''. \qquad (3)$$

Then, we should take into account that in the case of a large number of nuclei, the value of n_m is limited by their packing density. Upon random nucleation, the closest (octahedral) packing does not form and the degree of volume filling depends on the sequential formation of nuclei at different stages. To make allowance for the portion of the volume that is actually accessible to the nuclei, we introduce the factor k_1 equal to the ratio of this volume to the entire volume of the substance. Hence, we have $W = k_1 W''$. We should also take into account that a certain portion of the energy spent in the formation of the film can be released by merging of neighboring nuclei. This energy is proportional to the number of nuclei and hence to the sample mass. Therefore, the contribution of such an energy can be accounted for by introducing the coefficient k_2 in W''. In this coefficient, we also include the energy loss for overcoming the forces of inertia upon formation of nuclei with allowance for the effect of "overcrowding." Further on, we write equality $\Delta G = W$, introduce the notation $K = k_1 k_2$, and obtain the final relationship

$$\Delta G = K(p_s - p')(v'' - v)/2. \qquad (4)$$

The values of all parameters involved in (4) can be found in reference books, for example, in [2, 4]. The only exception is coefficient K, which can be calculated using data on the stochastic process of creating and merging nuclei with due account of their distortion. This is a quite complicated and cumbersome problem. A simpler method of determining K is based on the semiempirical approach using the parameters of the spinodal for a certain well-characterized reference substance, such as water. The temperature corresponding to the spinodal of the distilled and thoroughly purified water is 312°C at normal pressure [2], which yields $K = 9.29$.

A solution to Eq. (4) can be found either numerically or by a graphical method, i.e., by drawing $\Delta G(T)$ and $W(T)$ plots. The abscissa of the intersection point for these plots determines the required temperature value. The construction of such graphs for water is illustrated in Fig. 1. The $\Delta G(T) = \Delta H(T) - T\Delta S$ curves are calculated for the metastable region as monotonic functions of temperature. The latent heat of the phase transition is not included in these functions in the meta-

stable region, i.e.,

$$\Delta H(T) = \Delta H(T_0, p_0) + \int_{T_0}^{T} C_p(T)dT,$$

$$\Delta S(T) = \Delta S(T_0, p_0) + \int_{T_0}^{T} C_p(T)d\ln T,$$

where T_0 and p_0 are the initial temperature and pressure, respectively.

To test Eq. (4), we calculated the temperatures corresponding to the spinodal upon overheating of pure volatile liquids and compared the results with the experimental data reported in [2]. The calculated value for benzene is T_l = 491 K; the measurements of different researchers yield the following values: 473 K (F. Kernik, P.A. Gilbert, and K. Wismer), 498 K (E.N. Sinitsyn and V.P. Skripov), and 510 K (P.A. Pavlov and Skripov). Thus, the deviations of the calculated value from the experimental value range from 1.4 to 3.87%, which are admissible in applied calculations. The calculated value for *n*-heptane is T_l = 485 K; experiments yield 484 K (G. Wineshim and K. Tanata), 486 K (Skripov and V.I. Kukushkin), and 485.8 K (Skripov and Pavlov).

Equation (4) admits an approximate solution based on the assumption that ΔH = const and ΔS = const. Substituting relationship $\Delta G = \Delta H - T\Delta S$ into the left-hand side of (4), we obtain, after some transformations,

$$T_l = \Delta H/\Delta S + K(p_s - p')(v'' - v')/2.$$

Then, taking into account that $\Delta H/\Delta S = T_\infty$, we find the simple relationship

$$T_l = CT_\infty, \qquad (5)$$

where the proportionality coefficient is $C = 1 + K(p_s - p')(v'' - v')/2\Delta H$.

A solution to (5) can be close to an exact solution, if the temperature range T_l–T_∞ is sufficiently narrow, for example, at elevated pressures or for substances with small accessible overheating. The coefficient C turns out to be the same for substances with close chemical compositions. For example, for oxygen-containing organic compounds of small molecular mass (68–144 atomic units), the coefficient C, equal to the ratio T_l/T_∞, is nearly constant at atmospheric pressure and is 1.34 ± 1.5%. For ethanol, we have C = 463/361 = 1.32; for propyl alcohol, C = 495/370 = 1.34; etc. [2]. For a large number of high-boiling noncyclic hydrocarbons, C = 1.31 ± 5% at atmospheric pressure [2]. Such an accuracy is sufficient for many applied calculations. As the pressure rises, the difference $v'' - v'$ becomes smaller and the coefficient C also decreases, so that at the critical point, we have $v'' = v' = 0$ and C = 1.

Experimental data on attainable overheating of nonvolatile substances at normal pressure (T, K)

Substance	T_∞	T_l	T_l/T_∞
Polystyrene	653	803	1.23
Low-density polyethylene	593	773	1.3
Ammonium sulfate	483	643	1.33
Pentahydric copper sulfate	531	643	1.21
Potassium permanganate	513	648	1.25
Boric acid	343	493	1.43
Potassium hydrocarbonate	393	565	1.43
Gaseous carbon (G_6)	563	733	1.3
Celluloid	460	600	1.3
Lead azide	–	670	–

Note that a relationship similar to (5) puts the attainable values of overheating in correspondence with the equilibrium transformation temperature upon melting [5]. However, on melting, C is close to unity under overheating (1.01–1.02), whereas upon supercooling, it can be as low as 0.8 [5].

Equation (4) is valid both for volatile and nonvolatile substances, which, on heating, can undergo thermal decomposition without boiling. In this case, the changes in ΔG depend on the chemical potentials of the initial (μ_i) and final (μ_j) reaction products: $\Delta G = \sum \nu_i \mu_i - \sum \nu_j \mu_j$, where ν_i and ν_j are the coefficients accounting for the stoichiometry. In addition, when calculating the frequency J and the coefficient C, we should take into account the activation energy E of the reaction products at the phase boundary. With allowance for these arguments, we can write out the coefficient C as $C = 1 + K(p_s - p')\left(\sum \nu_j v_j - \sum \nu_i v_i\right) \times 2\Delta H + E_D/\Delta H$, where v_i and v_j are the specific volumes of the initial and final products, respectively. Experimental data demonstrate that the ratio $T_l/T_\infty = C$ lies within the range 1.1–1.46 for many nonvolatile thermally stable substances [3, 6, 7]. The values of this ratio for substances with different composition are presented in the table along with T_∞ and the initial temperature of decomposition. These temperatures were determined by thermal-analysis techniques [8, 9]. The values of T_l correspond to the first stages of thermal decomposition and characterize the temperatures to which the substance retains its initial composition as the heating rate increases above 10^2 K/s. We should note the agreement between the measured values of T_l for a number of materials and the calculations based on the wide-range

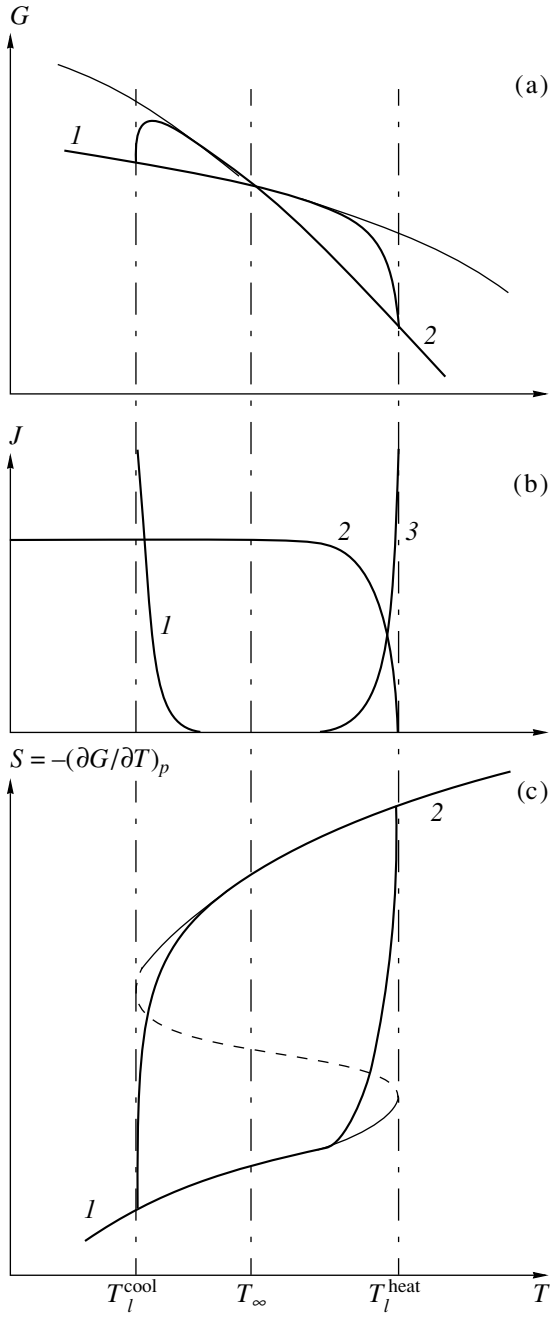

Fig. 2. Isobaric curves for potential- and kinetic-phase diagrams. (a) Variation in the Gibbs free energy: (*1*) condensed phase; (*2*) gaseous phase. (b) Variation in the nucleation rate: (*1*, *3*) nucleation flow J; (*2*) coefficient $\zeta = 1 - \frac{n}{n_m}$. (c) Variation in the entropy: (*1*) liquid phase branch; (*2*) gaseous phase branch. Thin lines: without taking nucleation into account; bold solid lines: nucleation is taken into account; dashed line: actually unrealizable branch of the labile state.

and other equations of state [10–12]. This confirms the relationships used in the calculations.

The above discussion of overheating and supercooling near the spinodal provides an opportunity to restore the missing portions of isobaric and isothermal curves in the plots of thermal potentials, which are usually drawn without taking nucleation into account, see, for example, [13]. In Fig. 2a, such plots are drawn by thick solid lines. The variation of relative filling of the volume by nuclei, $\zeta = 1 - n/n_m$, and the $J(T)$ and $S(T)$ curves are plotted in Figs. 2b and 2c in the vicinity of the spinodal.

As far as the practical implementations of the presented description of the metastable regions are concerned, we note the need to take the spinodal into account in calculating the thermal processes arising in materials under exposure to high-energy irradiation. The latter occurs, for example, in intense technological processes (plasma chemistry, laser irradiation, self-propagating high-temperature synthesis, cracking of petroleum and heavy-fraction petroleum products, etc.). The spinodal is also important in the analysis of combustion and explosion processes in condensed systems. The mathematical models used in the calculation of such processes, are often developed for equilibrium thermal conditions and do not involve information on the spinodal. The implementation of these models at high temperatures in the vicinity of the spinodal without taking into account its parameters may lead to inaccurate determination of the evaporation rates and the rates of thermal decomposition, to the overestimation of the concentration of the condensed phase in the reacting systems, and to other significant errors. Note that the lack of information on spinodals in the reference literature (reference book [2] is a rare exception) leads to the use of various and often baseless extrapolations of the data obtained for the stable phases to the region of metastable states in thermal calculations. The correlations obtained above allow us to avoid the errors caused by such an extrapolation.

Due account of the spinodal parameters provides an opportunity to improve the accuracy in the calculations of the temperature of reagents in the intense thermal processes in condensed systems. Note here the calculation of the reaction-zone size and of the operation-channel length in the plasmachemical reactors [12], the calculations of the evaporation rate for highly overheated liquids [11], the determination of the yield of reaction products in the gasification of solid fuels under intense heating [7, 9], the calculation of the adiabatic delay period before the ignition of energy-consuming materials [7, 14], and the calculation of the propagation rate for the combustion front [7, 15]. Other examples illustrating the use of improved mathematical models in the calculations of thermal processes are discussed in [7].

REFERENCES

1. A. Münster, *Chemische Thermodynamik* (Academie-Verlag, Berlin, 1969; Mir, Moscow, 1971).

2. V. P. Skripov, E. N. Sinitsyn, P. A. Pavlov, *et al.*, *Thermophysical Properties of Liquids in Metastable States* (Atomizdat, Moscow, 1960).
3. P. A. Pavlov, *Dynamics of Boiling of Strongly Overheated Liquids* (Sverdlovsk, 1968).
4. *Concise Handbook of Physicochemical Quantities*, Ed. by A. A. Ravdel' and A. M. Ponomareva (Spetsial'naya Literatura, St. Petersburg, 1999).
5. A. R. Ubbelohde, *Melting and Crystal Structure* (Clarendon Press, Oxford, 1965; Mir, Moscow, 1969).
6. O. F. Shlenskiĭ and N. M. Ievleva, Khim. Fiz. **18** (2), 67 (1999).
7. O. F. Shlenskiĭ, N. V. Afanas'ev, and A. G. Shashkov, *Thermal Destruction of Materials* (Énergoatomizdat, Moscow, 1996).
8. *Chemical Encyclopedia*, Ed. by I. L. Knunyants (Sovetskaya Éntsiklopediya, Moscow, 1983).
9. M. G. Sklyar, *Intensification of Coking and Quality of Coke* (Metallurgiya, Moscow, 1976).
10. K. V. Khishchenko, I. V. Lomonosov, V. E. Fortov, and O. F. Shlenskiĭ, Dokl. Akad. Nauk **349**, 322 (1996) [Phys. Dokl. **41**, 304 (1996)].
11. O. F. Shlenskiĭ, N. M. Ievleva, and N. N. Lyasnikova, Teplofiz. Vys. Temp. **38** (1), 41 (2000).
12. N. A. Zyrichev and O. F. Shlenskiĭ, Khim. Vys. Énerg. **33**, 484 (1999).
13. É. É. Shpil'raĭn and P. M. Kessel'man, *Foundations of Theory of Thermophysical Properties of Substances* (Énergiya, Moscow, 1977).
14. O. F. Shlenskiĭ, Khim. Fiz. **14** (6), 54 (1995).
15. O. F. Shlenskiĭ, Khim. Fiz. **17** (4), 116 (1998).

Translated by K. Kugel

Doklady Physics, Vol. 46, No. 4, 2001, pp. 232–236. Translated from Doklady Akademii Nauk, Vol. 377, No. 5, 2001, pp. 608–612.

PHYSICS

Peculiarities in the Excitation by Slow Electrons of the $^1D_2$ Levels in a Strontium Atom

Yu. M. Smirnov

Presented by Academician V.V. Osiko November 3, 2000

Received October 10, 2000

1. Study of inelastic collisions of slow electrons with strontium atoms is of considerable interest from the standpoint of fundamental science. The valence shell of a strontium atom in the ground state is characterized by the presence of two equivalent *s*-electrons, as for a helium atom. However, in contrast to the latter, the strontium atom has an atomic skeleton with a rather complicated structure. This structure involves filled $1s^22s^22p^63s^23p^63d^{10}4s^24p^6$ electron shells. This atom differs from those of lighter alkaline-earth elements, namely, magnesium and calcium, in the existence of the 3*d*-shell in it.

On the other hand, in the last few years, strontium acquired an important practical significance associated with the appearance of metal-vapor lasers. For the first time, laser generation based on a transition with wavelength $\lambda = 6.45$ μm was observed in [1] for a strontium atom. Later [2], such a generation was found for the SrI spectral lines, namely, $\lambda = 3.0665$ and 3.0111 μm. The generation on 9 transitions of a single-charged strontium ion was also obtained. The majority of these transitions correspond to IR lines with a wavelength of approximately 1 μm [3].

Thus, information on cross sections for the excitation of a strontium atom by electron impact can be used in solving both theoretical problems of atomic physics and electron–atom collisions and in developing new-types of lasers (e.g., lasers with electron pumping [4]). However, the processes occurring in the collisions of slow electrons with strontium atoms cannot be referred to as thoroughly studied. The first and most detailed experimental data concerning excitation cross sections for singlet atomic states of a strontium atom were obtained in [5]. A subsequent experimental study [6] was devoted to the thorough investigation of only one SrI transition, namely, the 460.733-nm resonance spectral line. Then, a unique theoretical study [7] appeared in which the calculation of the excitation cross sections for a strontium atom was performed in the Born–Ochkur approximation. Finally, quite recently, two papers [8, 9] were published devoted to discussing the peculiarities of the excitation of n^3P_1 levels for alkaline-earth metals and also of two-electron excitation. However, these studies are completely based on the results of the original paper [5] and do not contain new experimental information.

It should be noted that calculations [7] have only been performed for the lowest lying levels; the difference between theoretical and experimental cross sections for certain levels attains one decimal order. In the experimental study [5], the dependence of the cross sections on the principal quantum number *n* of the upper level (i.e., in spectral series) was approximated by a power function. At the same time, it was noted that considerable deviations from the power dependence took place in some singlet series. Since only 3 to 4 experimental points were measured for each of the singlet series, the reliability of the approximation at the available experimental errors of 30 to 40% is not high.

2. In this paper, a thorough investigation of the excitation of the $^1D_2$ level of a strontium atom by slow homogeneous-energy electrons is carried out. The main goal of this study was to determine the behavior of the excitation cross sections in the $5s5p^1P_1^\circ$–$5snd^1D_2$ spectral series. We used the method of extended intersecting beams in combination with the optical-spectroscopy method [10]. The technique and instrumentation for investigations using extended beams have been discussed in detail [11, 12]. Thus, the description of these methods seems to be unnecessary in this paper. However, the basic conditions of the experiments performed with strontium should be presented here.

Metallic strontium with a total impurity content not exceeding 0.02% (the main impurities are Si, Zn, Cu, Fe) was evaporated from a tantalum crucible by electron-beam heating of its external surface. Defocusing of the electron beam to a diameter of approximately 40 mm made it possible to provide a more uniform temperature field. In the operation regime at a crucible temperature of 1000 K, the concentration of Sr atoms within the region of intersection for atomic and electron beams attained 2.5×10^{10} cm^{-3}. However, when inves-

Moscow Power Institute (Technical University), Krasnokazarmennaya ul. 14, Moscow, 105835 Russia

1028-3358/01/4604-0232$21.00

tigating the resonance atomic lines, we lowered the concentration to 1×10^9 cm^{-3} with the goal of minimizing the role of reabsorption. It should be noted that in [5], the atomic concentration attained 10^{11}–10^{12} cm^{-3}.

As do atoms of other metals of the second group, strontium has an isolated ground level $^1S_0$ separated from the nearest excited levels by an interval exceeding 14000 cm^{-1}. For the evaporation temperature of 1000 K indicated above, the thermal equilibrium population of these levels is extremely low and excitation occurs only from the ground level.

The electron-beam current density in the entire operating energy range from 0 to 200 eV did not exceed 1.0 mA cm^{-2}, i.e., was several times lower than in [5]. The width of the electron energy distribution, which was measured at the entry of the electron collector by the retarding-potential method, was 0.9 eV at an energy of 100 eV and 1.0 eV at energies of 20 and 200 eV.

While scanning spectra, the actual spectral resolution of the setup, with allowance for the high operation speed of the electronic modules forming the registration system, was approximately 0.1 nm in the UV and visible spectral regions at $\lambda \leq 600$ nm. In the longer wave spectral region, the resolution dropped to 0.2 nm due to the necessity of changing the monochromator diffraction grating. Owing to the fact that only reflecting elements (with the exception of the quartz window applied for extracting the radiation from the vacuum chamber) were used in the optical system, it is achromatic and needs no additional adjustment in the entire operating spectral range from 190 to 850 nm.

The error in the measurements of relative cross sections amounts to 3 to 15% depending on the intensity of the spectral line and its position in the spectrum. The error in the absolute values of cross sections lies within the limits of ±20 to ±32%. A detailed discussion of error sources and test experiments can be found in [10–12].

3. We measured approximately 220 excitation cross sections for spectral lines within the spectral range from 242 to 768 nm in the case of exciting electrons with an energy of 30 eV. In this paper, we consider the behavior of the excitation cross sections for spectral lines arising in transitions from $^1D_2$ levels. The interest in the cross sections of these transitions is stimulated first of all by the fact that in a number of previous studies, an anomalous behavior of radiation lifetimes for $5snd\,^1D_2$ levels was observed. These anomalies in the behavior of low-lying [13] and higher-lying [14] $^1D_2$ levels were found experimentally and were predicted theoretically in a wide range (n = 6–25) [15]. Analogous data for cross sections are absent, although the anomalous behavior of the excitation cross section for the $5s5p\,^1P_1^\circ$–$5s7d\,^1D_2$ transition was noted in [15] without other comments.

The experimental results are presented in the table, in which the wavelength λ, the kind of the transition,

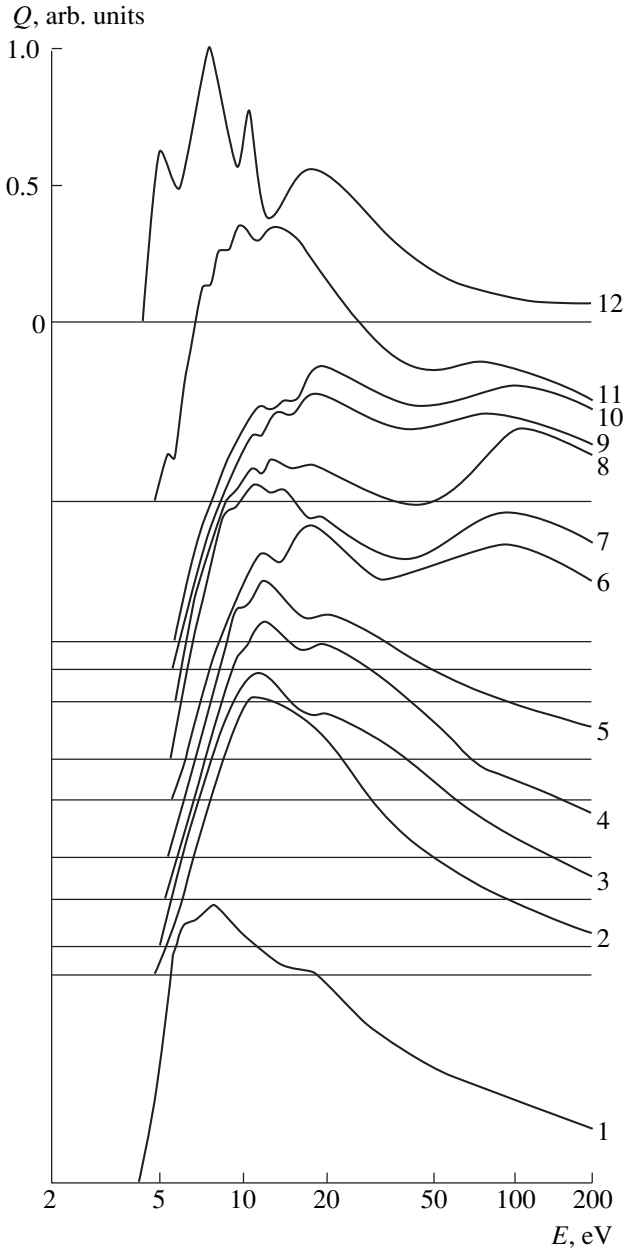

Fig. 1. Optical excitation functions for the excitation of strontium atoms.

the internal quantum number J, the energies E_l and E_u of the low-lying and high-lying layers, the cross-section values Q_{30} and Q_{max} at an energy of exciting electrons of 30 eV and in the maximum of the optical excitation function (OEF), respectively, and the position $E(Q_{max})$ of the maximum are listed. In the OEF column, the numbers of OEFs are indicated in accordance with their numbering in Fig. 1. Although in the present study the spectral resolution is much better than in [5], and all the more in [6], certain pairs of lines in the dense SrI spectrum could not be experimentally resolved. To do this, we used the entire available information concerning SrI atomic constants. The cross sections obtained as

Cross sections for strontium atoms

λ, nm	Transition	J	E_l, cm^{-1}	E_u, cm^{-1}	Q_{30}, 10^{-18} cm^2	Q_{max}, 10^{-18} cm^2	$E(Q_{max})$, eV	OEF
(329.662	$5s5p^3P°–5s12d^1D$	1–2	14504	44829)	0.48	0.63	11.0	7
(334.005	$5s5p^3P°–5s12d^1D$	2–2	14898	44829)	1.47	1.93	11.0	7
(355.485	$5s5p^3P°–5s8d^1D$	2–2	14898	43021)	0.22	0.27	12.0	4
(365.833	$5s5p^3P°–5s7d^1D$	1–2	14504	41831)	0.79	1.04	11.5	3
(371.188	$5s5p^3P°–5s7d^1D$	2–2	14898	41831)	0.051*	0.067	11.5	3
(396.261	$5s5p^3P°–5s6d^1D$	1–2	14504	39733)	1.10	1.77	11.0	2
416.931	$5s5p^1P°–5s23d^1D$	1–2	21698	45676	0.10	–	–	–
417.388	$5s5p^1P°–5s22d^1D$	1–2	21698	45650	0.115	–	–	–
417.920	$5s5p^1P°–5s21d^1D$	1–2	21698	45619	0.125	–	–	–
418.542	$5s5p^1P°–5s20d^1D$	1–2	21698	45584	0.14*	–	–	–
419.278	$5s5p^1P°–5s19d^1D$	1–2	21698	45542	0.16*	–	–	–
420.153	$5s5p^1P°–5s18d^1D$	1–2	21698	45492	0.185*	–	–	–
421.204	$5s5p^1P°–5s17d^1D$	1–2	21698	45433	0.22	–	–	–
422.470	$5s5p^1P°–5s16d^1D$	1–2	21698	45362	0.19	0.21	9.5	10
424.240	$5s5p^1P°–5s15d^1D$	1–2	21698	45263	0.165	–	–	–
426.232	$5s5p^1P°–5s14d^1D$	1–2	21698	45153	0.32	0.35	9.0	9
428.814	$5s5p^1P°–5s13d^1D$	1–2	21698	45012	0.40	0.53	110.0	8
432.195	$5s5p^1P°–5s12d^1D$	1–2	21698	44829	0.20	0.26	11.0	7
436.936	$5s5p^1P°–5s11d^1D$	1–2	21698	44578	0.37	0.46	18.0	6
445.180	$5s5p^3P°–5p^2\,^1D$	1–2	14504	36960	0.45	0.76; 0.76	9.5; 13	11
453.135	$5s5p^3P°–5p^2\,^1D$	2–2	14898	36960	1.27	2.15; 2.15	9.5; 13	11
453.237	$5s5p^1P°–5s9d^1D$	1–2	21698	43755	1.44	1.81	12.0	5
468.855	$5s5p^1P°–5s8d^1D$	1–2	21698	43021	3.21	3.91	12.0	4
(494.346	$5s5p^3P°–5s5d^1D$	1–2	14504	34727)	0.115	0.205	7.8	1
496.558	$5s5p^1P°–5s7d^1D$	1–2	21698	41831	8.18	10.8	11.5	3
(504.174	$5s5p^3P°–5s5d^1D$	2–2	14898	34727)	2.46	4.39	7.8	1
554.336	$5s5p^1P°–5s6d^1D$	1–2	21698	39733	21.0	33.8	11.0	2
644.668	$5s4d^3D–4d5p^1D°$	3–2	18319	33826	0.54	1.50	7.4	12
655.024	$5s5p^1P°–5p^2\,^1D$	1–2	21698	36960	64.1	109.0; 109.0	9.5; 13.0	11
730.942	$5s4d^1D–4d5p^1D°$	2–2	20149	33826	5.61	15.6	7.4	12
767.308	$5s5p^1P°–5s5d^1D$	1–2	21698	34727	42.1	75.2	7.8	1

a result of this procedure are marked by stars. Moreover, some intercombination lines (mainly in the UV spectral region) are not contained in any of the spectroscopic papers, and their classification is performed in the framework of this study. The data related to these lines are put in brackets.

As is seen from the table, the most complete data are obtained for the $5s5p^1P_1^\circ–5snd^1D_2$ spectral series in which cross sections are measured for all transitions having n = 5–23, with the exception of the transitions with n = 10. This transition is also absent in all preceding experimental studies devoted to the determination of atomic constants for SrI [5–9, 13, 14]. Seemingly, the excitation probability for this transition is rather small, so that this transition could not be experimentally detected to date.

The behavior of the excitation cross sections in the spectral series for atoms of alkaline-earth atoms have been previously discussed many times (see, e.g., [5, 10]);

however, these discussions were often done on the basis of scarce experimental data. Only investigations using extended beams made it possible to measure 15 to 20 cross-section values for certain series. It was established that in many cases, the dependence of the excitation cross section on the principal quantum number of the upper level obeys the power law

$$Q = A_i n^{-\alpha_i}. \quad (1)$$

Here, A_i and α_i are constants with their own characteristic values for each spectral series. However, in a number of cases, deviations from the power law were observed; therewith, no explanation was proposed to this effect in [5]. At the same time, the analysis performed for the calcium atom [10] allowed the undoubted close relation of the deviations from the dependence (1) with the existence of perturbances of the spectral series to be revealed.

The power dependence (1) is best presented in logarithmic coordinates, in which it is mapped by a straight line. This plot is depicted in Fig. 2 for the spectral series under discussion in the case of a Sr atom at an electron energy of 30 eV. As is seen, the reduction in the cross section with increasing n is substantially nonmonotone. For comparison, Fig. 3 shows a similar dependence of the natural lifetime $\tau = f(n)$ for $5snd\,^1D_2$ levels as a function of the principal quantum number n, which is taken from [14]. The theory predicts a monotonous growth $\tau \sim n^3$; however, this dependence takes place only for unperturbed series. Comparing Figs. 2 and 3, we may conclude that a correlation in the behavior of the dependences $Q = f(n)$ and $\tau = f(n)$ is observed. This behavior of the radiation lifetimes near $n = 15$ is explained in [14] by the perturbing effect of the $4d6s^{1,3}D_2$ levels. On the other hand, at $n \sim 10$, the basic perturbing cause is, apparently, the $4d^2\,^3P_{0,1,2}$ levels. For the lower lying $^1D_2$ levels, the perturbance is provided, first of all, by the interaction with the $4d^2\,^1D_2$ level.

Quite recently, in [15], the effect of perturbances on the behavior of the radiation lifetime for levels of Sr atoms (including $5snd\,^1D_2$ levels) was subjected to theoretical analysis. It was shown that application of the multichannel quantum-defect theory makes it possible to obtain satisfactory agreement between calculated and experimental lifetimes even for strongly perturbed series, including the series under discussion for a Sr atom. Unfortunately, the behavior of Sr-atom excitation cross sections was not considered from this standpoint. In fact, the behavior of the cross sections for this series is in agreement with formula (1) only when $n \geq 17$, which corresponds to the values $\alpha_i = 2.64$ and $A_i = 3.84 \times 10^{-16}$ cm^2.

When analyzing the OEFs shown in Fig. 1, we can conclude that the existence of a perturbance also affects the OEF shape. The most likely explanation of this fact

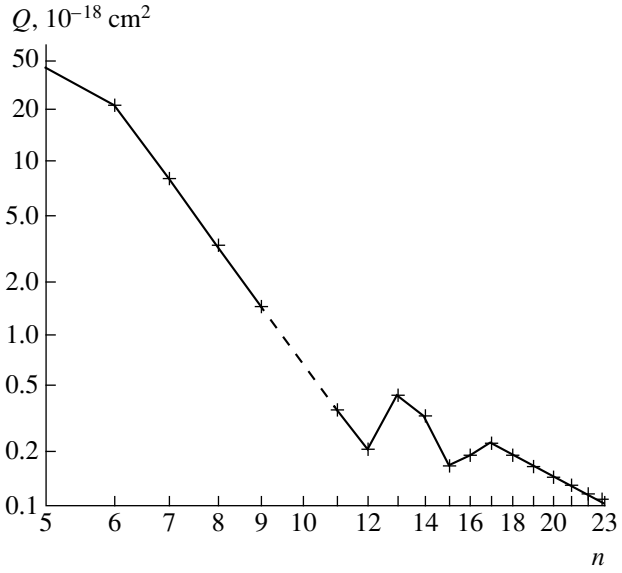

Fig. 2. Dependence $Q = f(n)$ for the $5s5p\,^1P_1^0$–$5snd\,^1D_2$ spectral series.

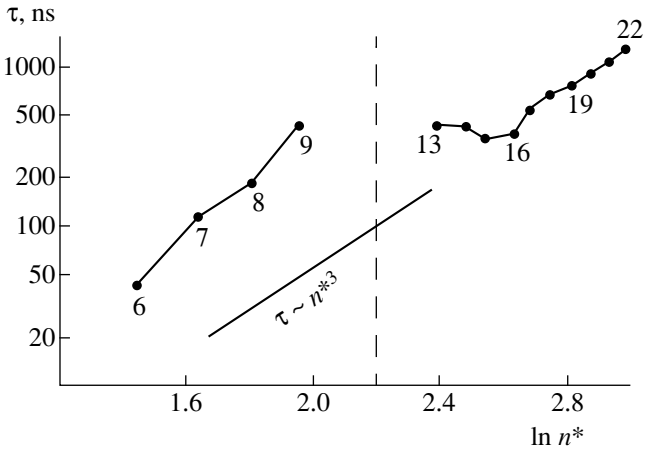

Fig. 3. Dependence $\tau = f(n)$ for $5snd\,^1D_2$ levels [14].

is that in the presence of a perturbance, the relation between contributions of different excitation channels varies with n and causes the appearance of additional features of the OEF. Previously, it was established that a similar behavior of the cross sections and the OEF in the perturbed $^1D_2$ series for a calcium atom occurs [10]. In this case, the basic perturbing levels are $3d^2\,^1D_2$ and $3d5s\,^1D_2$.

Alongside the transitions arising as a result of single-electron excitation of $5snd\,^1D_2$ levels, several of the transitions observed occur as a result of two-electron excitation of the even $5p^2\,^1D_2$ level and odd $4d5p\,^1D_2^\circ$ level. Although the cross sections for some of them are rather large, (e.g., for transitions at 655.024 and 730.942 nm), the information concerning the excitation

of these levels is scarce, which makes detailed discussion of these cases impossible. Nevertheless, it should be noted that the excitation cross section for the 655.024-nm spectral line is the greatest among those measured for $^1D_2$ levels of SrI.

4. While investigating the dependence $Q = f(n)$ for the $5s5p\,^1P_1^\circ$–$5snd\,^1D_2$ spectral series, it was established that this dependence is substantially nonmonotone. As in the case of the similar dependence $\tau = f(n)$, a suggested cause of this behavior can be a perturbance of the series under consideration. For $n \le 10$ and $n \sim 15$, the levels of the $4d^2$ and $4d6s$ configurations can be considered, respectively, perturbing levels.

REFERENCES

1. J. S. Deech and J. H. Sandes, IEEE J. Quantum Electron. **QE-4** (7), 474 (1968).
2. A. V. Platonov, A. N. Soldatov, and A. G. Filonov, Kvant. Élektron. (Moscow) **5**, 198 (1978).
3. I. G. Ivanov, E. L. Latush, and M. F. Sém, *Metal-Vapor Ion Lasers* (Énergoatomizdat, Moscow, 1990).
4. S. V. Arlantsev, B. L. Borovich, V. V. Buchanov, and N. I. Yurchenko, Kvant. Élektron. (Moscow) **23**, 977 (1996).
5. V. P. Starodub, I. S. Aleksakhin, I. I. Garga, and I. P. Zapesochnyĭ, Opt. Spektrosk. **35**, 1037 (1973).
6. S. T. Chen, D. Leep, and A. Gallagher, Phys. Rev. A **13**, 947 (1976).
7. R. K. Peterkop and A. K. Liepin'sh, Izv. Akad. Nauk Lat. SSR, Ser. Fiz. Tekh. Nauk, No. 2, 3 (1979).
8. V. P. Starodub, Opt. Spektrosk. **85**, 24 (1998) [Opt. Spectrosc. **85**, 19 (1998)].
9. V. P. Starodub, Zh. Prikl. Spektrosk. **65**, 433 (1998).
10. A. N. Kuchenev and Yu. M. Smirnov, Phys. Scr. **51**, 578 (1995).
11. Yu. M. Smirnov, in *Physics of Electron and Atomic Collisions* (Fiz.-Tekh. Inst. Akad. Nauk SSSR, Leningrad, 1985), pp. 183–193.
12. Yu. M. Smirnov, J. Phys. II France. **4**, 23 (1994).
13. A. L. Osherovich, Ya. F. Verolaĭnen, S. A. Pul'kin, *et al.*, Opt. Spektrosk. **46**, 243 (1979) [Opt. Spectrosc. **46**, 134 (1979)].
14. P. Grafström, J. Zhan-Kui, G. Jönsson, *et al.*, Phys. Rev. A **27**, 947 (1983).
15. C. J. Dai, Phys. Rev. A **52**, 4416 (1995).

Translated by G. Merzon

Doklady Physics, Vol. 46, No. 4, 2001, pp. 237–241. Translated from Doklady Akademii Nauk, Vol. 377, No. 5, 2001, pp. 613–617.

PHYSICS

On Evaporation of a Spherical Particle at Arbitrary Knudsen Numbers

Yu. I. Yalamov and E. I. Alekhin

Presented by Academician A.M. Fridman October 21, 2000

Received October 24, 2000

INTRODUCTION

The description of drop growth in certain devices or under natural conditions (e.g., in clouds), as well as of thermophoresis and diffusiophoresis phenomena, needs a quantitative theory capable of treating the gas flow around a particle immersed in gas aerosol in a wide range of Knudsen numbers. This theory must be based on solving the Boltzmann kinetic equation.

To date, there exists a number of approaches related to solving the Boltzmann equation for arbitrary Knudsen numbers. Among them, we note the Lees method [1, 2] with certain modifications [3, 4] and a method based on solving integro-moment equations by the variational Bubnov–Galerkin method [5–7].

Each of these methods have advantages and shortcomings. For example, the Lees method describes gas flows at large Knudsen numbers ($\mathrm{Kn} \gg 1$) well but fails at small Knudsen numbers ($\mathrm{Kn} \ll 1$). In the intermediate range of Knudsen numbers ($\mathrm{Kn} \sim 1$), the accuracy of the method is, generally speaking, unknown. The integro-moment Bubnov–Galerkin method is variational and makes it impossible to find the distribution function.

In this study, we use the method proposed previously in [8] for solving the Boltzmann equation at arbitrary Knudsen numbers. This method can be considered a natural generalization of the method of half-space moments with allowance for the ideas applied in the Lees method [1, 2].

The essence of the method is the following. A gas flow is described by a distribution function that has a discontinuity in the velocity space (as in the method of half-space moments [9]). However, as in the Lees method, the discontinuity takes place in the influence cone (Fig. 1) rather than in the half-plane $v_n = 0$ (v_n is the molecule velocity component normal to the particle surface). The procedure of constructing a system of moment equations is similar to the method of half-space moments [9]. Thus, the method proposed combines the advantages of the methods preceding it. Owing to the presence of the influence cone, this method allows us to describe the flows at arbitrary Knudsen numbers. On the other hand, the procedure of constructing the system of moment equations is similar to that in the method of half-space moments. This makes it possible to eliminate the inconsistency intrinsic to the Lees method in the choice of moments, while constructing the system of moment equations. Thus, in the limiting case as $\mathrm{Kn} \longrightarrow 0$, the system of moment equations is reduced to that derived by the method of half-space moments, since, in this case, the influence cone is transformed into a half-plane $v_n = 0$. In the other limiting case, i.e., as $\mathrm{Kn} \longrightarrow \infty$, the system of equations describes a free molecular flow.

FORMULATION OF THE PROBLEM

We consider a volatile spherical particle of radius a which is placed into its own vapor. Let the vapor temperature T_0 and its concentration n at a great distance from the particle (compared with the mean free path λ) be known. Let also $n = n_0(1 + s)$, where $n_0 = n_{\mathrm{sat}}(T_0)$ is the concentration of the saturated vapor at temperature T_0. The parameter s, depending on its sign, characterizes either supersaturation or incomplete saturation of the vapors. The Knudsen number is defined as $\mathrm{Kn} = \dfrac{\lambda}{a}$.

We restrict ourselves to a small temperature drop T_w between the surface of the particle and the gas; i.e., we assume the validity of the relation

$$\left|\frac{T_w - T_0}{T_0}\right| \ll 1.$$

In this case, the state of the gas differs slightly from the equilibrium state and the velocity distribution function f of the gas molecules can be expanded near the equilibrium Maxwellian distribution function f_0:

$$f^{\pm} = f_0(1 + \Phi), \qquad (1)$$

Moscow State Pedagogical University,
ul. Malaya Pirogovskaya 1, Moscow, 119435 Russia

1028-3358/01/4604-0237$21.00

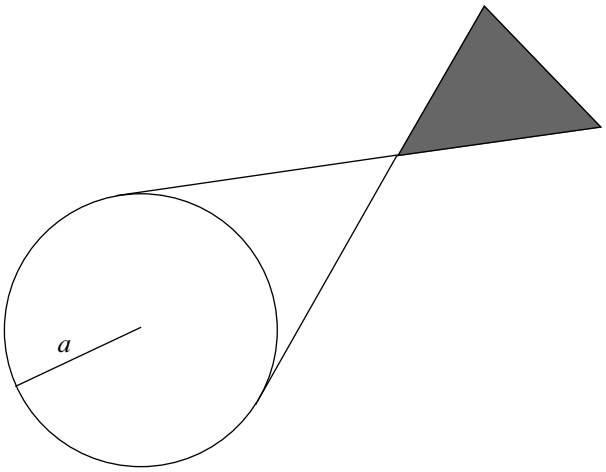

Fig. 1. Influence cone.

where

$$f_0 = n_0\left(\frac{m}{2\pi kT_0}\right)^{3/2}\exp(-c^2), \qquad (2)$$

m is the mass of a molecule, and $\mathbf{c} = \sqrt{\frac{m}{2kT_0}}\mathbf{v}$ is its reduced velocity.

The steady gas flow is described by the linearized Boltzmann equation [10] written out in the spherical coordinate system:

$$(\mathbf{c}\nabla)\Phi = I_c(\Phi), \qquad (3)$$

where $I_c(\Phi)$ is the linearized collision integral [10] and r, φ, and θ are spherical coordinates.

CONSTRUCTING THE SYSTEM OF MOMENT EQUATIONS

We represent the distribution function of vapor molecules, which is discontinuous on the influence cone (Fig. 1), in the following form:

$$\Phi \equiv \Phi^{\pm} = \begin{cases} \Phi^{+} & \text{inside the influence cone} \\ & \text{(hatched region in Fig.1)} \\ \Phi^{-} & \text{outside the influence cone} \end{cases}$$

We expand the function $\Phi^{\pm}$ into a series in terms of Sonin polynomials:

$$\Phi^{\pm} = \sum_{k=0}^{\infty} a_k^{\pm} S_{1/2}^k(c^2) + \sum_{k=0}^{\infty} b_k^{\pm} c_r S_{3/2}^k(c^2),$$

where $S_\nu^k(c^2)$ is the Sonin polynomial [10]. In the expansion of function $\Phi^{\pm}$, we preserve the terms up to $k = 1$ inclusively. Note that in the conventional Lees method [1], only the first two terms of the first summand are preserved. Renaming the expansion coefficients and omitting the argument in the Sonin polynomials, we have

$$\Phi^{\pm} = a_0^{\pm} + c_r a_1^{\pm} - S_{1/2}^1 a_2^{\pm} + c_r S_{3/2}^1 a_3^{\pm}. \qquad (4)$$

To simplify the calculation of the moments from the collision integral, the BGK-model [11] was chosen:

$$I_c = \frac{16}{15\sqrt{\pi}} f_0 \frac{1}{\lambda}(\Phi_{eq} - \Phi^{\pm}).$$

Here,

$$\Phi_{eq} = \nu + 2cG - S_{1/2}^1\tau,$$

$$\nu = \int f_0\Phi^{\pm}d^3c, \quad G = \sqrt{\frac{m}{2kT_0}}\int c f_0\Phi^{\pm}d^3c,$$

$$\tau = \int\frac{mv^2}{2kT_0} f_0\Phi^{\pm}d^3c.$$

Evaluating the parameters ν, G, and τ and substituting them together with function (4) into Eq. (3), we obtain the differential equation with respect to the expansion coefficients $a_0^{\pm}$, $a_1^{\pm}$, $a_2^{\pm}$, and $a_3^{\pm}$. Furthermore, this equation is multiplied by the same velocity polynomials [which were used when distribution function (4) was expanded into a series] and, finally, integrated over regions both inside and outside the influence cone. As a result, after simple rearrangements, we obtain the following system of moment equations:

$$\frac{4\sqrt{\pi}}{r^2}\frac{\partial a_0^{\pm}}{\partial r} + 2\pi(\pm 1 - x^3)\frac{\partial a_1^{\pm}}{\partial r} + \frac{2\sqrt{\pi}}{r^2}\frac{\partial a_2^{\pm}}{\partial r}$$

$$+ \frac{\pi}{r}\left(\pm 4 - \frac{2x}{r^2} - 4x\right)a_1^{\pm} = \frac{16}{15\sqrt{\pi}}\frac{a}{\lambda}\left\{\frac{2}{r^2}\left(\frac{2}{r^2} - \pi\right)\right.$$

$$\times(a_0^{+} - a_0^{-}) - \frac{2\sqrt{\pi}}{r^2}x\left(2 - \frac{1}{r^2}\right)(a_1^{+} - a_1^{-}) \qquad (5)$$

$$\left. + \frac{2}{r^4}(a_2^{+} - a_2^{-}) - \frac{\sqrt{\pi}}{r^2}x(a_3^{+} - a_3^{-}) - \frac{\sqrt{\pi}}{r^2}(a_3^{+} + a_3^{-})\right\};$$

$$12\sqrt{\pi}(1 \mp x^3)\frac{\partial a_0^{\pm}}{\partial r} \pm \frac{24\sqrt{\pi}}{r^2}\left(2 - \frac{1}{r^2}\right)\frac{\partial a_1^{\pm}}{\partial r}$$

$$+ 12\pi(1 \mp x^3)\frac{\partial a_2^{\pm}}{\partial r} \mp \frac{12\sqrt{\pi}}{r^2}\left(2 - \frac{1}{r^2}\right)\frac{\partial a_3^{\pm}}{\partial r}$$

$$\pm\frac{24\sqrt{\pi}}{r^5}a_1^{\pm} \mp \frac{12\sqrt{\pi}}{r^5}a_3^{\pm}$$

$$= \frac{16}{15\sqrt{\pi}}\frac{a}{\lambda}\left\{\mp\frac{12\sqrt{\pi}}{r^2}x\left(2-\frac{1}{r^2}\right)(a_0^+ - a_0^-)\right. \quad (6)$$

$$\pm\left(\pi\left(\frac{18}{r^4}-\frac{18}{r^2}-\frac{6}{r^6}\right)+\frac{14}{r^4}\right)(a_1^+ - a_1^-)$$

$$\left.\mp\frac{6\sqrt{\pi}}{r^2}x\left(2-\frac{1}{r^2}\right)(a_2^+ - a_2^-) \mp \frac{1}{r^4}(a_3^+ - a_3^-)\right\};$$

$$\frac{4\sqrt{\pi}}{r^2}\frac{\partial a_0^\pm}{\partial r} + 4\pi(\pm 1 - x^3)\frac{\partial a_1^\pm}{\partial r} + \frac{18\sqrt{\pi}}{r^2}\frac{\partial a_2^\pm}{\partial r}$$

$$-10\pi(\pm 1 - x^3)\frac{\partial a_3^\pm}{\partial r} + \frac{4\pi}{r}\left(\pm 2 - \frac{x}{r^2} - 2x\right)a_1^\pm$$

$$+\frac{10\pi}{r}\left(\frac{x}{r^2}+2x\mp 2\right)a_3^\pm = \frac{16}{15\sqrt{\pi}}\frac{a}{\lambda}\left\{\frac{4}{r^4}(a_0^+ - a_0^-)\right. \quad (7)$$

$$-\frac{2\sqrt{\pi}}{r^2}x\left(2-\frac{1}{r^2}\right)(a_1^+ - a_1^-) - \frac{2}{r^2}\left(3\pi - \frac{1}{r^2}\right)(a_2^+ - a_2^-)$$

$$\left.+\frac{7\sqrt{\pi}}{r^2}(a_3^+ + a_3^-) + \frac{7\sqrt{\pi}}{r^2}x(a_3^+ - a_3^-)\right\};$$

$$\pm\frac{24\sqrt{\pi}}{r^2}\left(2-\frac{1}{r^2}\right)\frac{\partial a_1^\pm}{\partial r} + 60\pi(1\mp x^3)\frac{\partial a_2^\pm}{\partial r}$$

$$\mp\frac{156\sqrt{\pi}}{r^2}\left(2-\frac{1}{r^2}\right)\frac{\partial a_3^\pm}{\partial r} \pm \frac{24\sqrt{\pi}}{r^5}a_1^\pm \mp \frac{156\sqrt{\pi}}{r^5}a_3^\pm$$

$$= \frac{16}{15\sqrt{\pi}}\frac{a}{\lambda}\left\{\frac{12\sqrt{\pi}}{r^2}x(1\pm x)(a_0^+ - a_0^-) \pm \frac{2}{r^4}(a_1^+ - a_1^-)\right. \quad (8)$$

$$-\frac{42\sqrt{\pi}}{r^2}(1\pm x)\left((a_2^+ - a_2^-) \mp \frac{55}{r^4}(a_3^+ - a_3^-)\right)$$

$$\left.+60\pi(1\mp x^3)a_3^\pm\right\}.$$

Here, r is the distance from the origin, which is normalized to the particle radius a, and $x = \sqrt{1-\frac{1}{r^2}}$.

As Kn $\longrightarrow$ 0, the system of differential equations (5)–(8) transforms into the system obtained by the method of half-space moments in [12, 13]. Formally, the passage to a limit can be performed by taking $x = 0$ in (5)–(8). As Kn $\longrightarrow \infty$, evidently, $\frac{a}{\lambda} \longrightarrow 0$. As a result, the terms standing in the right side and representing the moments of the collision integral vanish. In this case, collisions between molecules cease to influence the distribution function and Eqs. (5)–(8) describe the free molecular flow.

KINETIC BOUNDARY CONDITIONS ON A VOLATILE SURFACE

To solve the system of equations (5)–(8), it is necessary to set kinetic boundary conditions. Using the well-known Maxwellian model, we assume that a vapor molecule incident onto the drop surface can be either condensed on it (with probability α^-) or diffusely reflected backward into the gas (with probability $1 - \alpha^-$). Hence, the molecular flow directed outward from the particle surface consists of two parts. The first one represents the flow of molecules evaporated from the surface [their distribution function is characterized by the temperature T_w and the density $n_w = n_{sat}(T_w)$]. The second part represents the flow of reflected molecules (their distribution function is characterized by the unknown parameters T_s and n_s). As a result, the distribution function for molecules flying from the surface can be represented in the form

$$f^+ = \alpha^- n_w\left(\frac{m}{2\pi k T_w}\right)^{3/2}\exp\left(-\frac{mv^2}{2kT_w}\right)$$

$$+(1-\alpha^-)n_s\left(\frac{m}{2\pi k T_s}\right)^{3/2}\exp\left(-\frac{mv^2}{2kT_s}\right).$$

Linearizing this function near the f_0 absolute Maxwellian, we obtain

$$f^+ = \alpha^- f_0(1 + \nu_w - S^1_{1/2}\tau_w) + f_0(1-\alpha^-)(1 + \nu_s - S^1_{1/2}\tau_s), \quad (9)$$

where

$$\tau_w = \frac{T_w - T_0}{T_0}, \quad \nu_w = \frac{n_w - n_0}{n_0},$$

$$\tau_s = \frac{T_s - T_0}{T_0}, \quad \nu_s = \frac{n_s - n_0}{n_0},$$

and $n_0 = n_{sat}(T_0)$. Comparing this expression with the distribution function $f^+ = f_0(1 + \Phi^+)$, we obtain the following boundary conditions:

$$a_0^+ = \alpha^-\nu_w + (1-\alpha^-)\nu_s, \quad a_1^+ = 0,$$

$$a_2^+ = \alpha^-\tau_w + (1-\alpha^-)\tau_s, \text{ and } a_3^+ = 0.$$

To determine the four unknown quantities ν_w, τ_w, ν_s, and τ_s, we use the following relationships:

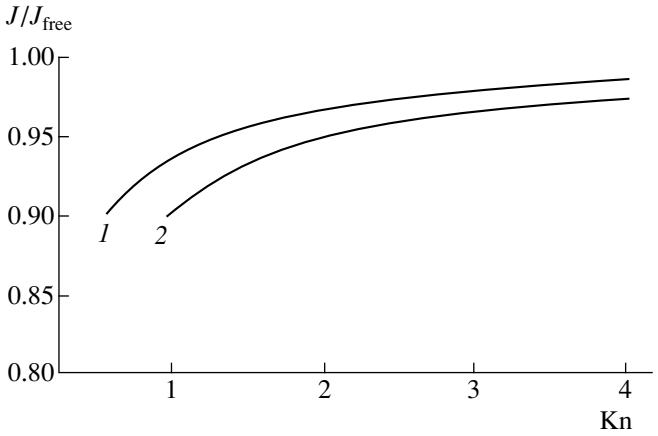

Fig. 2. Reduced mass flow at different values of the Knudsen number Kn: (*1*) the combined method; (*2*) the Lees method [1, 2].

(i) the Clausius–Clapeyron equation

$$p_{\text{sat}}(T_w) = p_{\text{sat}}(T_0)\exp\left(\frac{q}{kT_0} - \frac{q}{kT_w}\right); \qquad (10)$$

(ii) the energy-balance equation

$$J_q^+ + J_q^- = -q(J_m^+ + J_m^-); \qquad (11)$$

(iii) the equation for the balance of molecule flow

$$(1-\alpha^-)J^- + J'' = 0, \qquad (12)$$

where J'' is the part of the flow which was diffusely reflected from the drop surface;

(iv) the thermal-accommodation condition [14]

$$\alpha_T = \frac{(1-\alpha^-)J_q^- + J_q''}{(1-\alpha^-)J_q^- + J_{qw}''}. \qquad (13)$$

Here, α_T is the energy accommodation coefficient, J_q'' is the energy flux transferred by molecules reflected from the phase boundary, and J_{qw}'' is the energy flux transferred by molecules reflected from the phase boundary provided that complete thermal accommodation takes place.

Solving the system of equations (10)–(13) with respect to the unknown quantities ν_w, τ_w, ν_s, and τ_s and substituting the solutions obtained into (9), we arrive at the system of boundary conditions which links the expansion coefficients for the functions f^+ and f^-.

The boundary conditions at infinity have the form

$$\left.\frac{n-n_0}{n_0}\right|_{r\to\infty} = s, \quad \left.\frac{T-T_0}{T_0}\right|_{r\to\infty} = 0. \qquad (14)$$

SOLUTION TO THE SYSTEM OF EQUATIONS AND ANALYSIS OF THE RESULTS OBTAINED

The system of equations (5)–(8) with boundary conditions (10)–(13) was solved by the Galerkin method.

Since the heat flow and mass flow are proportional to each other, we restrict ourselves to analysis of the results concerning the mass flow J_m only. While calculating this flow, we assumed that complete thermal accommodation of the molecules occurs on the particle surface (i.e., $\alpha_T = 1$). In addition, we assumed that $s = 0.5$.

The plots obtained by both methods are shown in Fig. 2. Curves *1* and *2* were obtained by the combined method proposed in [8] and developed here and by the Lees method [1], respectively. All the results are normalized to the mass-flow density in a free molecular regime J_{free}. As is seen, at Knudsen numbers on the order of unity, significant discrepancies are observed in the values of the flows, which were evaluated by both methods. At Kn < 1, curve *2* is cut off since the Lees method is not applicable in this region.

Thus, we can state that the combined method of calculating the heat flow and mass flow is valid in the entire range of Knudsen numbers. Comparing the results obtained by the combined method and Lees methods, we can solve the problem of the validity of the latter method in the intermediate range of Knudsen numbers, i.e., at Kn ≈ 1.

Since the Galerkin method makes it possible to minimize the residual of kinetic equations only on the average, the representation of the distribution function in the form of an expansion in terms of basic functions only approximately describes its true behavior. Therefore, the calculated values of the heat flow and mass flow are not exactly constant and vary around their mean values. The average magnitude of these deviations may be taken as the estimated calculation accuracy. At Kn ≈ 0.5 and 4.0, the calculation error determined by this manner is approximately 7%. At Kn ≈ 1, this error does not exceed 4%.

ACKNOWLEDGMENTS

We are grateful to Professor A.A. Yushkanov for extremely fruitful discussions of the results of this work.

REFERENCES

1. L. Lees and Liu Chung-Yen, Phys. Fluids **5**, 1137 (1962).
2. L. Lees, J. Soc. Ind. Appl. Math. **13** (1) (1965).
3. I. N. Ivchenko and Yu. I. Yalamov, Izv. Akad. Nauk SSSR, Mekh. Zhidk. Gaza, No. 3, 164 (1974).
4. Yu. I. Yalamov, I. N. Ivchenko, and S. M. Muradyan, Dokl. Akad. Nauk SSSR **258**, 1106 (1981) [Sov. Phys. Dokl. **26**, 610 (1981)].

5. V. G. Chernyak and A. E. Margilevskiĭ, Teplofiz. Vys. Temp. **18**, 1032 (1980).
6. S. A. Beresnev and V. G. Chernyak, Teplofiz. Vys. Temp. **24**, 313 (1986).
7. S. A. Beresnev and V. G. Chernyak, Teplofiz. Vys. Temp. **24**, 549 (1986).
8. E. I. Alekhin, Available from VINITI No. 477-V97 (Moscow, 1997).
9. E. P. Gross, E. A. Jaeckson, and S. Ziering, Ann. Phys. **1** (2), 141 (1957).
10. M. N. Kogan, *Dynamics of Rarefied Gas* (Nauka, Moscow, 1967).
11. P. L. Bhatnagar, E. P. Gross, and M. A. Krook, Phys. Rev. **94**, 511 (1954).
12. A. B. Poddoskin, A. A. Yushkanov, and Yu. I. Yalamov, Zh. Tekh. Fiz. **52**, 2253 (1982) [Sov. Phys. Tech. Phys. **27**, 1383 (1982)].
13. Yu. I. Yalamov, A. B. Poddoskin, and A. A. Yushkanov, Dokl. Akad. Nauk SSSR **254**, 343 (1980) [Sov. Phys. Dokl. **25**, 734 (1980)].
14. Yu. I. Yalamov, E. R. Shchukin, and E. I. Alekhin, Teplofiz. Vys. Temp. **28**, 256 (1990).
15. C. A. J. Fletcher, *Computational Galerkin Methods* (Springer-Verlag, New York, 1984; Mir, Moscow, 1988).

Translated by Yu. Vishnyakov

Doklady Physics, Vol. 46, No. 4, 2001, pp. 242–246. Translated from Doklady Akademii Nauk, Vol. 377, No. 6, 2001, pp. 749–753.

PHYSICS

Properties of a Catalytically Active Pulsed Microwave Discharge at Atmospheric Pressure

Academician V. D. Rusanov, A. I. Babaritskiĭ, M. B. Bibikov, E. N. Gerasimov, V. K. Zhivotov, A. A. Knizhnik, B. V. Potapkin, and R. V. Smirnov

Received December 6, 2000

A pulse-periodic pseudocorona microwave discharge at atmospheric pressure [4] is of interest from both the fundamental and applied standpoints. This phenomenon attracts attention as a complicated object for investigation in the field of gas-discharge physics. For practice, this type of discharge is important by virtue of its catalytic properties in the chemical processes of hydrocarbon conversion with participation of plasma [1–3]. The effect of discharge-plasma catalytic activity in the process of thermal decomposition of methane into hydrogen and carbon consists in a significant (by several times) increase in the degree of preheated-methane decomposition under the action of discharge plasma. In this case, the microwave energy introduced into the system in the form of plasma represents a small fraction (smaller than 20%) of the thermal energy required for heating the methane. The process occurs mainly owing to accumulated thermal energy, so that the energy cost for the additional decomposition of methane molecules under the action of plasma, as compared with the energy introduced only in the plasma form, turns out to be lower than the enthalpy inherent in the process [3].

To explain the mechanism of plasma catalytic activity and to optimize reactors based on the effect of plasma catalysis, detailed information on the discharge space-time structure and parameters is required. We imply the electric-field amplitude in the plasma, the concentration of the charged particles, and the temperature of the neutral component. The electric-field amplitude determines the efficiency of accumulation of active-particles (electrons, ions, and clusters) in plasma, the chain reactions of which are the most probable mechanism determining the effect of plasma catalysis [2].

The discharge is formed at the point of a needle introduced into a microwave waveguide system as an initiator (Fig. 1). The parameters of the microwave radiation are the following: the pulse power is 30 to 100 kW, the frequency is 9.04 GHz (the wavelength is 3.3 cm), and the pulse duration is 0.1 to 1 μs. The discharge is produced from the initiator point in the form of a bundle (about ten filaments) of fine plasma formations with the following geometric parameters: the length is ~1 cm, the radius is ~0.1 mm, and the length growth rate is $\sim 10^6$ cm/s. The results of investigation of the discharge spatial-structure evolution are described in [4].

In a number of studies (see, e.g., [5, 6]), mechanisms of arising and developing filamentary discharge structures in a microwave field under conditions of high pressure were analyzed. The following two of them are the most probable. The first is the microwave-streamer mechanism that corresponds to microwave-field amplitudes close to threshold (discharge) amplitudes. The second is the development of ionization-overheating instability which is characterized by gas heating in the initially weakly irregular plasma, gas expansion, and an increase in the $\frac{E}{N}$ (field-intensity/concentration) parameter with a subsequent charge development in thin strongly heated channels. Each of these mechanisms can be realized experimentally. In these cases, discharge-plasma parameters may significantly differ depending on the mechanism. Theoretically, it is quite difficult to predict plasma properties in a particular experiment, since the system is too complicated for detailed numerical simulations. Therefore, direct experimental investigations of discharge properties are of great importance.

This study is devoted to the diagnostics of the time dependences of microwave-field amplitude, the concentration of electrons, and the gas temperature in plasma discharge channels in both methane and hydrogen. We analyzed the experimental profiles of spectral H_α and H_β lines from the hydrogen Balmer series, as well as the rotational spectrum in the V_{0-0} transition of Swan bands for a C_2 molecule. The spectral measurements were performed with a high (20 ns) time resolution. The discharge radiation from the region near the needle point was detected with the help of a MDR-23

Institute of Hydrogen Energetics and Plasma Technologies, Russian Research Center Kurchatov Institute, pl. Akademika Kurchatova 1, Moscow, 123182 Russia

1028-3358/01/4604-0242$21.00 © 2001 MAIK “Nauka/Interperiodica”

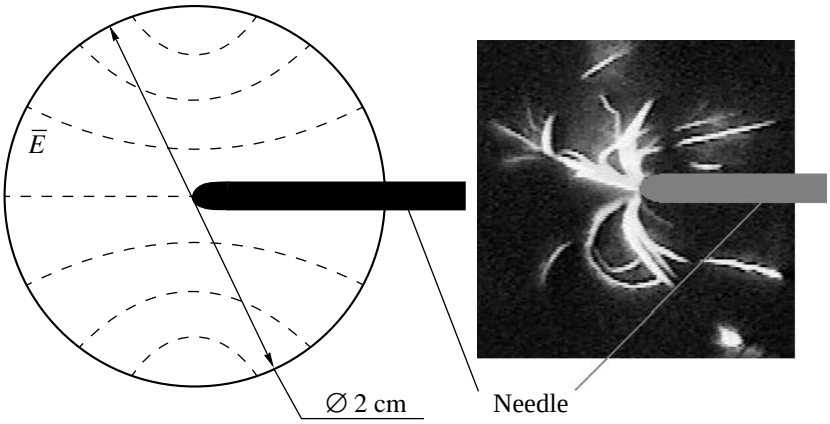

Fig. 1. Cross section of the discharge chamber and an external view of the discharge.

monochromator, a FEU-79 photomultiplier, and a high-speed analog-to-digital converter. For resolving the spectra in time, we applied the strobing-integrator method. Several tens of thousands of spectral dots were recorded in the pulse-periodic regime of the discharge (with a repetition frequency of 1 kHz) by uniform scanning using a monochromator. Each dot of the spectrum was measured for every sequential microwave pulse during a short period of time (5 ns), which was shifted with respect to the pulse onset for a fixed time interval. Thus, the spectrum obtained related to a certain time moment counted off from the beginning of the charge development. Varying the time delay, we recorded the time evolution of the spectra in a certain fixed cross section of the plasma channel. The measurements were performed without resolution with respect to the channel radius; therefore, the measured charge parameters should be considered to be averaged values.

An interesting feature of the measured time dependences was observed for the profiles of the H_α and H_β lines. For discharge in methane, at a time moment of about 0.4 μs from the beginning of the discharge development, the half-width of the profiles sharply increased (during about 100 ns) from approximately 1 and 4 Å to 6 and 40 Å for the H_α and H_β lines, respectively. This jump was explained by a sharp rise of the electron concentration in the plasma. For the time interval <0.4 μs, we observed a structure of satellite peaks on the line profiles (Fig. 2). Such a structure is characteristic for Stark splitting of atomic sublevels in an external electric field. At later time moments, this structure was not observed. For discharge in hydrogen, the jump in the line widths occurred earlier, namely, at $t \approx 250$ ns from the beginning of the discharge development. The Stark structure of the lines was also observed before the time moment mentioned above.

The feature indicated made it possible to conclude that the discharge development has two time stages: before the jump in concentration of charged particles and after this jump. At the initial stage ($t < 250$ ns in hydrogen and $t < 400$ ns in methane), the time dependence of the microwave-field amplitude was measured according to the observed Stark structure of the line profiles (Fig. 2). In these measurements, we used a method of profile modeling for which the measured values of parameters provided the best coincidence of the experimental and model profiles. To obtain a model profile, it is necessary to calculate the Blokhintsev profiles [7] for each side Stark component and, furthermore, to sum them over all side components with their relative intensities taken into account. Then, the convolution of the profile obtained with the monochromator instrumental profile and the Doppler profile was performed at $T \sim 1000$ K (this is the approximate temperature in the initial stage of a discharge). The fundamental component H_α of the Stark structure is not affected by the field, but it is significantly broadened by the electron impact. Therefore, in addition to the broadening causes listed above, we have performed a convolution of the Lorentz impact profile, whose half-width was fitted for the best coincidence of the calculated profile with the experimental profile. For a particular case, the experimental (curve *1*) and calculated (curve *2*) pro-

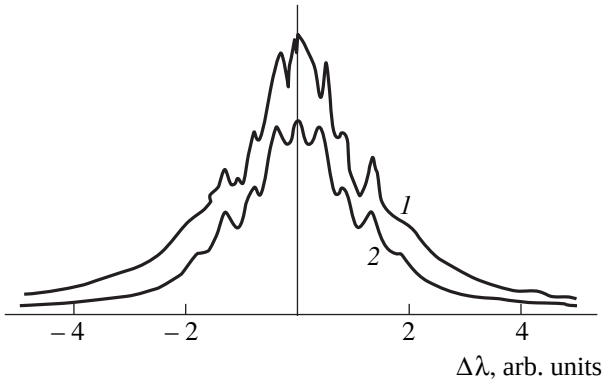

Fig. 2. H_α profiles in the 20-kV/cm microwave field: (*1*) the measured profile; (*2*) the calculated profile.

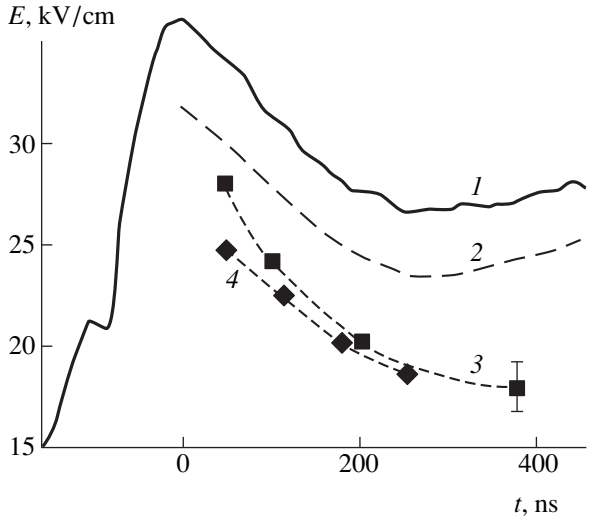

Fig. 3. Amplitude of the microwave field in plasma: (*1*) microwave pulse; (*2*) field amplitude in the discharge chamber in the absence of a needle and plasma; (*3*) discharge in methane; (*4*) discharge in hydrogen.

files of the H_α line for the discharge in methane are shown in Fig. 2. For clarity, the profiles were plotted with slightly different amplitudes. A similar structure was also observed for the H_β line. The effect of the microwave field on a radiating atom gives rise to a characteristic structure of satellite peaks representing the Stark system of sublevels. It is worth noting that the spacing between neighboring satellites along the wavelength scale is proportional to the field amplitude (the linear Stark effect). It is possible to fit this spacing within an accuracy of no worse than 10%, which, by virtue of the linearity, is the measurement accuracy for the field in itself.

Figure 3 shows the measurement results for the field amplitude of the H_α and H_β lines in the case of discharge in both hydrogen and methane. The moment of the discharge appearance coinciding with the microwave-field maximum was chosen as the onset of counting time. In the discharge chamber, in the absence of the needle and plasma (curve *2*), the field amplitude was calculated for the instantaneous value of the microwave power (curve *1*). We managed to measure the amplitude of the microwave field for discharges in hydrogen and methane within the time intervals of 50 to 250 ns and 50 to 400 ns, respectively. At later time moments, because of the drastic drop in the electron density, the line profile is already determined by other broadening causes. As is seen from Fig. 3, for discharge in methane, the field amplitude decreases from 28 to 18 kV/cm (the corresponding average electron energy calculated for this field amplitude varies within the range of 3 to 2 eV). For discharge in hydrogen, the field is somewhat lower than that for methane. In the time interval from 0 to 50 ns, the radiation intensity was insufficient for reliable recording of the spectral-line profiles. However, it is this time interval that corresponds to the maximum field (in the microwave-streamer head). At earlier time moments, we determined the field evolution by modeling the propagation of an ionization front in the framework of the diffusion model [4] using the measured propagation velocities for microwave streamers. The estimated maximum field in the microwave-streamer head attains 100 and 75 kV/cm for discharges in hydrogen and methane, respectively. This field rapidly drops (in a time on the order of 1 ns) to 25–30 kV/cm. The maximum mean electron energy in the streamer head attains 7 to 8 eV.

Beginning from the time moments of 250 and 400 ns in hydrogen and methane, respectively, we observed a drastic change in the half-widths of both the H_α and H_β lines, which was accounted for by a significant increase in the concentration of the charged particles in the plasma. Under these conditions, the predominant mechanism of line broadening became the broadening due to the presence of ions and electrons.

Analysis of the experimental profiles for the H_α and H_β lines was performed in order to determine the concentration of the charged particles. This procedure also consisted in modeling calculated profiles and comparing them with experimental profiles. We took into account both the quasi-static ion broadening (when the ion field was described by the Holtsmark distribution) and the electron-impact broadening of Stark components provided that the ion and electron concentrations were the same. The calculation procedure of the impact half-widths is described in [7]. The ion concentration can be evaluated within acceptable accuracy from the line half-width with the help of the relationship [8]

$$\Delta\lambda_{1/2} = \frac{\lambda^2}{2\pi c} 12.5 (n_u^2 - n_L^2) N^{2/3}, \qquad (1)$$

where λ is the wavelength, n_u and n_l are the principal quantum numbers of the transition upper and lower levels, respectively, and N is the ion concentration. This simplified procedure yields values of the concentration which are close to the results of detailed modeling.

The measurements results are shown in Fig. 4. For the concentration obtained, the normal Holtsmark ion field, $E_0 = 2.6031\, eN^{2/3}$, is higher than 50 kV/cm, which considerably exceeds the intensity of the microwave field at a given time moment (about 18 kV/cm at t = 0.4 μs in Fig. 3). In addition, at such values of electron concentration, the screening effect must be noticeable, which reduces the microwave field in the plasma. This arguments confirm that the procedure of ion-concentration determination is correct.

The concentration of free electrons in the plasma was evaluated from the broadening of the central component of the H_α line by electron impact. It turned out that this component can be isolated from the summary profile, since the side components of Stark structures are affected by the ion field similarly to the components

of H_β. For them, relationship (1) with the corresponding quantum numbers and wavelength is also applicable. The electron concentration estimated from the width of the central H_α component yields a value close to that of the ionic concentration (Fig. 4). Therefore, the electron and ion concentrations were considered to be identical. For discharge in methane, the electron concentration exceeds that for the discharge in hydrogen by approximately a factor of two. As is seen from Fig. 4, the concentration slightly drops with time, which might be related to the dynamics of the microwave-radiation absorption by the discharge, which is beyond the scope of this discussion.

During the initial 0.4 μs, when the broadening of lines by the microwave field prevails, the electron concentration was evaluated from the power W absorbed by the discharge, the measured propagation velocity, the field amplitude E, and the spatial parameters with the help of the relationship

$$W = \frac{1}{2}V\sigma E^2.$$

Here, V is the volume and σ is the plasma conductivity. The plasma conductivity was estimated for the frequency of the pulse loss, which was found from the electron mobility in methane and is approximately constant in a wide range of variation of the ratio $\frac{E}{N}$ ($\nu = 6.5 \times 10^{12}$ s^{-1}). The estimated value (curve *4* in Fig. 4) is approximately constant in time and is equal to $(1–2) \times 10^{15}$ cm^{-3}.

The time dependence of gas temperature for the discharge in methane was measured according to the rotational structure of the Swan-band spectrum ($V_{0–0}$ and $V_{1–1}$ transitions). The Swan-band spectra resolved in time were obtained by a method similar to that applied in measuring the H_α and H_β profiles. Then, we calculated the modeling spectrum, performed the convolution with the instrumental function of the monochromator, and compared the spectrum obtained with the experimental spectrum. The measurement results are shown in Fig. 4. In our experimental conditions, the rotational temperature of a C_2 molecule was identified with the gas temperature.

In conclusion, we briefly review the basic results of the diagnostic investigations which were presented above. The discharge time evolution can be described in the following way. The discharge development is characterized by two stages. The first is microwave-streamer development. The basic characteristics of the streamer head (i.e., of the ionization front) are a high electric-field intensity (100 kV/cm) and a high mean electron energy (8 eV). Under these conditions, the electron concentration can be as high as 10^{14} to 10^{15} cm^{-3}, which leads to screening of the microwave field. As a result, this field (along with the mean energy and the electron concentration) attains a steady-state

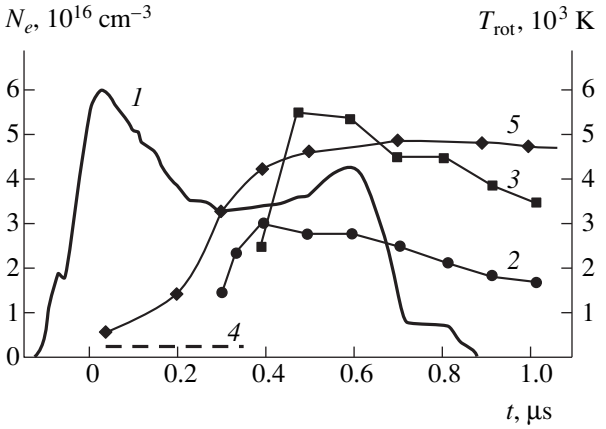

Fig. 4. Electron concentration N_e and rotational temperature T_{rot} as functions of time. (*1*) Microwave pulse; (*2*) N_e for the discharge in hydrogen; (*3*) N_e for discharge in methane; (*4*) N_e obtained from measurements of the absorbed power and field intensity; (*5*) T_{rot}.

value of 30 kV/cm in times (as is indicated by the numerical simulation of the ionization front) on the order of 1 ns. The electric-field intensity measured within the intervals of 50 to 250 ns in hydrogen and of 50 to 400 ns in methane (Fig. 3) characterizes the streamer column. The electron concentration in the streamer column is maintained at a level of ~10^{15} cm^{-3} (curve *4* in Fig. 4). Such a quasi-stationary state of the streamer-column parameters corresponds to streamer models of the discharge development [5]. Furthermore, as is seen from Fig. 4, in the streamer column, a rather rapid rise of the gas temperature is observed. Approximately simultaneously with attainment of a stationary gas temperature in methane at $t = 0.4$ μs, a sharp jump in the electron concentration (Fig. 3) is observed. This is apparently caused by gas expansion and an increase in the reduced field $\frac{E}{N}$, i.e., development of ionization-superheating instability. The concentration of 5×10^{16} cm^{-3} characterizing the stage of the developed instability is in good agreement with the results obtained by other authors in discharge channels for a prebreakdown field [10].

The high values of electron concentration and gas temperature in discharge channels testify to the high magnitude of the energy contribution. At the second stage of discharge, the estimated energy contribution obtained on the basis of diagnostic investigations attains approximately 3 eV per CH_4 molecule. This value is considerably higher than that of the microwave energy (0.4 eV per molecule) required for decomposition of a single methane molecule [1]. Thus, the assumption that the acceleration of the methane decomposition by chain ionic-molecular reactions must proceed not only in the plasma discharge channels but also in the weakly ionized peripheral regions of these chan-

nels necessarily follows. The problem associated with the formation of these ranges remains, to a large extent, open since the low electron concentration in them (presumably, 10^{11} to 10^{12} cm^{-3}) and weak luminosity strongly hamper direct measurements of plasma parameters. In [11], it was assumed that a weakly ionized periphery is formed owing to UV-radiation from strongly heated channels. It is also worth noting the possibility of the reaction proceeding both in the process of decomposition and the diffusive plasma expansion of the channel in itself.

REFERENCES

1. V. D. Rusanov, K. Étivan, A. I. Babaritskiĭ, *et al.*, Dokl. Akad. Nauk **354**, 213 (1997).
2. A. I. Babaritskiĭ, M. A. Deminskiĭ, S. A. Demkin, *et al.*, Khim. Vys. Énerg. **33**, 49 (1999).
3. A. I. Babaritskiĭ, I. E. Baranov, S. A. Demkin, *et al.*, Khim. Vys. Énerg. **33**, 458 (1999).
4. V. D. Rusanov, A. I. Babaritskiĭ, E. N. Gerasimov, *et al.*, Dokl. Akad. Nauk **366**, 323 (1999) [Dokl. Phys. **44**, 283 (1999)].
5. V. B. Gil'denburg, I. S. Gushchin, S. A. Dvinin, and A. V. Kim, Zh. Éksp. Teor. Fiz. **97**, 1151 (1990) [Sov. Phys. JETP **70**, 645 (1990)].
6. A. L. Vikharev, A. M. Gorbachev, O. A. Ivanov, and A. L. Kolysko, Zh. Éksp. Teor. Fiz. **106**, 172 (1994) [JETP **79**, 94 (1994)].
7. *Plasma Spectroscopy with Quasi-Monochromatic Electric Fields*, Ed. by E. A. Oks (Énergatomizdat, Moscow, 1990).
8. G. V. Sholin, A. V. Demura, and V. S. Lisitsa, Preprint IAÉ-2232 (Kurchatov Institute of Atomic Energy, Moscow, 1972).
9. I. I. Sobelman, *Atomic Spectra and Radiative Transitions* (Fizmatgiz, Moscow, 1963; Springer-Verlag, Berlin, 1979).
10. S. I. Gritsinin, A. A. Dorofeyuk, I. A. Kossyĭ, *et al.*, Teplofiz. Vys. Temp. **25**, 1068 (1987).
11. G. M. Batanov, S. I. Gritsinin, I. A. Kossyĭ, *et al.*, Tr. Fiz. Inst. Akad. Nauk SSSR **160**, 174 (1985).

Translated by Yu. Vishnyakov

Doklady Physics, Vol. 46, No. 4, 2001, pp. 247–250. Translated from Doklady Akademii Nauk, Vol. 377, No. 6, 2001, pp. 754–757.

PHYSICS

A Set of Phase-Equilibrium Equations in Covariant Form and Its Use for Developing a General Method of Calculation of Two-Phase Conodes in Multicomponent Systems

A. L. Udovskiĭ

Presented by Academician I.I. Novikov November 29, 2000

Received November 30, 2000

In the last 25–30 years, thermodynamic calculations of phase diagrams for both binary and multicomponent systems received wide application. The computer programs [1–7] developed in various research centers of the world are of wide use. The numerical methods involved in these programs can be divided into two classes. In studies of the first class [2], the Gibbs-energy minimum is sought for a heterogeneous system. In studies of the second class, the set of phase-equilibrium equations (establishing the equality of chemical potentials for the components of various phases) is solved [1, 3–7]. In this case, either the Newton–Raphson iterative method [1] or the Nelder–Mead modified simplex method is used to minimize the objective function representing the sum of residuals of the phase-equilibrium equations [7]. An essential constraint of the former methods is the impossibility of guaranteeing attainment of the global minimum of the Gibbs energy for a heterogeneous system. This means that the calculated phase diagram can be both stable and metastable. An essential disadvantage of the latter methods is the necessity of selecting a successful initial approximation for starting the iterative process, for which there is no assurance that the iterations will converge to the desired solution. Thus, the calculating methods of both the first and second class render it principally impossible to create autonomous computer programs for calculating phase diagrams and thermodynamic properties of multicomponent alloys of systems with three or more components.

Previously, we succeeded [8] in developing a general method of calculation and an autonomous computer program for calculating phase diagrams of binary systems which were not hampered by the above disadvantages. However, the problem of developing a general method of calculation of phase diagrams and thermodynamic properties for multiphase alloys of systems with three or more components is much more complicated.

The purpose of this study is to develop a reasonably general method for calculating two-phase equilibria in systems with three or more components.

FORMULATION OF THE PROBLEM

First, the number of unknown quantities in the set of equilibrium equations for two phases in the n-component system, which is written for constant temperature and pressure conditions, is equal to $2(n - 1)$ and exceeds the number n of set equations by $n - 2$. Thus, the set of equilibrium equations for two phases is parametric. Therefore, our first task is to perform unambiguous parameterization of the set of phase-equilibrium equations and, specifically, to obtain the principal possibility of unambiguous description of the two-phase equilibrium in an n-component system with a chosen set of parameters. Second, the problem involves searching for a stable conode, which should correspond to the two-phase stable equilibrium at the isothermal cross section of the phase diagram of an n-component system at a constant pressure.

SOLUTION TO THE PROBLEM

For solving the problem formulated, we use the vector approach [9]. The closed n-component systems involving components A_1–A_2–…–A_n are considered. A composition vector $\mathbf{x}$ is posed in correspondence to every point of a regular $(n - 1)$-dimensional simplex Δ_{n-1} of the compositions. We introduce the covariant basis $\{\mathbf{e}_1, \mathbf{e}_2, \ldots, \mathbf{e}_{n-1}\}$, each unit vector of which coincides with the ribs of the simplex Δ_{n-1} and is directed from the common simplex apex corresponding to component A_n to the simplex apices, which correspond to components $A_1, A_2, \ldots$, and A_{n-1}. In this case, the com-

Baĭkov Institute of Metallurgy, Russian Academy of Sciences, Leninskiĭ pr. 49, Moscow, 117334 Russia

1028-3358/01/4604-0247$21.00

position vector $\mathbf{x}$ in the covariant basis can be written as follows:

$$\mathbf{x} = \sum_{i=1}^{n-1} x^i \mathbf{e}_i, \quad 0 \le x^i \le 1,$$
$$x^n = 1 - \sum_{i=1}^{n-1} x^i, \quad \mathbf{e}_i\mathbf{e}_j = \begin{cases} 1, & i = j \\ 1/2, & i \ne j. \end{cases} \tag{1}$$

Here, x^i is the molar fraction of component A_i. It is evident that the molar Gibbs energy of a closed n-component system in the q-phase system, $G^{\alpha_1+\alpha_2+\ldots+\alpha_q}$, is related to the molar Gibbs energies of all the phases $G^{\alpha_1}, G^{\alpha_2}, \ldots, G^{\alpha_q}$ by the equation

$$G^{\alpha_1+\alpha_2+\ldots+\alpha_q}(\mathbf{x}, \mathbf{x}_1, \mathbf{x}_2, \ldots, \mathbf{x}_q, T, P) = \sum_{i=1}^{q} \alpha_i G^{\alpha_i}(x_i, T, P), \tag{2}$$

where α_i is the fraction of the ith phase, i.e., the ratio of the number of moles of atoms in the ith phase to the total number of moles of atoms, $1 \le i \le q$; and $\mathbf{x}_i$ is the composition vector for the ith phase. In a closed n-component system, the normalizing conditions are fulfilled:

$$\sum_{i=1}^{q} \alpha_i \mathbf{x}_i = \mathbf{x} = \text{const}, \quad \sum_{i=1}^{q} \alpha_i = 1. \tag{3}$$

The equilibrium of all q phases at a constant temperature T and a constant pressure P is attained provided that

$$dG^{\alpha_1+\alpha_2+\ldots+\alpha_q} = 0, \quad d^2G^{\alpha_1+\alpha_2+\ldots+\alpha_q} > 0. \tag{4}$$

Using Eqs. (2) and (3), we obtain from (4) the set of equilibrium equations in the vector form for all q phases on the condition that temperature and pressure are constant:

$$\text{grad}G^{\alpha_1}\big|_{\mathbf{x}_1} = \text{grad}G^{\alpha_2}\big|_{\mathbf{x}_2} = \ldots = \text{grad}G^{\alpha_q}\big|_{\mathbf{x}_q},$$
$$G^{\alpha_1}(\mathbf{x}_1) - \mathbf{x}_1\text{grad}G^{\alpha_1}\big|_{\mathbf{x}_1} = \ldots = G^{\alpha_q}(\mathbf{x}_q) - \mathbf{x}_q\text{grad}G^{\alpha_q}\big|_{\mathbf{x}_q}. \tag{5}$$

The vector form of equilibrium equations was originally obtained by Wilson [10] for two phases in the four-component system and by Udovskiĭ [11] for q phases in the n-component system. The vector form of the phase-equilibrium equations (5) is invariant relative to an arbitrary system of coordinates. Because the gradient of a scalar function G is a covector, Eqs. (5) in a generally covariant form and in an arbitrary covariant basis for the case of equilibrium of two phases, for example, for α and β phases in the n-component system, take the following form:

$$\left(\sum_{i=1}^{n-1} \frac{\partial G^\alpha}{\partial \gamma^i} g^{ij}\right)\Bigg|_{\mathbf{x}_\alpha} = \left(\sum_{i=1}^{n-1} \frac{\partial G^\beta}{\partial \gamma^i} g^{ij}\right)\Bigg|_{\mathbf{x}_\beta}, \quad j = 1, 2,$$
$$G^\alpha(\gamma_\alpha^1, \gamma_\alpha^2, \ldots, \gamma_\alpha^{n-1}) - \sum_{i=1}^{n-1}\left(\frac{\partial G^\alpha}{\partial \gamma^i}\Big|_{\mathbf{x}_\alpha} \gamma_\alpha^i\right)$$
$$= G^\beta(\gamma_\beta^1, \gamma_\beta^2, \ldots, \gamma_\beta^{n-1}) - \sum_{i=1}^{n-1}\left(\frac{\partial G^\beta}{\partial \gamma^i}\Big|_{\mathbf{x}_\beta} \gamma_\beta^i\right). \tag{6}$$

Here, $\mathbf{x}_\alpha = (\gamma_\alpha^1, \gamma_\alpha^2, \ldots, \gamma_\alpha^{n-1})$ and $\mathbf{x}_\beta = (\gamma_\beta^1, \gamma_\beta^2, \ldots, \gamma_\beta^{n-1})$ are the composition vectors for the equilibrium α and β phases, each having $n - 1$ contravariant curvilinear coordinates, that is, $(n - 1)$ components of the composition vector. The quantity g^{ij} in Eq. (6) is the contravariant metric tensor. The set of phase-equilibrium equations (6) are presented in an arbitrary covariant basis. In the particular case when the curvilinear set is orthogonal, the metric tensors, both covariant and contravariant, are diagonal:

$$g_{ij} = \begin{cases} g_{ii}, & i = j \\ 0, & i \ne j, \end{cases} \quad g^{ij} = \begin{cases} g^{ii}, & i = j \\ 0, & i \ne j. \end{cases}$$

In this case, the set of equations (6) for the equilibrium of two phases are as follows:

$$\left(\frac{\partial G^\alpha}{\partial y^i} g^{ii}\right)\Bigg|_{\mathbf{x}_\alpha} = \left(\frac{\partial G^\beta}{\partial y^i} g^{ii}\right)\Bigg|_{\mathbf{x}_\beta}, \quad i = 1, 2, \ldots, n-1,$$
$$G^\alpha(\gamma_\alpha^1, \gamma_\alpha^2, \ldots, \gamma_\alpha^{n-1}) - \sum_{i=1}^{n-1}\left(\frac{\partial G^\alpha}{\partial \gamma^i}\Big|_{\mathbf{x}_\alpha} \gamma_\alpha^i\right)$$
$$= G^\beta(\gamma_\beta^1, \gamma_\beta^2, \ldots, \gamma_\beta^{n-1}) - \sum_{i=1}^{n-1}\left(\frac{\partial G^\beta}{\partial \gamma^i}\Big|_{\mathbf{x}_\beta} \gamma_\beta^i\right). \tag{7}$$

For simplicity, we first consider the use of (7) for a three-component system. In the simplex of compositions, we introduce the polar system of coordinates whose pole with respect to the origin of coordinates arranged at a point where the third component is located is set by the vector $\mathbf{x}_0$. In this case, the composition vectors for equilibrium phases are written as

$$\mathbf{x}_\alpha = \mathbf{x}_0 + \mathbf{u}_\alpha, \quad \mathbf{x}_\beta = \mathbf{x}_0 + \mathbf{u}_\beta. \tag{8}$$

The family of poles of the polar system can be found in the curve of the intersection of the Gibbs molar energies for the α and β phases:

$$G^\alpha(\mathbf{x}_0) = G^\beta(\mathbf{x}_0). \tag{9}$$

We write the vector specifying the pole of the polar system of coordinates both in the covariant basis $(\mathbf{e}_1, \mathbf{e}_2)$,

through the oblique coordinates (x_0^1, x_0^2), and in the orthonormalized basis $(\mathbf{s}_1, \mathbf{s}_2)$ arranged with respect to the oblique basis $(\mathbf{e}_1, \mathbf{e}_2)$ so that the bisectrices of angles between the unit vectors of the corresponding bases coincide:

$$\mathbf{x}_0 = x_0^1\mathbf{e}_1 + x_0^2\mathbf{e}_2 = z_0^1\mathbf{s}_1 + z_0^2\mathbf{s}_2. \quad (10)$$

In this case, the polar coordinates of the composition vectors for the α and β phases completely specify the oblique coordinates of these vectors:

$$x_\alpha^i = u_1^i(r_\alpha\cos\varphi^\alpha + z_0^1) + u_2^i(r_\alpha\sin\varphi^\alpha + z_0^2),$$
$$x_\beta^i = u_1^i(-r_\beta\cos\varphi^\beta + z_0^1) + u_2^i(-r_\beta\sin\varphi^\beta + z_0^2); \quad i = 1, 2. \quad (11)$$

With allowance for (11), the dependence of the Gibbs molar energies for the α and β phases on composition is expressed through the polar coordinates and through the coordinates of the pole. In these coordinates, the physical components of the gradient from scalar function G take the form

$$\mathrm{grad}G = \frac{\partial G}{\partial r}\mathbf{r}_0 + \frac{1}{r}\frac{\partial G}{\partial\varphi}\boldsymbol{\varphi}_0, \quad (12)$$

where $\mathbf{r}_0$ and $\boldsymbol{\varphi}_0$ are the unit vectors of the basis of the polar system of coordinates. Let the pole (x_0^1, x_0^2) be inside the two-phase (α + β) region. In this case, with allowance for the fact that the vectors $\mathbf{r}^\alpha$ and $\mathbf{r}^\beta$ are antiparallel, set (7) in the polar system of coordinates becomes

$$\left.\frac{\partial G^\alpha}{\partial r}\right|_{(r_\alpha, \varphi^\alpha)} = -\left.\frac{\partial G^\beta}{\partial r}\right|_{(r_\beta, \varphi^\beta = \pi + \varphi^\alpha)},$$
$$\left.\frac{1}{r_\alpha}\frac{\partial G^\alpha}{\partial\varphi^\alpha}\right|_{(r_\alpha, \varphi^\alpha)} = -\left.\frac{1}{r_\beta}\frac{\partial G^\beta}{\partial\varphi^\beta}\right|_{(r_\beta, \varphi^\beta = \pi + \varphi^\alpha)}, \quad (13)$$
$$(r_\alpha + r_\beta)\left.\frac{\partial G^\alpha}{\partial r}\right|_{(r_\alpha, \varphi^\alpha)} = G^\alpha(r_\alpha, \varphi^\alpha) - G^\beta(r^\beta, \varphi^\beta = \pi + \varphi^\alpha).$$

It is worthwhile to divide the process of solving set (13) into three stages. At the first stage, from the equality of the Gibbs molar energies (9) for competitive phases, we find the curve that unambiguously parameterizes the two-phase conodes. In this curve, a pole for the polar system of coordinates is chosen. At the second stage, we fix a certain value of the angle $\varphi^\alpha = \varphi_i^\alpha$; then, the set of equations (13) describes the tentative conode, which depends parametrically on φ_i^α and represents the solution to set (14):

$$\left.\frac{\partial G^\alpha}{\partial r}\right|_{(r_\alpha(\varphi_i^\alpha))} = -\left.\frac{\partial G^\beta}{\partial r}\right|_{(r_\beta(\varphi_i^\beta = \pi + \varphi_i^\alpha))},$$
$$(r_\alpha(\varphi_i^\alpha) + r_\beta(\varphi_i^\beta))\left.\frac{\partial G^\alpha}{\partial r}\right|_{(r_\alpha(\varphi_i^\alpha))} \quad (14)$$
$$= G^\alpha(r_\alpha(\varphi_i^\alpha)) - G^\beta(r^\beta(\varphi_i^\beta = \pi + \varphi_i^\alpha)).$$

The set of equations (14) is solved using the generalizing Maxwell "rule of equal areas" in the coordinates $\frac{\partial\tilde{G}}{\partial r} - r$, where

$$\tilde{G}(r, \varphi_i^\alpha) = \begin{cases} G^\alpha(r, \varphi_i^\alpha), & r \le z^{\alpha\beta} \\ G^\beta(r, \varphi_i^\beta = \pi + \varphi_i^\alpha), & r \ge z^{\alpha\beta}; \end{cases} \quad (15)$$

and r is the modulus of the radius vector directed along the unit vector $\mathbf{r}_0$ at an angle φ_i^α to, e.g., the first unit vector of the covariant basis $\mathbf{e}_1$. Alternatively, one can use the condition of continuity of the radial component of the gradient for the Gibbs molar energy at the phase boundaries α/(α + β) and β/(α + β) of the phase diagram for a fixed value of the angle φ_i^α between the single-phase and heterophase regions:

$$\left.\frac{\partial G^\alpha}{\partial r}\right|_{r_{j+1}^\alpha(\varphi_i^\alpha)} = \frac{G^\alpha(r_j^\alpha(\varphi_i^\alpha)) - G^\beta(r_j^\beta(\varphi_i^\beta))}{r_j^\alpha(\varphi_i^\alpha) - r_j^\beta(\varphi_i^\beta)},$$
$$\left.\frac{\partial G^\beta}{\partial r}\right|_{r_{j+1}^\beta(\varphi_i^\beta)} = \frac{G^\alpha(r_j^\alpha(\varphi_i^\alpha)) - G^\beta(r_j^\beta(\varphi_i^\beta))}{r_j^\alpha(\varphi_i^\alpha) - r_j^\beta(\varphi_i^\beta)}. \quad (16)$$

Here, $r_j^\alpha(\varphi_i^\alpha)$, $r_j^\beta(\varphi_i^\beta)$ and $r_{j+1}^\alpha(\varphi_i^\alpha)$, $r_{j+1}^\beta(\varphi_i^\beta)$ are the modules of the radius vectors $\frac{\alpha}{\alpha+\beta}$ and $\frac{\beta}{\alpha+\beta}$ of the ends of the test two-phase conode calculated at the jth and $(j + 1)$th cycles, respectively, for the same fixed angle φ_i^α.

At the third stage, we compose an objective function which is equal to the sum of residuals squared of all three equations of set (13). This function is minimized using the values of the angular variable φ_i^α from a minimum to a maximum value of this angle in the domain of its admissible values. As a result, we find a stable two-phase conode in the family of tentative conodes for a fixed pole. Conducting the cycle over the family of points lying in the curve specified by equality (9), we obtain a family of stable two-phase conodes on the isothermal–isobaric cross section of the phase diagram for the three-component system.

In the general case, set (7) of phase-equilibrium equations is written in the hyperspherical system of coordinates which represents the generalization of the spherical system of coordinates (see, e.g., [12]). This set is divided into two subsets of equations. The first involves the equalities of the angular components of the gradients of the Gibbs molar energies for two phases

with respect to the vector of phase compositions calculated at the points of composition vectors for the equilibrium phases. The second subset is close to set (14) except that, instead of a single direction angle for the composition vector of the α phase, as was the case for the three-component system, $n-2$ angles appear for the composition vector of the α phase in the n-component system. Further, the entire procedure is also divided into three stages in searching for a two-phase conode in the isothermal-isobaric section of the phase diagram in the n-component system. At first, from (9), we seek the surface which localizes the family of single-phase and two-phase ends of conodes and represents the family of poles for the hyperspherical system of coordinates. Thereafter, all the space of independent variables (r^α, r^β, θ_1^α, θ_2^α, …, θ_{n-2}^α) is divided into two subspaces: the first is a two-dimensional subspace E_r^2 formed by the radial components of the composition vectors for both phases (r^α, r^β); the second is the $(n-2)$-dimensional subspace E_θ^{n-2} formed by the angular variables (θ_1^α, θ_2^α, …, θ_{n-2}^α). For every fixed pole of the hyperspherical system of coordinates in the space E_r^2 and for every fixed angle (θ_1^α, θ_2^α, …, θ_{n-2}^α), we solve the set of two equations using the generalized Maxwell equal-area rule in coordinates $\frac{\partial \tilde{G}}{\partial r} - r$ and seek the tentative conode. Finally, at the third stage, we compose an objective function equal to the sum of residuals squared of all n phase-equilibrium equations of set (7) written in the hyperspherical system of coordinates, which is minimized over all the values of angular variables (θ_1^α, θ_2^α, …, θ_{n-2}^α) in the domain of admissible values. As a result, we find a stable two-phase conode in the family of tentative conodes for a fixed pole in the n-component system.

ACKNOWLEDGMENTS

This work was supported by the President's Federal Target-Oriented Program "Integration," project nos. K0573 and A0075.

REFERENCES

1. L. Kaufman and H. Bernstein, *Computer Calculation of Phase Diagrams* (Academic, New York, 1970; Mir, Moscow, 1972).
2. J. F. Counsell, E. B. Less, and P. J. Spencer, Met. Sci. J. **5**, 210 (1971).
3. H. Gaye and C. H. P. Lupis, Metall. Trans. A **6**, 1049 (1975); **6**, 1057 (1975).
4. H. L. Lukas, E. Th. Henig, and B. Zimmerman, CALPHAD: Comput. Coupling Phase Diagrams Thermochem. **1** (3), 225 (1977).
5. H. L. Lukas, J. Weiss, and E. Th. Henig, CALPHAD: Comput. Coupling Phase Diagrams Thermochem. **6** (3), 229 (1982).
6. B. Sundman, B. Jansson, and J. O. Andersson, CALPHAD: Comput. Coupling Phase Diagrams Thermochem. **9** (2), 153 (1985).
7. L. Lin, P. Wollants, O. van der Biest, and L. Delaye, CALPHAD: Comput. Coupling Phase Diagrams Thermochem. **18** (1), 89 (1994).
8. A. L. Udovsky, V. N. Karpushkin, and E. A. Kozodaeva, CALPHAD: Comput. Coupling Phase Diagrams Thermochem. **19** (3), 245 (1995).
9. A. L. Udovskiĭ, in *Phase Diagrams in Material Science* (Naukova Dumka, Kiev, 1984), pp. 112–147.
10. A. J. C. Wilson, Proc. Cambridge Philos. Soc. **37**, 95 (1941).
11. A. L. Udovskiĭ, in *Mathematical Problems of Chemical Thermodynamics* (Nauka, Novosibirsk, 1985), pp. 132–142.
12. A. L. Udovskiĭ, A. M. Gaĭdukov, and O. S. Ivanov, Dokl. Akad. Nauk SSSR **231**, 671 (1976).

Translated by V. Bukhanov

Doklady Physics, Vol. 46, No. 4, 2001, pp. 251–253. Translated from Doklady Akademii Nauk, Vol. 377, No. 4, 2001, pp. 477–480.

MECHANICS

A Stationary Cylindrical Vortex in a Viscous Fluid

S. N. Aristov

Presented by Academician L.V. Ovsyannikov August 30, 2000

Received September 26, 2000

Localized vortex flows are widely distributed in nature and may easily arise under very diversified conditions. Their sizes range from whirlpools produced by vigorous stirring of tea to tornados and tropic cyclones. Though these vortices were studied for a long time, many features of their structure remain unanswered. In this study, an attempt is made to describe a stationary cylindrical vortex in a viscous fluid in the framework of a new class of exact solutions of Navier–Stokes equations.

FORMULATION OF THE PROBLEM

We consider a stationary axisymmetric flow of an incompressible fluid inside an infinite cylinder. Adherence conditions are given on the lateral boundary of the cylinder, and one of its cross sections is taken to be an impermeable partition. It is necessary to find the velocity and pressure on the assumption that the fluid is set in rotation far from the partition.

In the case of stationary and axisymmetric fluid motion, the Navier–Stokes equation can be written as follows [1]:

$$\begin{gathered} V_r\frac{\partial V_r}{\partial r}+V_z\frac{\partial V_r}{\partial z}-\frac{V_\varphi^2}{r}=-\frac{\partial P}{\partial r}+\nu\left(\frac{\partial}{\partial r}\frac{1}{r}\frac{\partial rV_r}{\partial r}+\frac{\partial^2 V_r}{\partial z^2}\right),\\ V_r\frac{\partial V_z}{\partial r}+V_z\frac{\partial V_z}{\partial z}=-\frac{\partial P}{\partial z}+\nu\left(\frac{1}{r}\frac{\partial}{\partial r}r\frac{\partial V_r}{\partial r}+\frac{\partial^2 V_z}{\partial z^2}\right),\\ V_r\frac{\partial V_\varphi}{\partial r}+V_z\frac{\partial V_\varphi}{\partial z}+\frac{V_rV_\varphi}{r}=\nu\left(\frac{\partial}{\partial r}\frac{1}{r}\frac{\partial rV_\varphi}{\partial r}+\frac{\partial^2 V_\varphi}{\partial z^2}\right),\\ \frac{1}{r}\frac{\partial rV_r}{\partial r}+\frac{\partial V_z}{\partial z}=0, \end{gathered} \tag{1}$$

where V_φ, V_z, and V_r are the velocity components in the cylindrical coordinate system, P is the pressure divided by the density, and ν is the viscosity factor.

We seek the solution of Eqs. (1) in the following form:

$$\begin{gathered} V_r=\frac{\nu}{r}U(x),\quad V_z=-\frac{2\nu z}{R^2}\frac{\partial U}{\partial x},\quad V_\varphi=\frac{\nu z}{Rr}\sqrt{2}V(x),\\ P=P_0+\frac{2\nu^2}{R^2}\left(B(x)-2\frac{z^2}{R^2}G(x)\right), \end{gathered} \tag{2}$$

where U, V, B, and G are the unknown functions of the dimensionless coordinate $x=\dfrac{r^2}{R^2}$, R is the radius of the cylinder, and P_0 is the external pressure. The impermeable partition is taken as the zero of the longitudinal coordinate.

Substituting (2) into Eqs. (1) and collecting the terms at identical powers of the longitudinal coordinate, we obtain the system of ordinary differential equations:

$$2(xU'')'=2G+UU''-U'U', \tag{3}$$

$$2xV''=UV'-VU', \tag{4}$$

$$4x^2G'=-V^2, \tag{5}$$

$$B=U'-\frac{U^2}{4x}, \tag{6}$$

where the prime denotes the derivative with respect to coordinate x. In view of (2), the incompressibility condition is automatically fulfilled and relationships (5) and (6) follow from the equation for the radial velocity component. Equation (5) defines the balance between the centrifugal force and part of the pressure gradient. According to (6) and (3), the pressure is determined in an explicit form after the velocity components have been found. Equations (3)–(5) form an isolated system describing the mutual influence of poloidal and azimuthal circulations. This makes it possible to assign such flows to self-induced vortices. To formulate the boundary conditions, we assume that adherence condi-

Institute of Mechanics of Continua, Ural Division, Russian Academy of Sciences, ul. Akademika Koroleva 1, Perm, 614061 Russia

tions are given on the lateral boundary and all hydrodynamical fields are regular in the center of the cylinder. This leads to the following conditions:

$$x = 0: U = V = 0, \quad U'' = G - \frac{U'U'}{2}, \qquad x = 1: U = U' = V = 0. \tag{7}$$

Thus, we have the following problem to be solved: To find the possible solutions of Eqs. (3)–(5) satisfying boundary conditions (7).

ANALYSIS OF THE PROBLEM

Before analyzing Eqs. (3)–(5), it is pertinent to begin with the study of an ideal fluid. It will suffice to drop the linear terms in Eqs. (3)–(6). This means that the inertial effects dominate the viscous effects. Entering (3) into (5) and performing several identical transformations, we obtain

$$2G = -UU'' + U'U',$$

$$B = -\frac{U^2}{4x},$$

$$UV' = VU',$$

$$\frac{V^2}{2x^2} = U^2\left(\frac{U''}{U}\right)'.$$

The last two equations have evident integrals that coincide with the linear variant of the Grad–Shafranov equations; namely,

$$V = \alpha U, \quad U'' = \left(\beta - \frac{\alpha^2}{2x}\right)U, \tag{8}$$

where α and β are arbitrary constants. The investigation of (8) demonstrates that it has no solutions satisfying conditions (7). However, there exist localized solutions decaying at infinity. One among them, for $\beta = \frac{\alpha^4}{16}$, is expressed via analytical functions:

$$U = Ax\exp\left(-\frac{\alpha^2 x}{4}\right), \quad G = \frac{U^2}{2x^2}, \quad B = -\frac{U^2}{4x}. \tag{9}$$

The characteristic property of this solution is that the pressure dependence on the distance to the axis of the cylindrical vortex is nonmonotonic. For other values of parameter β, the mentioned single-cellular regime gives way to the multicellular regime. It is significant that poloidal circulation can be directed arbitrarily in accordance with the reversibility of the Euler equations.

In the case of a viscous fluid, the solutions were found numerically by the Runge–Kutta method. All required derivatives at the axis of the cylinder were found using the system of equations (3)–(5). This led to the Cauchy problem with three arbitrary parameters that were derivatives with respect to velocity components $U'(0)$ and $V'(0)$ and pressure $G(0)$. Note that the equations were integrated to the point where the radial velocity was equal to zero. Further, the problem was solved again with the use of the following transformation, which did not change the form of the input equations:

$$x = \varepsilon^2 x, \quad V = \varepsilon^{-1}V, \quad G = \varepsilon^{-4}G, \quad B = \varepsilon^{-2}B, \quad U = U,$$

where ε is an arbitrary number and the notation of the variables is the same as before. In addition, this transformation restricts our consideration to analysis of a two-parameter problem. The results of solving this problem are shown in Figs. 1 and 2. It is possible to use, as the Reynolds number, either the average angular momentum in a certain cross section of the cylinder or

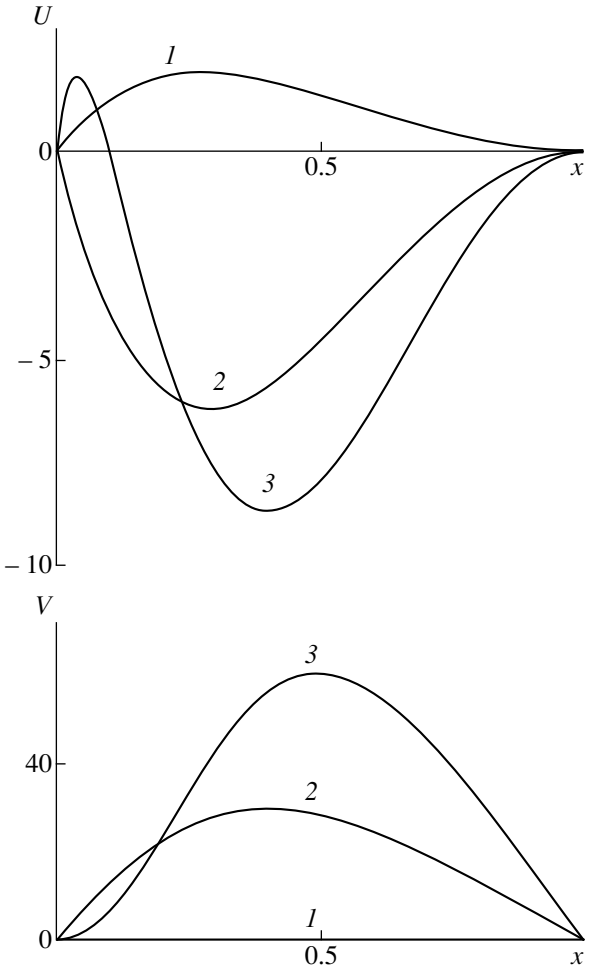

Fig. 1. Dependence of the velocity components on the dimensionless coordinate for three different regimes of the fluid flow.

the value of the vertical pressure gradient on its axis. In this case, figures on the curves correspond to the successive rise in the Reynolds numbers. To describe the results obtained, it is convenient to take the impermeable partition as the cup bottom and to discuss the flows in the range of positive values of the longitudinal coordinate.

The first type of solution is determined by the following parameters of the Cauchy problem: $U'(0) = 17.657$, $V'(0) = 0$, and $G(0) = 43.581$. In this case, the fluid does not rotate and its motion must be caused by a fluid flow directed along the axis to the cup bottom. The fluid on the axis flows in the direction of the pressure increase. The profiles of the pressure components and the radial velocity are marked on the curves by number *1*. This regime does not seem to be of great interest, and it was known before since in the absence of rotation, the problem in question coincides with the formulation of the problem on a flow in a porous pipe [2, 3].

In the second case (curves *2*; $U'(0) = -47.756$; $V'(0) = 136.719$, and $G(0) = 1342.790$), the fluid flow is directed upward from the cup bottom, i.e., in the opposite direction as compared with the nonrotating fluid. The azimuthal velocity near the axis depends almost linearly on the radial coordinate. The pressure on the axis decreases with distance from the cup bottom; conversely, near the edges, it, correspondingly, rises. Thus, near the axis and near the edges, the fluid moves in the direction of the pressure increase.

With a further increase in the rotation velocity, the solution exists for the following set of parameters: $U'(0) = 121.501$, $V'(0) = 22.089$, and $G(0) = 1891.179$. In this case, there is a central zone in the cylinder, where the fluid flows toward the partition, and an external range, where the flow is directed away from the wall of the cylinder to its axis (see curves *3*). The occurrence of a two-cellular poloidal circulation is a characteristic feature of powerful atmospheric vortices. In our case, such a flow is characterized by the maximal Reynolds number. Due to the insufficient accuracy of the method chosen, we failed to find any solutions with further increase of parameter $G(0)$.

CONCLUSION

Qualitatively, the solutions obtained adequately describe vortex flows produced in the process of stirring tea in a cup. It is known that the forced fluid rotation near the free surface of the cup bottom is responsible for a powerful vertical flow, owing to which tea-leaves move upward. The increase in the velocity rotation gives rise to the formation of a funnel at the center of the cup where the fluid sinks. This is also a characteristic feature of powerful atmospheric vortices. It is evident that the results presented here do not exhaust all possible problems that can be studied in the framework of the above new class of exact solutions.

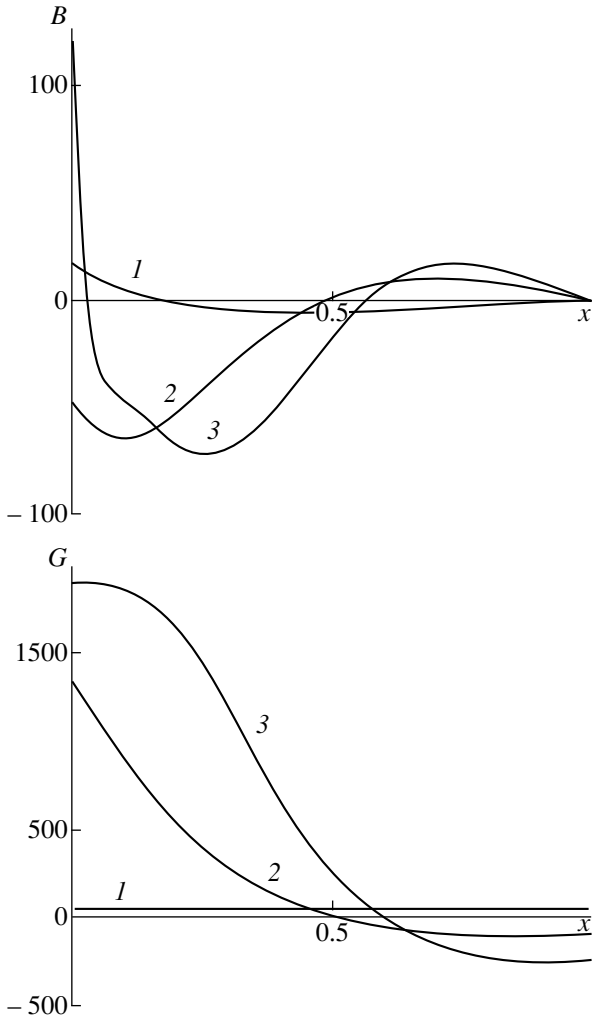

Fig. 2. Dependence of the pressure components on the dimensionless coordinate for three different regimes of the fluid motion.

ACKNOWLEDGMENT

This work was financially supported in part by the Russian Foundation for Basic Research.

REFERENCES

1. L. D. Landau and E. M. Lifshitz, *Course of Theoretical Physics*, Vol. 6: *Fluid Mechanics* (Nauka, Moscow, 1986; Pergamon, New York, 1987).
2. C. Y. Wang, Annu. Rev. Fluid Mech. **23**, 159 (1991).
3. M. A. Goldshtik, Annu. Rev. Fluid Mech. **22**, 441 (1990).

Translated by Yu. Vishnyakov

Doklady Physics, Vol. 46, No. 4, 2001, pp. 254–257. Translated from Doklady Akademii Nauk, Vol. 377, No. 4, 2001, pp. 481–484.

MECHANICS

Weak Discontinuities in Flows of a Heat-Conducting Inviscid Gas

S. P. Bautin

Presented by Academician G.G. Chernyĭ October 16, 2000

Received October 27, 2000

The set of gas-dynamic equations describing the flows in a heat-nonconducting inviscid compressible continuum are of the hyperbolic type, and there are possible gas flows with weak discontinuities of sonic or contact characteristics [1]. This property of the set of gas-dynamic equations makes it possible to solve complicated and important problems (see, e.g., [2]). The complete set of the Navier–Stokes equations [3] describing the flows of a heat-conducting viscous gas belongs to a mixed type. In flows of such a continuum, weak discontinuities are also possible on either the thermal-wave front [4] or the contact surface [5]. The investigation of flows in a heat-conducting inviscid gas (see, e.g., [6]) is of interest in connection with the problem of obtaining high energy densities [7].

In this study, we prove that, in flows of a heat-conducting inviscid gas, there are characteristic surfaces of three types and, consequently, weak discontinuities are possible on all of these surfaces.

First, there are two sound characteristics whose propagation velocities are independent of the thermal-conductivity coefficient and strictly lower than the sound velocity in a heat-nonconducting gas. Using the transport equation derived for these characteristics, we argue that in flows of a heat-conducting inviscid gas, the gradient-catastrophe phenomenon is possible. In the class of analytical functions, we prove the theorems on the existence and uniqueness of solutions to problems on a piston and on obtaining preassigned distributions in the flows of a heat-conducting inviscid gas. We also consider two mechanisms of perturbation transfer, namely, elastic interaction and the thermal conductivity process.

Second, the contact surface in unsteady flows is a second-type characteristic that has a multiplicity of two or one for three- or two-dimensional cases, respectively. We showed that, in the two-dimensional case, the transport equation for the characteristics of this type is a linear partial differential equation.

Ural State University of Railway Communication, ul. Kolmogorova 66, Yekaterinburg, 620034 Russia

Third, we also prove that, if the gas thermal-conductivity coefficient depends on temperature and has certain properties, then the given trajectory of motion of the heat-wave front and the given cold flow of gas unambiguously determine the heat compression wave propagating through this background and continuously joining it at the wave front.

A thermodynamically perfect gas is described by the equation of state

$$p = R\rho T, \quad e = c_{v0}T, \quad R, c_{v0} = \text{const} > 0. \qquad (1)$$

Here, p is pressure, ρ is density, T is temperature, and e is internal energy. To describe the flows of such a gas, we can take ρ, T, and, in particular, the sound velocity squared $c^2 = \left(\frac{\partial p}{\partial \rho}\right)\Big|_{S = \text{const}}$, as independent thermodynamic variables; the latter is determined by the relationship $c^2 = R\gamma T$, where S is the entropy and $\gamma = 1 + \frac{R}{c_{v0}} > 1$ is the gas adiabatic index. For the gas described by equations of state (1), we also consider the complete set of Navier–Stokes equations for a heat-conducting inviscid gas (i.e., we assume the coefficients of dynamic and volume viscosities to be zero):

$$\begin{aligned} &D\rho + \rho \operatorname{div}\mathbf{u} = 0, \\ &D\mathbf{u} + \frac{1}{\gamma}\left(\frac{T}{\rho}\nabla\rho + \nabla T\right) = \mathbf{0}, \\ &DT + (\gamma - 1)T\operatorname{div}\mathbf{u} = \frac{1}{\rho}(\kappa\Delta T + \nabla\kappa\cdot\nabla T). \end{aligned} \qquad (2)$$

Here, $D = \frac{\partial}{\partial t} + \mathbf{u}\cdot\nabla$, t is time, $\mathbf{u} = \{u, v, w\}$ is the vector of gas velocity, $\mathbf{0}$ is the zero vector, and $\kappa = \kappa(\rho, T)$ is the thermal-conductivity coefficient. In set (2), we introduce dimensionless variables, including the dimensionless sound velocity $c = \sqrt{T}$.

1028-3358/01/4604-0254$21.00

We now consider, in a conventional manner, the case when the surface C, determined by the functions $\varphi(t, x, y, z)$ as

$$C\colon \varphi(t, x, y, z) = 0, \quad \left(\frac{\partial\varphi}{\partial t}\right)^2 + (\nabla\varphi)^2 \neq 0,$$

is a characteristic surface of set (2). For this purpose, we make the corresponding change of variables for which the surface C under consideration becomes a new coordinate plane $\theta = 0$. In addition to the change of variables, we pass to a quasilinear set containing only the first-order derivatives. In the set of partial differential equations obtained in this way, the determinant of the matrix A_0, which is multiplied by the vector of the derivatives with their components normal to the plane $\theta = 0$, is factored:

$$\det A_0 = \frac{1}{\rho}(\nabla\varphi)^2\kappa(D\varphi)^2\left[(D\varphi)^2 - \frac{1}{\gamma}T(\nabla\varphi)^2\right].$$

Thus, the presence of characteristics in the flows of a heat-conducting inviscid gas is possible only if one of the following three factors is zero:

$$\kappa = 0, \quad D\varphi = 0, \quad (D\varphi)^2 - \frac{1}{\gamma}T(\nabla\varphi)^2 = 0.$$

The change from $\kappa = 0$ to $\kappa > 0$ leads to a heat wave propagating through the cold background. The second and third equalities determine, respectively, contact surface C^0 and two characteristics denoted below as $C_\kappa^\pm$ and also referred to as sonic characteristics. In this case, the propagation velocity

$$c_\kappa = \frac{1}{\sqrt{\gamma}}\sqrt{T} \tag{3}$$

(with respect to the flow under consideration) for such characteristics in a heat-conducting gas is independent of the thermal conductivity coefficient, i.e., independent of the heat-conduction properties of the gas. Since $c_\kappa = \frac{c}{\sqrt{\gamma}}$, the sound velocity in a heat-conducting gas is strictly lower than the sound velocity in a heat-nonconducting gas. It is this fact that seems to be responsible for the lagging of the compression-wave front in a heat-conducting gas with respect to that in a heat-nonconducting gas (this effect was found in calculations [8]).

In the case of one-dimensional flows, it is convenient to introduce the new variable $\theta = x - \psi(t)$; then, set (2) takes the form

$$\begin{aligned}
&\rho_t + (u - \psi')\rho_\theta + \rho u_\theta = 0,\\
&u_t + (u - \psi')u_\theta + \frac{1}{\gamma}\left(\frac{T}{\rho}\rho_\theta + T_\theta\right) = 0,\\
&T_t + (u - \psi')T_\theta + (\gamma - 1)Tu_\theta\\
&\quad = \frac{1}{\rho}(\kappa T_{\theta\theta} + \kappa_\rho\rho_\theta T_\theta + \kappa_T T_\theta^2).
\end{aligned} \tag{4}$$

For components of the derivatives which are normal to the characteristic under consideration, we accept the notation $f_k = \left.\frac{\partial^k f}{\partial\theta^k}\right|_{\theta = 0}$, $k = 0, 1, 2, \ldots$

Let one of the characteristics $C_\kappa^\pm$: $x = \psi(t)$, all the desired functions, and [by virtue of the form of set (4)] the heat flux on this characteristic be given by

$$\begin{aligned}
&\rho|_{\theta = 0} = \rho_0(t) > 0, \quad u|_{\theta = 0} = u_0(t),\\
&T|_{\theta = 0} = T_0(t) > 0, \quad T_\theta|_{\theta = 0} = T_1(t).
\end{aligned} \tag{5}$$

In this case,

$$\begin{aligned}
u_0 - \psi' &= \mp\sqrt{\frac{T_0}{\gamma}}, \quad \rho_1 = \pm\sqrt{\frac{\gamma}{T_0}}(\rho_0 u_1 + \rho_0'),\\
T_1 &= \mp\frac{\sqrt{\gamma T_0}\rho_0'}{\rho_0} - \gamma u_0',\\
T_2 &= \frac{\rho_0}{\kappa^0}\left[T_0' \mp \sqrt{\frac{T_0}{\gamma}}T_1 + (\gamma - 1)T_0 u_1\right]\\
&\quad - \frac{1}{\kappa^0}(\kappa_\rho^0\rho_1 T_1 + \kappa_T^0 T_1^2).
\end{aligned} \tag{6}$$

In this and subsequent formulas, the zero superscript in the thermal conductivity coefficient and in its partial derivatives with respect to ρ and T implies that these functions are considered for $\rho = \rho_0$ and $T = T_0$.

We differentiate the first two equations of set (4) with respect to θ, put θ equal to 0, and take into account relations (5) and (6). Then, their linear combination yields the transport equation for $u_1(t)$:

$$u_1' + u_1^2 + A(t)u_1 + B(t) = 0, \tag{7}$$

where the functions $A(t)$ and $B(t)$ are expressed through $f_0(t)$. They are not written out here owing to their awkwardness.

If constant values of the desired functions are given on the characteristic $C_\kappa^\pm$,

$$\begin{aligned}
\rho_0(t) = \rho_{00} = \text{const} > 0, \quad u_0(t) = 0,\\
T_0(t) = T_{00} = \text{const} > 0,
\end{aligned} \tag{8}$$

then, in transport equation (7), $A(t) = \alpha$ and $B(t) = 0$, where the constant $\alpha = \frac{(\gamma - 1)\rho_{00}T_{00}}{2\gamma\kappa^0}$ is positive. In this case, Eq. (7) has a particular solution in the form

$$u_1(t) = \frac{\alpha u_{10}}{(u_{10} + \alpha)e^{\alpha t} - u_{10}}, \quad u_1(0) = u_{10}.$$

For example, if $u_{10} < 0$ and $u_{10} + \alpha < 0$, the gradient catastrophe occurs at the moment $t_* = \frac{1}{\alpha}\ln\frac{u_{10}}{u_{10} + \alpha} > 0$.

The existence of certain flows in the neighborhood of the characteristics $C_\kappa^\pm$ is established with the help of the two following theorems.

Theorem 1. *Let initial conditions* (5) *satisfying equalities* (6) *be given on one of the characteristics* $C_\kappa^\pm$ *for the set of equations* (4)*, and let either the condition*

$$\rho(t, \theta)|_{t=0} = \rho^0(\theta), \quad \rho^0(\theta)|_{\theta=0} = \rho_0(t)|_{t=0} \qquad (9)$$

or the condition

$$u(t, \theta)|_{t=0} = u^0(\theta), \quad u^0(\theta)|_{\theta=0} = u_0(t)|_{t=0} \qquad (10)$$

also be given. In this case, there exist unique analytic solutions to both problem (4), (5), (9) *and problem* (4), (5), (10) *if all the initial data are analytical in a certain neighborhood of the point* ($t = 0$, $\theta = 0$).

This theorem formulates problems with initial values for either the density $\rho = \rho^0$ or the velocity $u = u^0$ of the gas, which are given at the moment $t = 0$ and continuously join the background flow through a weak discontinuity on $C_\kappa^\pm$.

Theorem 2. *Let initial conditions* (5) *satisfying equalities* (6) *be given on one of the characteristics* $C_\kappa^\pm$ *for the set of equations* (4)*, and let the condition*

$$\begin{gathered} u(t, \theta)|_{\theta = x_p(t) - \psi(t)} = x_p'(t), \\ x_p(0) = \psi(0), \quad u_0(0) = x_p'(0) \end{gathered} \qquad (11)$$

also be given. In this case, there exists a unique analytic solution to problem (4), (5), (11) *if all the initial data are analytical in a certain neighborhood of the point* ($t = 0$, $\theta = 0$).

Relationship (11) is the condition of zero flow through a piston moving along the trajectory $x = x_p(t)$. Therefore, relations (4), (5), and (11) describe the problem of a smooth motion of an impenetrable piston.

The proof of Theorems 1 and 2 consists in reducing the formulated problems to the Cauchy characteristic problem of the standard form [2].

Theorems 1 and 2 admit corresponding generalizations to the case of three-dimensional unsteady flows.

Let conditions (8) for a quiescent homogeneous heat-conducting gas and a sonic characteristic in this gas be given (for definiteness, C_κ^+ is assumed to move from the left to the right). This characteristic originates when an incompressible piston smoothly [$x_p''(0) > 0$] moves into the gas. Such a piston generates a compression wave with $u_x|_{C_\kappa^+} < 0$ and $\rho_x|_{C_\kappa^+} < 0$. However, it follows from (6) in this case that $T_2 < 0$ and, at small t, in the entire compression-wave region including the piston, the gas temperature is lower than that of the homogeneous background through which the characteristic C_κ^+ propagates. This implies that, simultaneously with gas compression, heat outflows from the gas through the piston. If the compressing piston is heat-insulating or the heat inflows through it to the gas, the inequality $T_x|_{C_\kappa^+} > 0$ is satisfied necessarily. However, by virtue of relationship (6), condition (8) is already not satisfied on such a characteristic C_κ^+ and the background flow ceases to be a homogeneous quiescent gas. The same conclusion also follows from general physical considerations. Indeed, the heat wave overtakes characteristic C_κ^+ moving with a finite velocity. It affects the gas parameters in front of it and, consequently, affects its propagation velocity. Along with this, the calculations of the compression wave in a heat-conducting gas show [8] that the weak-discontinuity front is nevertheless retained; this fact is confirmed by the presence of the $C_\kappa^\pm$ characteristics in heat-conducting gas flows.

The formulas and arguments presented above are particular mathematical confirmations of the general conclusion that the solutions to the set of equations (2) allow for both mechanisms of perturbation transfer, namely, that caused by elastic interactions and that induced by heat conduction. Each of these processes is characterized by its inherent rate (finite or infinite, respectively) of perturbation transfer.

Furthermore, in the case of $\frac{\partial}{\partial z} = w = 0$, we use the change of variables $\theta = x - \psi(t, y)$, $\xi = y$, and $\tau = t$ for the set of equations (2) in order to give the characteristic C^0: $x = \psi(t, y)$ in the form of $\theta = 0$. In this case, the transport equation, which is an equation for the derivative $v_1(\tau, \xi)$ normal to the surface C^0, is obtained from the corresponding linear combination of the second and third equations differentiated previously with respect to θ and considered for $\theta = 0$:

$$v_{1\tau} + v_0(\tau, \xi) v_{1\xi} + C(\tau, \xi) v_1 + D(\tau, \xi) = 0.$$

Here, the functions $C(\tau, \xi)$ and $D(\tau, \xi)$ are not written out owing to their awkwardness. The equation obtained is a linear transport equation, and the singularities of the solutions to this equation are known.

Finally, a weak discontinuity in flows of a heat-conducting inviscid gas can originate in the case of the passage from $\kappa = 0$ to $\kappa > 0$. For simplicity, we consider this problem only in the one-dimensional case.

Theorem 3. *Let the thermal-conductivity coefficient* $\kappa(\rho, T)$ *satisfy the conditions*

$$\begin{gathered} \kappa(\rho, T)|_{T=0} = 0, \quad \kappa_\rho(\rho, T)|_{T=0} = 0, \\ \kappa_T(\rho, T)|_{T=0} > 0. \end{gathered} \qquad (12)$$

Let set (4) *have the solution*

$$\rho = \rho_{00} = \text{const} > 0, \quad u \equiv 0, \quad T \equiv 0 \qquad (13)$$

and be referred to as a cold homogeneous background. If the given function $x = \psi(t)$ is such that

$$\psi'(0) \neq 0,$$

and if all the initial data for the problem under consideration are analytical in a certain neighborhood of the point $t = 0$ and $x = \psi(0)$, then, in addition to solution (13), *there exists one more analytical solution continuously joining it in the line $\theta = 0$, i.e., for $x = \psi(t)$.*

This second solution is constructed in the form of an infinite series:

$$f(t, \theta) = \sum_{k=0}^{\infty} f_k(t)\frac{\theta^k}{k!}, \tag{14}$$

where f can be ρ, u, or T, with

$$\rho_0 = \rho_{00}, \quad u_0 = 0, \quad T_0 = 0;$$
$$\rho_1 = \frac{\rho_{00}u_1}{\psi'}, \quad u_1 = \frac{T_1}{\gamma\psi'}, \quad T_1 = -\frac{\psi'\rho_{00}}{\kappa_T^0}. \tag{15}$$

For proof of the convergence of series (14) (as done in [4]), we construct a majorant problem with an analytical solution.

Solution (14) is a heat wave propagating through cold homogeneous background (13) and joining it continuously on a heat-wave front whose trajectory of motion is described by the function $x = \psi(t)$. From formulas (15), it follows that heat wave (14) is a compression wave. Indeed, the density and the gas velocity, as well as temperature, increase behind the wave front.

Theorem 3 admits a natural generalization to the case of a spatial heat wave propagating through an arbitrary cold flow which is the solution to the set of equations (2) with $T \equiv 0$. The heat wave also exists in the case of $\kappa = \kappa_0\sqrt{T}$, $\kappa_0 = \text{const} > 0$, when the last condition of (12) is not satisfied.

REFERENCES

1. G. G. Chernyĭ, *Gas Dynamics* (Nauka, Moscow, 1988).
2. S. P. Bautin, *Mathematical Theory of Shock-Free Strong Compression of Ideal Gas* (Nauka, Novosibirsk, 1997).
3. V. M. Kovenya and N. N. Yanenko, *Splitting Method in Problems of Gas Dynamics* (Nauka, Novosibirsk, 1983).
4. S. P. Bautin, Dinamika Sploshnoĭ Sredy **83**, 11 (1987).
5. S. P. Bautin, Prikl. Mat. Mekh. **51**, 574 (1987).
6. E. I. Zababakhin and V. A. Simonenko, Prikl. Mat. Mekh. **29**, 334 (1965).
7. E. I. Zababakhin and I. E. Zababakhin, *Phenomena of Unbounded Cumulation* (Nauka, Moscow, 1988).
8. M. G. Anuchin, Prikl. Mekh. Tekh. Fiz. **39** (4), 25 (1998).

Translated by V. Bukhanov

Doklady Physics, Vol. 46, No. 4, 2001, pp. 258–260. Translated from Doklady Akademii Nauk, Vol. 377, No. 4, 2001, pp. 485–487.

MECHANICS

On the Uniform Stability of an Equilibrium State for a Differential Equation Depending on a Multidimensional Parameter

O. V. Druzhinina and A. A. Shestakov

Presented by Academician V.V. Rumyantsev September 5, 2000

Received September 15, 2000

In this paper, we prove a theorem on the uniform stability with respect to a multidimensional parameter for an equilibrium state of the nonlinear time-independent differential equation

$$\dot{x} = g(x, h), \quad x \in R^n, \quad h \in H \subset R^k, \tag{1}$$

which is defined on the set $B(r) \times H$, where $B(r) = \{x \in R^n: |x| \le r\}$ with $r > 0$. We assume that

$$g(0, h) = 0 \quad \forall h \in H. \tag{2}$$

The problem on the uniform stability of an equilibrium state with respect to a multidimensional parameter is of both theoretical and applied importance [1]. It is closely related to the problem of studying the stability of the equilibrium state $x = 0$ for Eq. (1) under permanently acting perturbations [2–4]. Indeed, for a fixed $h = h_0$, differential equation (1), rewritten in the form

$$\dot{x} = g(x, h^0) + [g(x, h) - g(x, h^0)]$$

can be considered a perturbed equation with respect to the differential equation

$$\dot{x} = g(x, h^0). \tag{3}$$

It is known [3, 5] that the stability of the equilibrium state $x = 0$ for Eq. (1) under permanently acting perturbations follows from the asymptotic stability of the equilibrium state for Eq. (3). The concept of stability under permanently acting perturbations of the form $R(x, h) ::= g(x, h) - g(x, h^0)$ was introduced in [6]. This concept is rather useful for studying the stability of conservative mechanical systems under permanently acting perturbations of a given class.

Moscow State Open University of Railway Communication, ul. Obraztsova 15, Moscow, 103055 Russia

We assume that the function $g(x, h)$ satisfies the Lipschitz condition with respect to $x = (x_1, x_2, \ldots, x_n)$ for each $h \in H \subset R^k$; i.e.,

$$\exists L = L(h) > 0: \left|g(x^1, h) - g(x^2, h)\right| \le L\left|x^1 - x^2\right| \quad \forall x^1, x^2 \in B(r).$$

Moreover, we assume that the solutions $x(t, x_0, h)$ to Eq. (1), with $x(0, x_0, h) = x_0$, continuously depend on both the initial point x_0 and the parameter $h = (h_1, h_2, \ldots, h_k)$, with $k \ge 1$.

The solution $x = 0$ to Eq. (1) is referred to as uniformly stable with respect to the set $H \subset R^k$ if

$$\forall \varepsilon > 0 \quad \exists \delta = \delta(\varepsilon) \quad |x_0| < \delta \Rightarrow |x(t, x_0, h)| < \varepsilon \quad \forall t \in R^+, \quad \forall h \in H. \tag{4}$$

In (4), the number δ depends on ε but is independent of the choice of point $h \in H$.

We consider an example of an equation that depends on a parameter belonging to a noncompact set.

Example 1. Let $H = (0, 1]$. We introduce the notation $r^2 = x_1^2 + x_2^2$ and $\theta = \arctan\left(\frac{x_2}{x_1}\right)$ and consider the set of equations

$$\dot{r} = r^2(r - h), \quad \dot{\theta} = 1, \quad h \in H. \tag{5}$$

Then, for each point $h \in H$, the solutions to Eq. (5) which originate at the points of the set $\{r: r < h\}$ tend to zero as $t \longrightarrow +\infty$, while the solutions originating at the points of the set $\{r: r > h\}$ are unbounded as $t \longrightarrow +\infty$. The set $\{r: r = h\}$ is invariant with respect to (5). For any $\delta > 0$, there are unbounded solutions for $h < \delta$ belonging to the set $\{r: r < h\}$. Hence, the solution $x_1 = x_2 = 0$ to Eq. (5) is not uniformly stable with respect to the noncompact set $H = (0, 1]$.

1028-3358/01/4604-0258$21.00 © 2001 MAIK “Nauka/Interperiodica”

We now consider an example of the set of equations when the trivial solution is stable but not uniformly stable with respect to the compact set $H = [0, 1]$.

Example 2. Let $H = [0, 1]$ and $h \in H$. We consider the following set of equations:

$$\begin{aligned} \dot{r} &= 0, \text{ if } r \in [0, h]; \\ \dot{r} &= hr^5(r^2 - h^2), \text{ if } r \in (h, +\infty]; \\ \dot{\theta} &= 0. \end{aligned} \tag{6}$$

Here, r and θ are defined in the foregoing example.

For an arbitrary given number $\varepsilon > 0$ and each point $h \in [0, 1]$, a solution belonging to the set $\{r: r < \min(h, \varepsilon)\}$ will belong furthermore to the set $\{r: r < \varepsilon\}$ for all $t \in R^+$. For $h = 0$, any solution satisfying the inequality $r < \varepsilon$ should belong furthermore to the set $\{r: r < \varepsilon\}$ for all $t \in R^+$.

Therefore, for each $h \in H$, the solution $x_1 = x_2 = 0$ to set (6) is stable but not uniformly stable (in h) with respect to the set H.

The following theorem is valid.

Theorem. *Let the above conditions for differential equation* (1) *be valid. If the trivial solution $x = 0$ to Eq.* (1) *is asymptotically stable for each h belonging to the compact set H of the space R^k, then the trivial solution $x = 0$* to Eq. (1) is *uniformly stable with respect to the set H.*

Proof. By virtue of the inversion found in [7] for the Lyapunov theorem on the asymptotic stability, for each point $h \in H$, there exists a scalar Lyapunov function $V(h, x)$ defined for $0 \le |x| \le \sigma(h)$ (where σ is a number depending on h) and having the following properties:

(1) the function $V(h, x)$ and its partial derivative $V_x(h, x)$ are continuous in the sphere $B(\sigma(h))$ of radius $\sigma(h) > 0$;

(2) $V(h, 0) = 0$ and $V(h, x) > 0$ for $0 < |x| \le \sigma(h)$;

(3) $(V_x(h, x), g(x, h)) < 0$ for $0 < |x| \le \sigma(h)$.

For each point $h_0 \in H$, there exists an open set $N(h_0) \subset B(\sigma(h_0)) \times H$ containing $(B(\sigma(h_0)) - \{0\}) \times \{h_0\}$ such that

$$(V_x(h_0, x), g(x, h)) < 0, \quad (x, h) \in N(h_0).$$

Let a number $\varepsilon > 0$ be given. We choose a number $a > 0$ such that

$$Q_a ::= \{x \in B(\sigma(h_0)): V(h_0, x) \le a\} \subset \operatorname{int} B(\varepsilon).$$

We introduce the notation

$$P_a ::= \{x \in Q_a: V(h_0, x) = a\}$$

and

$$H_{h_0} ::= \{h \in H: P_a \times \{h\} \subset N(h_0)\}.$$

Since $h_0 \in H_{h_0}$ and the set $N(h_0)$ is open, we have

$$\exists \lambda = \lambda(h_0): |h - h_0| \le \lambda(h_0) \Rightarrow h \in H.$$

We now prove that there exists a number $\delta = \delta(\varepsilon, h_0) > 0$ such that

$$|x_0| < \delta \Rightarrow |x(t, x_0, h)| < \varepsilon \quad \forall t \in R^+, \quad |h - h_0| \le \lambda(h_0).$$

Indeed, we choose a number $\delta(\varepsilon, h_0)$ such that $|x| < \delta \Rightarrow V(h_0, x) < a$. If the inequalities

$$|p - h_0| \le \lambda(h_0), \quad |y| < \delta(\varepsilon, h_0)$$

are satisfied for certain points $p \in R^k$ and $y \in R^n$, then, for a certain $\tau > 0$, the equality $|x(\tau, y, p)| = \varepsilon$ is valid. It follows from the inequalities

$$V(h_0, y) < a < V(h_0, x(\tau, y, p))$$

that $\mu \in (0, \tau)$, where

$$\mu ::= \sup\{t < \tau: V(h_0, x(t, y, p)) = a\}.$$

Moreover, we have

$$V(h_0, x(\mu + \eta, y, p)) > a \quad \forall \eta \in (0, \tau - \mu).$$

There exists a number $\eta_0 \in (0, \tau - \mu)$ such that

$$(x(\tau, y, p), p) \in N(h_0) \quad \forall t \in [\mu, \mu + \eta_0].$$

Hence, the inequalities

$$\begin{aligned} a < V(h_0, x(\mu + \eta_0, y, p)) &= V(h_0, x(\mu, y, p)) \\ &+ \int_{\mu}^{\mu + \eta_0} (V_x(h_0, x(t, y, p)), q(x(t, y, p)))d\tau \\ &< V(h_0, x(\mu + \eta, y, p)) = a \end{aligned}$$

are valid. Therefore, the assumption on the existence of the point $(y, p) \in R^n \times R^k$ leads to a contradiction.

By virtue of the compactness of the set H, we can isolate a finite subcovering from the open covering of this set:

$$\bigcup_{h \in H} \left\{ q \in H: |q - h| < \frac{1}{2}\lambda(h) \right\}.$$

Let the points $h^1, h^2, \ldots, h^m$ belonging to the space R^k be such that

$$H \subset \bigcup_{i=1}^{m} \left\{ q \in H: |q - h^i| < \frac{1}{2}\lambda(h^i) \right\}.$$

For given $h \in H$ and $|x_0| < \delta(\varepsilon)$ [where $\delta(\varepsilon) ::= \min\{\delta(\varepsilon, h^1), \ldots, \delta(\varepsilon, h^m)\}$], there exist h^j, $1 \le j \le m$

such that $|h - h^j| < \frac{1}{2}\lambda(h^j)$. Since $|x_0| < \delta(\varepsilon) \le \delta(\varepsilon, h^j)$, we conclude that $|x(t, x_0, h)| < \varepsilon\ \forall h \in H, \forall t \in R^+$. Thus, the theorem is proven.

ACKNOWLEDGMENTS

We are grateful to Academician V.V. Rumyantsev for his valuable remarks and attention to this work.

REFERENCES

1. A. N. Tikhonov, Mat. Sb. **31**, 575 (1952).
2. G. N. Duboshin, Tr. Gos. Astron. Inst., Mosk. Gos. Univ. **14** (1) (1940).
3. I. G. Malkin, Prikl. Mat. Mekh. **8**, 241 (1944).
4. P. A. Kuz'min, Prikl. Mat. Mekh. **21**, 129 (1957).
5. L. Salvadori and A. Schiaffino, Nonlinear Anal. **1** (3) (1977).
6. L. Salvadori and F. Visentin, Nonlinear Anal. **40**, 549 (2000).
7. J. L. Massera, Ann. Math. **50**, 705 (1949).

Translated by V. Chechin

Doklady Physics, Vol. 46, No. 4, 2001, pp. 261–263. Translated from Doklady Akademii Nauk, Vol. 377, No. 5, 2001, pp. 618–620.

MECHANICS

Motion of the Earth's Poles under the Action of Gravitational Tides in the Deformable-Earth Model

L. D. Akulenko*, Yu. G. Markov, and L. V. Rykhlova*****

Presented by Academician A.A. Boyarchuk October 12, 2000

Received October 17, 2000

High-precision methods of observation for trajectories of Earth-pole motion testify to the rather complicated dynamic processes occurring in the Earth–Moon–Sun system [1, 2]. Development of an adequate mathematical model that makes it possible to describe the actual trajectories of the Earth-rotation axis (i.e., the instantaneous position of the angular-velocity vector) in a certain convenient coordinate system bound to the Earth seems to be extremely important in both astrometric and geophysical aspects. Based on mathematical modeling, the investigation of the evolution of the Earth's rotation and the translational-rotational motion of the Earth–Moon system can turn out to be quite interesting and useful [2–4]. Attempts to allow only for the perturbing hydrometeorological processes proceeding, particularly, in the Southern hemisphere in order to explain the phenomena correlated with the motion of poles are insufficiently convincing. These attempts are of a qualitative nature and correspond only to estimates of different-scale oscillation periods.

To describe the rotational motion of the deformable Earth and the mutations of its poles, we can use a mechanical model of a viscoelastic solid, which is based on rigorous theorems of mechanics and perturbation methods, i.e., methods of singular expansions and averaging [5]. The two-layer model of the Earth is used which corresponds to a continuous solid nucleus and a viscoelastic mantle [2]. The deformation process is assumed to occur quasistatically. The motion is considered to proceed with respect to the center of mass of the three-axis Earth with "frozen" principal central moments of inertia $\tilde{A}$, $\tilde{B}$, and $\tilde{C}$. At each time moment, this motion corresponds to instantaneous rotation about a certain axis under the action of perturbing gyroscope, gravitational, and tidal moments of force. The vector of the motion is inclined at variable angles to both the axis of the Earth figure and the vector of the kinetic moment. The problem of the dynamics and analysis of a possibility of approaching the axis of the Earth's maximum moment of inertia and the vector of the kinetic moment are of considerable importance for the investigation of steady-state motions. (Here, an analogy with a free solid having interior dissipative elements takes place [5].) It is of interest to clarify the mechanisms of external action that hamper this approach and lead to steady-state vibrations within time intervals on the order of 10^3T, where T = 433 to 441 sidereal days is the period of the Chandler wobble.

Below, for the system of "the binary Earth–Moon planet" in the attraction field of the Sun, we use the model of a viscoelastic solid. Based on both asymptotic methods of nonlinear mechanics and mathematical modeling equations of motion in terms of action-angle variables, we propose, for the first time, a qualitative analysis and quantitative estimates of the relevant complicated dynamic process. As a result, we can describe the mutual position of the instantaneous Earth-rotation axis, figure axis, and its kinetic-moment vector. The possibility of determining the system parameters and the consistency of the analytic model with the actual trajectory measurements for the motion of the Earth's poles are studied.

1. The setting of the dynamical problem under consideration is based on the spatial variant of the system composed of the deformable Earth and the Moon in the attracting central field of the Sun. The Moon and the Sun are considered to be gravitating mass points. In the initial theoretical model, the Earth–Moon system is assumed to be an "almost binary planet". This presupposes the existence of a barycenter and the necessity of allowing for its position in further calculations. The mutual orbital motion of the Earth's and Moon's centers of mass with respect to the barycenter is given in canonical Delone variables.

The most adequate generalized coordinates for describing the proper rotation of the Earth about its center of mass are the action-angle canonical variables (I_i, w_i, i = 1, 2, 3). The qualitative theory of dissipative

* *Institute of Problems in Mechanics, Russian Academy of Sciences, pr. Vernadskogo 101-1, Moscow, 117526 Russia*

** *Moscow Institute of Aviation (Technical University), Volokolamskoe sh. 4, Moscow, 125080 Russia*

*** *Institute of Astronomy, Russian Academy of Sciences, ul. Pyatnitskaya 48, Moscow, 109017 Russia*

1028-3358/01/4604-0261$21.00

systems is used as a basis for the dynamic model and for identification of its parameters, which correspond to the regime of the Chandler wobble of the Earth's pole at frequency $\dot{w}_1 = n_{w_1}$. The evolution of the mutation of the Earth's poles is studied on the basis of allowance for gravitational tides caused by the actions of the Moon and the Sun.

We introduce the perturbed Routh functional

$$R = R_0(I_1, I_2) + \varepsilon R_1(\{I\}, \{w\}, [\mathbf{u}], [\dot{\mathbf{u}}]) + \varepsilon^2 \ldots, \quad (1)$$

where $\varepsilon > 0$ is the dimensionless parameter, εR_1 is the perturbing functional caused by gravitational tides, I_2 is the modulus of the Earth's kinetic moment, I_1 is the projection of the kinetic moment on the figure axis, and $\mathbf{u}$ is the displacement vector for the elastic medium (mantle). The functional R_0 describes the intermediate trajectory for the Earth's rotation about the center of mass in the case of Euler–Poinsot-type motion:

$$R_0 = \frac{I_2^2}{2\tilde{A}}\left(1 - \frac{\tilde{C} - \tilde{A}}{\tilde{C}}\frac{\kappa^2}{\kappa^2 + \lambda^2}\right), \quad \tilde{C} > \tilde{B} > \tilde{A},$$
$$\kappa^2 = \frac{\tilde{C}(\tilde{A} - \tilde{B})}{\tilde{A}(\tilde{B} - \tilde{C})}, \quad \lambda^2 = \kappa^2\frac{2h\tilde{C} - I_2^2}{I_2^2 - 2h\tilde{A}}. \quad (2)$$

Here, κ^2 and λ^2 are the basic dynamic parameters: for the Earth, $0 < \lambda^2 < 1$; h is a constant corresponding to the integral of the intermediate-motion energy. The quantities $\tilde{A}$, $\tilde{B}$, and $\tilde{C}$, as was mentioned above, determine the principal central moments of inertia for the deformable Earth under the action of centrifugal forces caused by its proper motion and the Moon's gravitational field. All parameters introduced in (1) are known or must be evaluated using experimental data. The structure of the perturbing functional εR_1 is subjected to further analysis and simplification on the basis of the averaging method.

Numerical estimations show that the angle (phase) w_2 is a relatively rapid variable. The frequency $\dot{w}_2 = n_{w_2} = 7.29 \times 10^{-5}\ \mathrm{s}^{-1} \approx 10^{-4}\ \mathrm{s}^{-1}$ corresponds to the diurnal rotation of the Earth. The w_1 phase corresponds to the motion of the pole with period T of the Chandler wobble, $\dot{w}_1 = n_{w_1} = 1.7 \times 10^{-7}\ \mathrm{s}^{-1}$. Furthermore, this phase is considered a "semislow" variable, and averaging over this variable is not performed. In other words, partial averaging takes place (i.e., averaging over the rapid w_2 phase). The employment of averaged equations of motion leads to a relative error of 10^{-3} to 10^{-4} within the time interval $(10^3$–$10^4)T$, i.e., on the order of the Earth-axis precession period.

2. The qualitative analysis and numerical experiment for the model problem is performed on the basis of evolutionary (averaged over w_2) equations of the form

$$\dot{I}_1 = -\varepsilon\frac{\partial\langle R_1\rangle}{\partial w_1}, \quad \dot{w}_1 = n_{w_1} + \varepsilon\frac{\partial\langle R_1\rangle}{\partial I_1}, \quad n_{w_1} = \frac{\partial R_0}{\partial I_1},$$
$$\dot{\delta}_2 = +\varepsilon\frac{\partial\langle R_1\rangle}{\partial w_1}\frac{1}{I_2\sin\delta_2}\frac{1 + \kappa^2\mathrm{sn}^2 u}{\sqrt{1 + \kappa^2}\,\mathrm{dn}\,u}, \quad (3)$$
$$u = \frac{2\mathbf{K}(\lambda)}{\pi}w_1, \quad t \geq t_0.$$

Here, the angular brackets $\langle\ldots\rangle$ imply averaging over w_2, δ_2 is the angle between the axis of the Earth's figure and the kinetic-moment vector, the quantity δ_2 is $\delta_2 \simeq 0.''2 \simeq 10^{-6}$ rad, and n_{w_1} is the frequency of the Chandler wobble of the Earth's pole in the intermediate motion. Since the modulus λ is rather small, $\lambda \simeq 10^{-7}$, then $\mathbf{K}(\lambda) = \frac{\pi}{2} + O(10^{-14})$, and for the intervals of phase variation under consideration, $w_1 \simeq 10^4$–10^5, we can obtain $u \simeq w_1$, $\mathrm{sn}\,u \simeq \sin w_1$, and $\mathrm{dn}\,u \simeq 1$. It is worth noting that the averaged functional $\langle R_1\rangle$ depends on the parameters κ^2 and λ^2, the "semislow" w_1 phase, and the orbit parameters. The variables I_1 and δ_2 entering into (3) are related to slow variables.

Along with Eqs. (3), which were considered in absolute time t, for the qualitative and quantitative analysis of the pole trajectories, these equations should be analyzed on the manifold with argument w_1, i.e., the phase characterizing the mutations of the pole:

$$\frac{dI_1}{dw_1} = \frac{\dot{I}_1}{\dot{w}_1}, \quad \frac{d\delta_2}{dw_1} = \frac{\dot{\delta}_2}{\dot{w}_1}, \quad \dot{w}_1 \neq 0. \quad (4)$$

Qualitative analysis of systems of equations (3) and (4) shows that the right-hand sides of the equations for I_1 have zero average values over w_1. This property leads to a weak evolution (without secular variation) of the I_1 variable that contains a periodic component with frequency n_{w_1}, which is caused by the tidal moments of force. The variable w_1 changes with time almost linearly, so that this change is superimposed by similar periodic modulations. As follows from Eqs. (3) and (4), the character of this change for the variable δ_2 is essentially different. The secular variation of the quantity δ_2 may occur due to the existence of the function $\kappa^2\sin^2 w_1$: $\delta_2^2 - \delta_{20}^2 \simeq \varepsilon d(t - t_0)$, where d = const is determined by the resonance action of the tidal moments of force with the Chandler-wobble period.

The pole mutation is determined as the angular motion of the rotation axis with respect to the figure axis; the components of this motion are

$$x_p = \frac{\omega_x}{\omega} = \frac{\lambda I_2}{\tilde{A}\omega\sqrt{\kappa^2 + \lambda^2}}\mathrm{cn}u,$$

$$y_p = -\frac{\omega_y}{\omega} = -\frac{\lambda I_2\sqrt{1+\kappa^2}}{\tilde{B}\omega\sqrt{\kappa^2 + \lambda^2}}\mathrm{sn}u, \qquad (5)$$

$$\omega = \frac{I_2}{\tilde{A}\sqrt{\kappa^2 + \lambda^2}}\left[\lambda^2\mathrm{cn}^2u + \frac{\tilde{A}^2}{\tilde{C}^2}\kappa^2(1-\lambda^2\mathrm{sn}^2u)\right]^{1/2}.$$

In accordance with the generally accepted agreement, the angular coordinate y_p in (5) is directed along the 90° meridian of the western longitude [6]. Since $\lambda^2\kappa^{-2} \simeq 10^{-12}$, expressions (5) make it possible to establish the approximate shape of the virtually closed elliptical figure circumscribed by the axis of the instantaneous angular velocity of the rotation in the tangent plane:

$$X_p^2 D_x^{-2} + Y_p^2 D_y^{-2} = 1, \quad \frac{D_y}{D_x} = \frac{\tilde{A}}{\tilde{B}}\sqrt{1+\kappa^2} > 1,$$

$$D_x = R_\mathrm{E}\frac{\tilde{C}}{\tilde{A}}\frac{\lambda}{\kappa}, \quad D_y = R_\mathrm{E}\frac{\tilde{C}}{\tilde{B}}\frac{\lambda}{\kappa}\sqrt{1+\kappa^2}, \qquad (6)$$

$$X_p = D_x\cos w_1, \quad Y_p = -D_y\sin w_1.$$

Here, R_E is the Earth's radius and D_x and D_y are the ellipse semiaxes. We can find from (6) that the ellipse semiaxes weakly change with the variation of λ that has a small periodic component with frequency n_{w_1} caused by variations of I_1 (4). We note that the ratio of the ellipse semiaxes is virtually constant and close to unity; the ellipse is slightly extended along the *Y*-axis. Furthermore, as follows from (6), $D_{x,y} \simeq 7.7$ m; i.e., the ellipse linear size is 15.4 m. Data of pole-trajectory measurements made in the middle of the 1990s yielded trajectories of the elliptic-spiral type and magnitudes of the semiaxes close to 0.″45–0.″5, which is equivalent to a linear size $L \simeq 14.2$–15.7 m. Moreover, this elliptic spiral is extended along the *Y*-axis. Our estimates testify to the fact that theoretical and experimental data are both qualitatively and quantitatively well consistent with each other.

ACKNOWLEDGMENTS

This work was supported by the State Scientific and Technological Program "Astronomy," project no. 1.8.1.2 and by the Russian Foundation for Basic Research, project no. 01-02-17250.

REFERENCES

1. H. Moritz and A. Mueller, *Earth Rotation: Theory and Observation* (Ungar, New York, 1987; Naukova Dumka, Kiev, 1992).
2. Yu. G. Markov, L. V. Rykhlova, and N. V. Skorobogatykh, Dokl. Akad. Nauk **370**, 613 (2000) [Dokl. Phys. **45**, 70 (2000)].
3. P. Goldreich and S. J. Peale, Ann. Rev. Astron. Astrophys. **6**, 287 (1968).
4. N. N. Kozlov and T. M. Éneev, Preprint No. 134, IPM AN SSSR (Keldysh Institute of Applied Mathematics, Academy of Sciences of the USSR, Moscow, 1977).
5. F. L. Chernous'ko, Izv. Akad. Nauk SSSR, Mekh. Tverd. Tela, No. 1, 22 (1980).
6. H. Kinoshita, Celest. Mech., No. 15, 277 (1977).

Translated by G. Merzon

Doklady Physics, Vol. 46, No. 4, 2001, pp. 264–267. Translated from Doklady Akademii Nauk, Vol. 377, No. 5, 2001, pp. 621–625.

MECHANICS

On an Extension of the Concept of Orbital Stability for Trajectories of a Dynamical System

O. V. Druzhinina and A. A. Shestakov

Presented by Academician V.V. Rumyantsev September 7, 2000

Received September 15, 2000

In this paper, we consider three types of orbital stability for semitrajectories of a dynamical system, namely, metric stability, topological stability, and stability in a system of two neighborhood filters. We also introduce and study an essential extension of the concept of orbital stability for a trajectory, which we term the rigidity of the trajectory in the Poincaré sense. The orbital stability and the rigidity in the Poincaré sense are, in general, independent notions. We prove that the set Ω_O of all orbitally stable semitrajectories is a proper subset of the set Ω_P of all semitrajectories rigid in the Poincaré sense: $\Omega_O \subset \Omega_P$, $\Omega_O \neq \Omega_P$. Using a family of Lyapunov functions, we establish criteria for both orbital stability and rigidity in the Poincaré sense for semitrajectories and semihulls of motions for a dynamical system. In the developed theory, we propose a general approach to investigating properties, similar to stability, of compact and noncompact trajectories of a dynamical system.

The concept of orbital stability (but not this term) for a periodic trajectory is met within the studies of P. Laplace [1] and A. Poincaré [2]. Various approaches to defining the concept of orbital stability for an individual semitrajectory were developed in the papers of N.D. Moiseev [3], S. Lefshets [4], and B.P. Demidovich [5]. The same subjects for semiinvariant and invariant (both compact and noncompact) sets of trajectories were considered in the studies of V.I. Zubov [6], N.P. Bkhatia and G. Szegö [7], A.A. Shestakov [8, 9], Yu.V. Malyshev [10], T. Ura [11], J. Auslander [12], J. Auslander and P. Seibert [13], and other authors.

1. DEFINITIONS

We consider a continuous dynamical system φ: $R^n \longrightarrow R^n$ in the Birkhoff sense which is generated by the nonlinear steady-state equation

$$\frac{dx}{dt} = g(x), \quad g \in C^1(R^n \longrightarrow R^n). \tag{1}$$

In what follows, we denote a positive semitrajectory and a positive semihull of motions for dynamical system (1) as $C^+ = C^+(x)$ and $H^+ = H^+(x)$, respectively, provided that the trajectory and motions pass through the point $x \in R^n$, with $H^+(x) = \overline{C^+(x)}$, where the bar implies set closure.

The positive prolongation $P_1^+(x)$ of the point $x \in R^n$ and the positive prolongation $P_1^+(H^+)$ of the semihull $H^+ = H^+(x)$ of motions for the dynamical system φ are defined by the relationships

$$P_1^+(x) = \bigcap_{U \in N(x)} H^+(U), \quad P_1^+(H^+) = \bigcup_{x \in H^+} P_1^+(x),$$

where $N(x)$ is the set of all neighborhoods of point x.

The neighborhood filter Φ of set A is termed topological and denoted as T if Φ is the set of all open sets containing A. This filter is termed metric and is denoted as M if Φ is the set of all open balls $B(A, \varepsilon)$ containing A.

We define the prolongation of a semihull H^+ with respect to the neighborhood filter Φ of this semihull by the formula

$$P_\Phi(H^+) = \bigcap_{N \in \Phi} H^+(N).$$

The neighborhood filter Φ of the semihull H^+ is termed dense if $\bigcap \overline{U} = H^+$, where $U \in \Phi$. We denote the set of all positively invariant filters as $\{\Phi^+\}$.

For the two-dimensional case, the concept of prolongation was introduced by Poincaré [2] and used by Bendixson [14] for qualitatively studying systems (1) in the plane R^2. For the dynamical system in R^n, the concept of prolongation was introduced by Ura [11]. It follows from the definitions that (i) $H^+(x) \subset P_1^+(x)$; (ii) $P_1^+(x) = P_{R^n}^+(x)$; (iii) $P_D^+(x) = \varnothing$, $x \notin \overline{D}$, $D \subset R^n$;

Russian State Open Technical University of Rail Communication, ul. Chasovaya 22/2, Moscow, 125808 Russia

and (iv) $y \in P_D^+(x)$ if and only if there exist sequences $\{x_n\} \subset D$ and $\{t_n\} \subset R$ such that $x_n \longrightarrow x$, $t_n \geq 0$ and $\varphi(t_n, x_n) \longrightarrow y$.

It is evident that $P_\Sigma(H^+) \subset P_\Phi(H^+)$ if $\Phi \subset \Sigma$, where Φ and Σ are the neighborhood filters for $H^+ = H^+(x)$.

The semihull $H^+ = H^+(x)$ of motions for the dynamical system φ: $R^n \longrightarrow R^n$ is termed

(a) positively orbitally topologically stable if, for each neighborhood V of the semihull H^+, there exists a neighborhood U of the semihull H^+ such that $C^+(U) \subset V$;

(b) positively orbitally metrically stable if, for each number $\varepsilon > 0$, there exists a number $\delta > 0$ such that $C^+(B(H^+, \delta)) \subset B(H^+, \varepsilon)$, where $B(H^+, \mu)$ is an open ball with a center in H^+ and of radius $\mu > 0$;

(c) positively orbitally stable with respect to the neighborhood filters Σ and Φ ($\Sigma \supset \Phi$) if, for each neighborhood $U \in \Sigma$ of the semihull H^+, there exists a neighborhood $V \in \Phi$ of the semihull H^+ such that $C^+(U) \subset V$;

(d) positively rigid in the Poincaré sense if

$$P_T(H^+) = H^+, \tag{2}$$

where T is the topological filter of the semihull H^+; and

(e) positively nonrigid in the Poincaré sense if equality (2) is invalid.

The notions of the orbital topological stability and orbital metric stability of the semihull H^+ are particular cases of the concept of orbital stability with respect to a system of two neighborhood filters. Namely, the orbital topological (metric) stability is the orbital stability in the system of (T, T) [in the system of (M, M)].

2. EXAMPLES

The character of the metric orbital stability for a noncompact trajectory differs from that for a compact trajectory.

Example 1. Let the following dynamical system be given in R^2: $\dot{x} = 1$ and $\dot{y} = -2xy(1 + x^2)$ for $x \leq 0$ and $\dot{y} = 0$ for $x \geq 0$. The trajectory $y = 0$ is evidently an invariant set of the system, and this trajectory is orbitally unstable because the following condition (for brevity, it is referred to as condition A) is not met: for each $\varepsilon > 0$, there exists a number $\delta > 0$ such that the implication

$$x \in B(y = 0, \delta) \Rightarrow C^+(x) \subset B(y = 0, \varepsilon)$$

holds.

However, for the trajectory $y = 0$, the other contiguous property (for brevity, the property A_1) is fulfilled: for an arbitrary $\varepsilon > 0$ and an arbitrary compact set $Q \subset R^2$, there exists $\delta = \delta(\varepsilon, Q) > 0$ such that the implication

$$x \in B(y = 0, \delta) \cap Q \Rightarrow C^+(x) \subset B(y = 0, \varepsilon)$$

takes place.

Example 2. Let the dynamical system $\dot{x} = 1$ and $\dot{y} = 0$ for $x \leq 0$ and $\dot{y} = -2xy(1 + x)^{-1}$ for $x \geq 0$ be given in R^2. It is evident that the trajectory $y = 0$ is positively asymptotically orbitally stable because both condition A and the attraction condition (for brevity, it is referred to as condition B) are satisfied for it. Namely, there exists $\delta > 0$ such that the implication

$$x \in B(y = 0, \delta) \Rightarrow d(\varphi(t, x), y = 0) \to 0$$
$$\text{as } t \longrightarrow +\infty$$

holds, where d is the distance from the point $\varphi(t, x)$ to the axis Ox.

Example 3. Let the following dynamical system be given in R^2:

$$\dot{x} = 1, \quad \dot{y} = 0 \text{ for } x \leq 0 \text{ and } |y| \geq 2,$$

$$\dot{x} = -2xy(1 + x^2)^{-1} \text{ for } x \geq 0 \text{ and } |y|(1 + x^2) \leq 1,$$

$$\dot{x} = -[(2 - |y|) \times 2x[(1 + x^2)(1 + 2x^2)\operatorname{sgn} y]^{-1}$$
$$\text{for } x \geq 0, \quad |y| \leq 2, \text{ and } |y|(1 + x^2) \geq 1.$$

It is evident that the trajectory $y = 0$ is positively orbitally stable but not asymptotically stable because condition B is not satisfied for it. However, another attraction condition (for brevity, it is referred to as condition B_1) is satisfied for it. In other words, for each compact set $Q \subset R^2$, there exists a number $\delta > 0$ such that the implication $x \in B(y = 0, \delta) \cap Q \Rightarrow d(\varphi(t, x), y = 0) \longrightarrow 0$ holds as $t \longrightarrow +\infty$.

Example 4. Let the following dynamical system be given on R^2: $\dot{x} = 1$ and $\dot{y} = -2xy(1 + x^2)^{-1}$. The trajectory $y = 0$ is evidently an attractor (condition B is satisfied), but it is not positively orbitally stable (condition A is not satisfied). However, condition A_1 is satisfied for it.

Remarks. (1) In all these examples, we consider the noncompact trajectory $y = 0$ for which conditions B and B_1, as well as conditions A and A_1, are independent.

(2) It is easy to show that, for the compact semitrajectory C, conditions A and B follow from the conditions A_1 and B_1, respectively.

3. RELATION BETWEEN THE ORBITAL STABILITY OF A SEMIHULL AND ITS RIGIDITY IN THE POINCARÉ SENSE

We consider the semitrajectory $C^+(x)$ (generally speaking, noncompact) of continuous dynamical system (1). It follows from the definitions of orbital stability and rigidity in the Poincaré sense that the set Ω_O for all orbitally stable semitrajectories of dynamical system (1) is a proper subset of the set Ω_P of all semitrajectories rigid in the Poincaré sense; i.e., $\Omega_O \subset \Omega_P$ and $\Omega_O \neq \Omega_P$. Thus, the set of all trajectories rigid in the

Poincaré sense is wider than the set of all orbitally stable semitrajectories.

The following theorem establishes the relation between the first prolongation and the prolongation with respect to the neighborhood filter for the semihull H^+.

Theorem 1. *Let T be the topological filter of the semihull H^+. In this case,*

$$P_T(H^+) = \overline{P_1^+(H^+)}, \quad (3)$$

where $P_1^+(H^+)$ is the positive prolongation of the semihull H^+.

Proof. It is evident that the right-hand side of (3) is contained in its left-hand side. Let $q \in P_T(H^+)$. We show that there exists a sequence of points $p_n \in H^+$ such that $q_n \in P_1^+(p_n)$ and $q_n \longrightarrow q$. We assume the contrary. In this case, we can find a number $r > 0$ such that the closure $\overline{B(q, r)}$ is compact and $P_1^+(p) \cap B(q, r) = \varnothing$, $\forall p \in H^+$. Each point p has a neighborhood U_p such that $C^+(U_p) \cap B(q, r) = \varnothing$. Therefore, we have

$$H^+(U) \cap B\left(q, \frac{1}{2}r\right) = \varnothing, \quad q \in P_T(H^+).$$

The contradiction obtained proves the theorem.

Theorem 2. *Let H^+ be a positively rigid (in the Poincaré sense) semihull of motions for the dynamical system φ: $R^+ \longrightarrow R^n$. In this case, the following statements are equivalent*:

(A_1) *$P_\Phi(H^+) = H^+$ for a certain neighborhood filter Φ of the semihull H^+.*

(A_2) *$P_1^+(x) \subset H^+$ $\forall x \in H^+$.*

(A_3) *The semihull H^+ is orbitally stable with respect to its certain dense neighborhood filter G.*

(A_4) *The semihull H^+ is orbitally stable with respect to some of its dense neighborhood filters Σ and Φ.*

Proof. It is evident that statement (A_1) follows from the rigidity, in the Poincaré sense, of the semihull H^+. If (A_1) is valid, then the relation $P_1^+(p) \subset P_\Phi(H^+) = H^+$ takes place for $p \in H^+$. Hence, (A_2) is valid and we infer from Theorem 1 that

$$P_T(H^+) = \bigcup_{p \in H^+} P_1^+(p) = H^+.$$

Statement (A_1) is proven. It follows from statement (A_1) that the filter $\{\Phi^+\}$ is dense. The semihull H^+ is evidently always orbitally stable with respect to $\{\Phi^+\}$. Now, we assume that H^+ is orbitally stable with respect to G, with G being a dense filter for H^+. In this case, if $q \notin H^+$, there exists a neighborhood $N \in \Sigma$ such that $q \notin H^+$. Let $U \in G$ be such that $C^+(U) \subset G$ so that $q \notin C^+(U)$. Consequently, $P_G(H^+) = H^+$ and, therefore, (A_1) follows from (A_3). It is evident that (A_4) follows from (A_3). If (A_4) is valid, then $\Phi \subset \{\Sigma^+\}$ so that $\{\Sigma^+\}$ is a dense filter and (A_3) is valid with $G = \{\Sigma^+\}$.

The following theorem on the relation between the rigidity in the Poincaré sense and the orbital stability holds.

Theorem 3. *If the semihull H^+ is positively rigid in the Poincaré sense, there exists a unique maximum dense filter F with respect to which the semihull H^+ is orbitally stable.*

Theorem 4. *Let H^+ be a positive semihull of motions of a dynamical system. In order for H^+ to be topologically orbitally stable, it is necessary and sufficient that $P_1^+(x)$ be a compact subset of H^+, where $x \in H^+$.*

Proof. Theorem 4 is proven by contradiction with the use of Theorem 2.

The next theorem establishes a criterion of the rigidity in the Poincaré sense in terms of neighborhoods of the points belonging to a semitrajectory.

Theorem 5. *In order for the semitrajectory $C^+(x)$ of the dynamical system φ: $R^n \longrightarrow R^n$ to be positively rigid in the Poincaré sense, it is necessary and sufficient that the following condition take place*: *for arbitrary points $p \notin C^+(x)$ and $q \in C^+(x)$, neighborhoods U and V of these points exist such that*

$$U \cap C^+(V) = \varnothing. \quad (4)$$

Proof. Let the semitrajectory $C^+ = C^+(x)$ satisfy condition (4). In this case, there exist neighborhoods U and V of points p and q, respectively, which satisfy condition (4) for $p \notin C^+$ and $q \in C^+$. Consequently, $p \notin H^+(V)$ and, therefore,

$$p \notin \cap\{H^+(V): V \text{ is a neighborhood of } q\} = P_1^+(q).$$

Since $q \in C^+$ is an arbitrary point, then $p \notin P_1^+(C^+)$ so that $P_1^+(C^+) \subset C^+$. Hence, the condition $P_1^+(C^+) = C^+$ is satisfied and, therefore, the semitrajectory C^+ is rigid in the Poincaré sense. Now, let the semitrajectory C^+ be rigid in the Poincaré sense. In this case, $P_1^+(C^+) = C^+$. Let $p \notin C^+$ and $q \in C^+$. Hence, $p \notin P_1^+(q) \subset P_1^+(C^+)$. Because $P_1^+(q) = \cap\{H^+(V): V \text{ is a neighborhood of } q\}$, there exists a neighborhood V of point q for which $p \notin H^+(\varphi)$. In this case, $R^n = H^+(V) = U$ is a neighborhood of point q; consequently, condition (4) is satisfied.

Theorem 6. *If the semitrajectory $C^+ = C^+(x)$ is positively rigid in the Poincaré sense, it is positively invariant.*

Proof. Let the semitrajectory C^+ be positively rigid in the Poincaré sense. According to Theorem 5, this semitrajectory satisfies condition (4). Let $p \notin C^+$. In

this case, it follows from (4) that $p \notin C^+(q)$ for each point $q \in C^+$. Thus, $p \in C^+(C^+) = \cup\{C^+(q): q \in C^+\}$. Hence, $C^+(C^+) \subset C^+$ and the semitrajectory C^+ is positively invariant.

In the general case, the rigidity of a semitrajectory in the Poincaré sense and the orbital stability of this semitrajectory are independent notions. However, in a number of cases, these notions are equivalent, as follows from the definition of the topological orbital stability, the properties of the semihull H^+, and Theorem 5.

Theorem 7. *Let the semihull H^+ of motions of the dynamical system $\varphi: R^n \longrightarrow R^n$ have a compact omega-limiting set. In this case, the semihull H^+ is topologically orbitally stable if and only if it is rigid in the Poincaré sense.*

It is important to note that the concept of the rigidity for a trajectory in the Poincaré sense is an extension of the concept of the orbital stability for the trajectory, while the concept of stability in the Joukowski sense [15] is an extension of that in the Lyapunov sense with respect to coordinates.

4. THE USE OF A FAMILY OF LYAPUNOV FUNCTIONS FOR INVESTIGATING THE ORBITAL STABILITY AND RIGIDITY OF TRAJECTORIES

Let (Σ, Φ) be a system of two filters Σ and Φ, $\Phi \subset \Sigma$ for the semihull H^+, and let $N \in \Sigma$ be a positively invariant set of the dynamical system $\varphi: R^n \longrightarrow R^n$. The semihull H^+ may be noncompact.

The nonnegative function $v: N \longrightarrow R^n$ is termed a Lyapunov function for the semihull H^+ and its filter Σ if (a) $v^{-1}(0) = H^+$; (b) $v(\varphi(t, x)) \le v(x)\ \forall (t, x) \in R^+ \times N$; and (c) $v^{-1}([0, c)) \in \Sigma$, $c > 0$.

The family V of nonnegative functions in R^n is termed a (Σ, Φ)-family of the Lyapunov functions for the semihull H^+, if each function v of this family is a Lyapunov function for the semihull H^+ and its filter Σ and, for each neighborhood U of the filter $\Phi \subset \Sigma$, there exists a function $v \in V$ such that $\inf\{v(x): x \in U\} > 0$. This inequality is equivalent to the following property: for each neighborhood $U \in \Phi$, there exists a function $v \in U$ and a number $d > 0$ such that $v^{-1}([0, d)) \subset U$.

Theorem 8. *In order for the semihull H^+ of motions of the dynamical system $\varphi: R^n \longrightarrow R^n$ to be positively orbitally stable with respect to (Σ, Φ), it is necessary and sufficient that such a (Σ, Φ)-family $V = \{v\}$ of the Lyapunov functions exist for the semihull H^+ such that $\Phi \subset \Sigma$ and Φ are a dense filter.*

Theorem 9. *Let Φ be a dense neighborhood filter of the semihull H^+. In order for the semihull H^+ to be positively asymptotically orbitally stable with respect to Φ, it is necessary and sufficient that the Φ-family V of the Lyapunov functions v exist for H^+ and, moreover, that the following property be valid*:

$$\forall U \in \Phi, \quad \forall x \in U \quad \lim_{t \to +\infty} v(\varphi(t, x)) = 0.$$

Theorem 10. *Let the semihull H^+ of motions of the dynamical system $\varphi: R^n \longrightarrow R^n$ be positively rigid in the Poincaré sense, and let F be the unique dense filter of the semihull H^+ with respect to which H^+ is orbitally stable* (*such a filter always exists*). *In order for the semihull H^+ to be positively rigid in the Poincaré sense, it is necessary and sufficient that the F-family of the Lyapunov functions exist.*

Theorems 8–10 are criteria for the orbital stability and the rigidity in the Poincaré sense in terms of families of the Lyapunov functions which are, in general, discontinuous.

ACKNOWLEDGMENTS

The authors are grateful to Academician V.V. Rumyantsev for his valuable remarks and attention to this work.

REFERENCES

1. P. S. Laplace, *Traite de mecanique celeste* (Duprat, Paris, 1799, 1802), Vols. 1, 2.
2. H. Poincaré, *Sur les Courbes Definies par les Equations Differentielles: Oeuvres* (Gauthier-Villars, Paris, 1951; Gostekhteoretizdat, Moscow, 1947).
3. N. D. Moiseev, *Outlines of Stability Theory Development* (GITTL, Moscow, 1949).
4. S. Lefschetz, *Differential Equations: Geometric Theory* (Interscience, New York, 1957; Inostrannaya Literatura, Moscow, 1961).
5. B. P. Demidovich, *Lectures on Theory of Mathematical Stability* (Nauka, Moscow, 1967).
6. V. I. Zubov, *Lyapunov Methods and Their Application* (Len. Gos. Univ., Leningrad, 1957).
7. N. P. Bhatia and G. P. Szegö, *Stability Theory of Dynamical Systems* (Springer-Verlag, Berlin, 1970).
8. A. A. Shestakov, Diff. Uravn. **13**, 958 (1977).
9. A. A. Shestakov, Diff. Uravn. **13**, 1079 (1977).
10. Yu. V. Malyshev, Doctoral Dissertation in Mathematical Physics (Sverdlovsk, 1991).
11. T. Ura, Contribs. Different. Equat. **3**, 249 (1964).
12. J. Auslander, SIAM J. Math. Anal. **8**, 573 (1977).
13. J. Auslander and P. Seibert, Ann. Inst. Fourier **14**, 237 (1964).
14. I. Bendixson, Acta Math. **24**, 1 (1901).
15. O. V. Dunaeva, Dokl. Akad. Nauk **355**, 51 (1997) [Phys. Dokl. **42**, 374 (1997)].

Translated by V. Bukhanov

Doklady Physics, Vol. 46, No. 4, 2001, pp. 268–270. Translated from Doklady Akademii Nauk, Vol. 377, No. 5, 2001, pp. 626–628.

MECHANICS

On the Brockett Stabilization Problem

G. A. Leonov

Presented by Academician N.F. Morozov October 8, 2000

Received October 25, 2000

In the book by P. Brockett [1], the following problem was formulated.

Let three matrices A, B, and C be given. Under what conditions does there exist a matrix $K(t)$ such that the system

$$\frac{dx}{dt} = Ax + BK(t)Cx, \quad x \in R^n \tag{1}$$

is asymptotically stable?

It is worth noting that the problem of stabilizing system (1) by means of a constant matrix K is well known in the automatic-control theory [2, 3]. From this point of view, the Brockett problem can be reformulated in the following manner.

How much would introduction of a time-dependent matrix $K(t)$ improve the capabilities of the conventional stabilization?

In solving problems of stabilization of mechanical systems, a more narrow class of stabilizing matrices $K(t)$ should often be considered. These matrices must be periodic and have a zero mean value over their period $[0, T]$:

$$\int_0^T K(t)dt = 0. \tag{2}$$

Such stabilizing actions are realized in the problems of stabilization of pendulum systems.

We consider a pendulum with its point of support vibrating in the vertical direction. In the linear approximation, the pendulum vibrations in the vicinity of the upper equilibrium position are described by the equation

$$\ddot{\theta} + \alpha\dot{\theta} + (K(t) - \omega_0^2)\theta = 0, \tag{3}$$

where α and ω_0 are positive numbers. As a rule, the functions $K(t)$ are assumed to take either form $\beta\sin\omega t$ [4] or

$$K(t) = \begin{cases} \beta & \text{at } t \in [0, T/2) \\ -\beta & \text{at } t \in [T/2, T) \end{cases} \tag{4}$$

[5, 6]. For these functions $K(t)$, the effect of stabilization of the pendulum upper equilibrium position is well known for large ω or small T.

In this paper, we present algorithms for constructing periodic piecewise-constant functions $K(t)$, which allow us to solve the Brockett problem in a number of cases.

Theorem 1. *Let* $\alpha^2 < 4(\beta - \omega_0^2)$. *Then, for any* $\tau > 0$, *there exists a number* $T > \tau$ *such that Eq.* (3) *with a function* $K(t)$ *having form* (4) *is asymptotically stable.*

In particular, the possibility of stabilizing the upper equilibrium position for a pendulum point of support under low-frequency vibrations follows from this theorem.

We here outline the proof of Theorem 1. For $K(t) = -\beta$, Eq. (3) has two linear manifolds in its phase space, namely, a stable ($\eta = L_1\theta$) and an unstable ($\eta = L_2\theta$) one (with $\eta = \dot{\theta}$). In this case, the rate of solution convergence to the unstable manifold is higher than the divergence rate along this manifold. After a change at $K(t) = \beta$, this unstable manifold may turn along the trajectories of Eq. (3) and can then attain coincidence with the straight line $\eta = L_1\theta$ before the next change. (Large values of T imply that the pendulum vibrates many times during time T.) Since the above-mentioned convergence of the solution predominates over its divergence after the change at the moment $t = T$, any solution as a whole can be embedded into a sphere of arbitrarily small radius.

We now describe the similar algorithm for system (1).

We assume that there exists a matrix K_1 such that the system

$$\frac{dx}{dt} = (A + \mu BK_1C)x \tag{5}$$

with scalar parameter μ has a stable linear invariant manifold $L(\mu)$. Here, $\mu \geq \mu_0$ and μ_0 is a certain number.

St. Petersburg State University,
Universitetskaya nab. 7/9, St. Petersburg, 199164 Russia

1028-3358/01/4604-0268$21.00

We also assume that

$$\lim_{\mu \to +\infty} L(\mu) = L_0 \tag{6}$$

and, for any given number $\delta > 0$, there exists a number $\mu_1 \geq \mu_0$ such that

$$\begin{gathered} |x(1, x_0)| \leq \delta, \\ \forall x_0 \in \{|x| = 1\} \cap L(\mu), \quad \mu \geq \mu_1. \end{gathered} \tag{7}$$

Here, $x(0, x_0) = x_0$ and the existence of limit (6) implies that the set $L(\mu) \cap \{|x| \leq 1\}$ is in the ε-neighborhood $L_0 \cap \{|x| \leq 1\}$, where $\varepsilon \longrightarrow 0$ as $\mu \longrightarrow +\infty$.

The above-formulated assumption implies that the trajectories rapidly converge on manifold $L(\mu)$ for large values of parameter μ.

We denote by $M(\mu)$ the linear invariant manifold of system (5) such that for this manifold,

$$\lim_{\mu \to +\infty} M(\mu) = M_0,$$
$$\dim M(\mu) + \dim L(\mu) = n, \quad M(\mu) \cap L(\mu) = \{0\}.$$

We also assume that $M(\mu)$ is the manifold of slow motions; i.e., there exists a number R such that the inequality

$$\begin{gathered} |x(1, x_0)| \leq R, \\ \forall x_0 \in \{|x| = 1\} \cap M(\mu) \end{gathered} \tag{8}$$

is valid for arbitrary $\mu \geq \mu_0$. We then assume that a matrix K_2 exists such that for the system

$$\frac{dy}{dt} = (A + BK_2C)y, \tag{9}$$

the fundamental matrix $Y(t)$ can be found with $Y(0) = I$, which satisfies the condition

$$Y(\tau)M_0 \subset L_0 \tag{10}$$

for a certain number τ.

We now define the matrix $K(t)$ with period $(2 + \tau)$ in the following manner:

$$K(t) = \begin{cases} \mu K_1 & \text{for } t \in [0, 1) \\ K_2 & \text{for } t \in [1, 1 + \tau) \\ \mu K_1 & \text{for } t \in [1 + \tau, 2 + \tau). \end{cases} \tag{11}$$

Theorem 2. *System* (1) *with a matrix* $K(t)$ *having the form of* (11) *is asymptotically stable for sufficiently large* μ.

The following corollary of Theorem 2 takes place.

Theorem 3. *Let the matrices* K_1 *and* K_2 *exist and satisfy the following conditions*:

(i) *The matrix* BK_1C *has* $(n - 1)$ *eigenvalues with negative real parts, and* $\det BK_1C = 0$.

(ii) *For a certain number* λ *and a vector* $u \neq 0$ *satisfying the equality* $BK_1Cu = 0$, *the vector-function*

$$\exp[(A + BK_2C + \lambda I)t]u$$

is periodic.

Then, there exists a periodic matrix $K(t)$ *such that system* (1) *is asymptotically stable.*

In a two-dimensional case, Theorem 3 has the following simple formulation.

Theorem 4. *Let* $n = 2$ *and there exist matrices satisfying the following conditions*:

(I) $\det BK_1C = 0$ *and* $\mathrm{Tr} BK_1C \neq 0$.

(II) *The matrix* $A + BK_2C$ *has complex-valued eigenvalues.*

Then, there exists a periodic matrix $K(t)$ *having form* (11) *such that system* (1) *is asymptotically stable.*

A more complicated algorithm for constructing the piecewise stabilizing function $K(t)$ allows us to prove the following theorem.

Theorem 5. *Let* $n = 3$, B *be a column,* C *be a row, and the following conditions be satisfied*:

(*1*) $\det(B, AB, A^2B) \neq 0$.

(*2*) $CB \neq 0$.

(*3*) *There exists a number* k_1 *such that the matrix* $A + k_1BC$ *has two complex-valued and one negative eigenvalue.*

(*4*) *There exists a number* k_2 *such that the function*

$$C\exp[(A + k_2BC)t]B$$

has at least one zero in the interval $(-\infty, 0)$.

Then, there exists a periodic function $K(t)$ *such that the system of Eqs.* (1) *is asymptotically stable.*

We then consider system (1) provided that B is a vector column, C is a vector row, and $K(t)$ is a scalar piecewise continuous function $\mathbf{R}^1 \longrightarrow \mathbf{R}^1$. Assuming complete controllability of pair (A, B) and complete observability of pair (A, C), we reduce system (1) to the form [7]

$$\begin{aligned} \dot{x}_1 &= \dot{x}_2, \\ &\cdots\cdots\cdots \\ \dot{x}_{n-1} &= x_n, \\ \dot{x}_n &= -(a_nx_n + \ldots + a_1x_1) - K(t)(c_nx_n + \ldots + c_1x_1). \end{aligned}$$

Here, a_j and c_j are certain numbers. In the case of $c_n \neq 0$, without loss of generality, we can set $c_n = 1$.

Theorem 6. *Let the following inequalities be satisfied*:

(*i*) *for* $n > 2$, $c_1 \leq 0, \ldots, c_{n-2} \leq 0$;

(*ii*)
$$c_1(a_n - c_{n-1}) > a_1,$$
$$c_1 + c_2(a_n - c_{n-1}) > a_2,$$
$$\ldots\ldots\ldots\ldots\ldots\ldots$$
$$c_{n-2} + c_{n-1}(a_n - c_{n-1}) > a_{n-1}.$$

Then, there are no functions $K(t)$ for which system (1) *is asymptotically stable.*

Theorem 6 is a consequence of the positive invariance for the set

$$\{x_1 \geq 0, \ldots, x_{n-1} \geq 0,\ x_n + c_{n-1}x_{n-1} + \ldots + c_1x_1 \geq 0\}.$$

We now apply the above-formulated theorems provided that $n = 2$, B is a column, C is a row, and $K(t)$ is a scalar function. (This case is important in control theory.) To do this, we introduce the transfer function for system (1):

$$W(p) = C(A - pI)^{-1}B = \frac{\rho p + \gamma}{p^2 + \alpha p + \beta}.$$

Here, p is a complex-valued variable.

In what follows, we assume that $\rho \neq 0$. For the problem under consideration, without loss of generality, we can set $\rho = 1$. Moreover, we assume that the function $W(p)$ is nongenerate; i.e., the inequality

$$\gamma^2 - \alpha\gamma + \beta \neq 0$$

is met. It is well known [7] that system (1) can be rewritten in this case in the form

$$\begin{aligned} \dot\sigma &= \eta, \\ \dot\eta &= -\alpha\eta - \beta\sigma - K(t)(\eta + \gamma\sigma). \end{aligned} \tag{12}$$

It is easy to see that the stabilization of system (12) by means of a constant function $K(t) \equiv K_0$ is possible if and only if $\alpha + K_0 > 0$ and $\beta + \gamma K_0 > 0$. For the number K_0 to meet these inequalities, it is necessary and sufficient that either the condition $\gamma > 0$ or the relationships $\gamma \leq 0$ and $\alpha\gamma < \beta$ be satisfied.

We now consider the case when the stabilization by means of a constant function $K(t) \equiv K_0$ is impossible since $\gamma \leq 0$ and $\alpha\gamma > \beta$. To do this, we use Theorem 4. It is evident that hypothesis (i) of Theorem 3 is met because $\det BK_1C = K_1 \det BC = 0$ and $\mathrm{Tr}BK_1C = K_1CB = -K_1 \neq 0$.

Hypothesis (II) of Theorem 4 will be met if, for a certain K_2, the polynomial

$$p^2 + \alpha p + \beta + K_2(p + \gamma)$$

has complex-valued zeroes. It is easy to see that for such K_2 to exist, it is necessary and sufficient that the inequality

$$\gamma^2 - \alpha\gamma + \beta > 0 \tag{13}$$

be satisfied.

Hence, if inequality (13) holds true, there exists a periodic function $K(t)$ such that system (12) is asymptotically stable.

As is easy to see, the hypotheses of Theorem (6) are met if the inequality

$$\gamma^2 - \alpha\gamma + \beta < 0 \tag{14}$$

is satisfied.

Hence, we arrive at the following theorem [8].

Theorem 7. *If inequality* (13) *is met, then there exists a periodic function $K(t)$ such that system* (12) *is asymptotically stable*.

If inequality (14) *is valid, there are no functions $K(t)$ for which system* (12) *is asymptotically stable.*

This result was also obtained in [9] by the averaging method for another class of stabilizing functions $K(t)$ having the form

$$K(t) = (k_0 + k_1\omega\cos\omega t), \quad \omega \gg 1.$$

REFERENCES

1. R. Brockett, *Open Problems in Mathematical Systems and Control Theory. A Stabilization Problem* (Springer-Verlag, Berlin, 1999).
2. L. A. Zadeh and C. A. Desoer, *Linear System Theory: The Spatial State Approach* (McGraw-Hill, New York, 1963; Nauka, Moscow, 1970).
3. A. A. Pervozvanskiĭ, *Course of Automatic Control Theory* (Nauka, Moscow, 1986).
4. Yu. A. Mitropol'skiĭ, *Averaging Methods in Nonlinear Mechanics* (Naukova Dumka, Kiev, 1971).
5. V. I. Arnol'd, *Ordinary Differential Equations* (Nauka, Moscow, 1971; MIT Press, Cambridge, 1973).
6. V. I. Arnold, *Mathematical Methods of Classical Mechanics* (Nauka, Moscow, 1979; Springer-Verlag, New York, 1989).
7. S. Lefschetz, *Stability of Nonlinear Control Systems* (Academic, New York, 1965; Mir, Moscow, 1967).
8. G. A. Leonov, in *Proceedings of the International Conference on Control of Oscillations and Chaos*, St. Petersburg, 2000, p. 38.
9. L. Morean and D. Aeyels, in *Proceedings of the Conference of Decision and Control*, Phoenix, 1999, p. 108.

Translated by V. Chechin

Doklady Physics, Vol. 46, No. 4, 2001, pp. 271–275. Translated from Doklady Akademii Nauk, Vol. 377, No. 5, 2001, pp. 629–633.

MECHANICS

An Unsteady Model for Volcanic-Eruption Dynamics Involving Crystallization and Through-Magma Gas Filtration

O. É. Mel'nik

Presented by Academician G.G. Chernyĭ September 25, 2000

Received September 28, 2000

Manifestations of volcanic eruptions occur in great varieties: from slow lava outflow to catastrophic explosive eruptions. The eruption type is determined by the amount of gas initially dissolved in the magma, the magma viscosity, and the intensity of the gas withdrawal through the magma and into the volcano-conduit walls. Pure lava eruptions are typical of low-viscosity magma with a small amount of dissolved gas. Eruptions of magma saturated with gas are the most dangerous when an abrupt change from the lava outflow to gas-ashed jets is possible. In this case, the discharge rate can be briefly changed by several orders of magnitude [1].

In view of the difficulty of direct study, volcanic eruption modeling on the basis of continuum mechanics is of great importance. Special features of these flows are a high value of viscosity (up to 10^9 Pa s), strong dependence of viscosity on the concentration of magma gases in the melt and on temperature, an unusual pressure dependence of the volatile component content, a small value of the diffusion coefficient, etc. The eruption-magma flow is characterized by a strong pressure drop (from hundreds of MPa to atmospheric pressure), which results in changing from homogeneous flow to a bubble flow and then, possibly, to a flow with suspension of matter in gas.

A slow extrusion of a lava dome with an outflow of the gas present in magma through the dome surface is the most typical eruption regime for magma containing many crystals and a relatively small amount of dissolved gas. This type of volcanos is typified by Soufriere Hills (Montserrat Island, 1995–2000), Mount Unzen (Japan, 1990–1995), and Lascar (Chili, 1984–1996). In the models elaborated by the author in collaboration with A.A. Barmin [1–3], the possibility of such an eruption regime and its transition to the explosive phase was found in the quasi-stationary approach; however, the description was highly simplified.

Institute of Mechanics, Moscow State University, Michurinskiĭ pr. 1, Moscow, 117192 Russia

In papers [4, 5], where the results of field observations are generalized, it was shown that the lower the magma flow, the greater the quantity of crystals contained in the magma, the crystallization being at work in the volcano conduit when the magma is elevated. The gas outflow through magma is another peculiarity of such eruptions. This results in a relatively low fraction of bubbles at the dome surface: 10–30% instead of 99% for estimates ignoring gas loss [1].

A stationary model with a simplified equation of magma crystallization was published in [6]. In the present paper, an unsteady model for magma flow in a volcano conduit with an adequate equation for crystal growth is considered. The effect of the processes in the magmatic chamber on the magma discharge rate at the surface is studied.

The statement of the problem on a flow in a conduit in the case of a rising lava dome is similar to that of [1]. At depth L, there is a magmatic chamber connected with a growing dome by a conduit with diameter d. The magma parameters in the magmatic chamber (the pressure P_{ch}, the dissolved gas concentration c_{ch}, and the volumetric fraction of the crystals β_{ch}) are time-dependent. The magma is a four-component medium containing a melt, dissolved gas, bubbles, and crystals. The flow in the conduit is described by the system of equations

$$\frac{\partial}{\partial t}\rho_m + \frac{\partial}{\partial x}\rho_m V = -G, \quad \frac{\partial}{\partial t}\rho_c + \frac{\partial}{\partial x}\rho_c V = G; \quad (1a)$$

$$\frac{\partial}{\partial t}\rho_x + \frac{\partial}{\partial x}\rho_x V = -J, \quad \frac{\partial}{\partial t}\rho_g + \frac{\partial}{\partial x}\rho_g V_g = J; \quad (1b)$$

$$\frac{\partial p}{\partial x} = -\rho g - \frac{32\mu V}{d^2}, \quad V_g - V = -\frac{k(\alpha)}{\mu_g}\frac{\partial p}{\partial x}; \quad (1c)$$

$$J = n\rho_m(1-\beta) \times 4\pi a^2 \left.\frac{\partial c}{\partial r}\right|_{r=a}$$

$$= n\rho_m(1-\beta) \times 4\pi a(c - C_f\sqrt{p}),$$

1028-3358/01/4604-0271$21.00

$$G = 3\rho_m(1-\beta)U(t)\int_0^t I(\omega)\left(\int_\omega^t U(\lambda)d\lambda\right)^2 d\omega,$$

$$I(c) = I_0\frac{\mu(c_0)}{\mu(c)}\exp\left(-\zeta_i\frac{T_m(c)}{T}\right)$$

$$\times\exp\left(-\theta_i\frac{T_m^3(c)}{(T_m(c)-T)^2T}\right), \quad (1d)$$

$$U(c) = U_0\frac{\mu(c_0)(T_m(c)-T)}{\mu(c)T}\exp\left(-\theta_u\frac{T_m(c)}{T}\right);$$

$$\alpha = \frac{4}{3}\pi a^3 n, \quad \frac{\partial n}{\partial t}+\frac{\partial nV}{\partial x}=0, \quad p=\rho_g^0 RT,$$

$$\rho_m = \rho_m^0(1-\alpha)(1-\beta)(1-c), \quad \rho_c = \rho_c^0(1-\alpha)\beta, \quad (1e)$$

$$\rho_x = \rho_m^0(1-\alpha)(1-\beta)c, \quad \rho_g = \rho_g^0\alpha;$$

$$T_{liq} = 8.33c^2 - 139.40c + 1611.75,$$

$$T_{sol} = 5.74c^2 - 98.72c + 1281.23, \quad (1f)$$

$$T_m = T_{liq}(1-\beta) + T_{sol}\beta;$$

$$\mu = \theta(\beta)\mu_m(c), \quad \log\frac{\theta(\beta)}{\theta_0} = \arctan(\omega(\beta-\beta_*)) + \frac{\pi}{2},$$

$$\log\mu_m = -3.545 + 0.833\ln c + \frac{9601 - 2368\ln c}{T - (195.7 + 32.25\ln c)}, \quad (1g)$$

$$\log\frac{k(\alpha)}{k_0} = -10.2(\alpha\times 10^2)^{1.4\times 10^{-2}\alpha^{-1}}, \quad \alpha > 0.03.$$

Here, ρ_m, ρ_c, ρ_x, and ρ_g are the densities of the melt, crystals, bubbles, and dissolved gas, respectively; ρ is the mixture density; α and β are the volumetric concentrations of bubbles and crystals (the latter is taken relative to the condensed-phase volume, i.e., relative to the volume of the melt-and-crystal mixture); V and V_g are the magma and gas velocities, respectively; p is the pressure; c is the mass concentration of the dissolved gas; μ, μ_m, and μ_g are the viscosity of the mixture, melt, and gas, respectively; d is the conduit diameter; $k(\alpha)$ is the coefficient of gas filtration through the magma; R is the gas constant; T, T_m, T_{liq}, and T_{sol} are the magma temperature, the effective melting temperature, and the temperatures of liquidus and solidus, respectively; a is the bubble radius; n is the bubble number density; x is the vertical coordinate; and I and U are the rates of crystal growth and nucleation.

System (1) is written out under the following assumptions: the motion is one-dimensional and laminar; the magma is a Newtonian fluid with a viscosity dependent on the dissolved gas concentration and the volumetric fraction of crystals; and the mixture temperature is constant. The system consists of continuity equations for the melt and crystals (1a), for the dissolved gas and the gas in the free phase (1b), momentum equations for the condensed phase with allowance for gravity and volcanic conduit resistance, and the Darcy law for gas motion in porous magma (1c); equations accounting for the mass exchange intensity in the magma (1d); and equations describing physical properties of the magma, (1e)–(1g). Formula (1g) for $k(\alpha)$ was obtained by approximating the data of penetrability measurements for samples from the eruption of the Soufriere Hills volcano; the $\mu_m(c)$ was taken from [7]; the $\theta(\beta)$-dependence was obtained by approximating data on the dome growth for the Soufriere Hills volcano using a stationary model.

The following assumptions are taken in obtaining Eqs. (1d). The bubbleward gas diffusion is quasi-equilibrium, and the concentration profile is determined by solving a stationary diffusion equation [8]. The bubble nucleation is assumed to be instantaneous, and their concentration in a liquid particle is conserved. The magma crystallization is quasi-isothermal due to the change in the effective melting temperature when the amount of dissolved gas decreases. The expressions for the nucleation intensity of crystals and their growth are similar to that of [9]; however, the expressions take into account the decrease in the diffusivity with decreasing c.

For system (1), the boundary-value problem is solved for a given conduit length, the parameters in the magmatic chamber, and the conditions at the exit. For the magmatic chamber of spherical shape, the pressure is related to the discharge rates of the inflowing (Q_{in}) and outflowing (Q_{out}) magma through the equation

$$\frac{dP_{ch}}{dt} = -\frac{Q_{out}-Q_{in}}{\tau}, \quad \tau = \frac{V_{ch}\rho_{ch}}{\gamma},$$

where V_{ch} and ρ_{ch} are the volume of the magmatic chamber and the mean magma density in it and γ is the rock elastic modulus. The pressure at the upper edge of the conduit is equal to atmospheric pressure. For calculations, the same values of parameters as those in [6] were used.

System (1) was solved by an implicit method with a varied mesh in space, which provides first-order accuracy. The steady-state solution with a low (0.15 m^3/s) discharge rate was used as the initial condition; the discharge rate Q_{in} was taken to be constant (0.75 m^3/s).

In Fig. 1 we show, in the Q_e–P_{ch} plane (Q_e is the magma discharge rate at the volcano conduit exit), the steady-state solution to Eqs. (1) and a family of unsteady solutions corresponding to various τ values

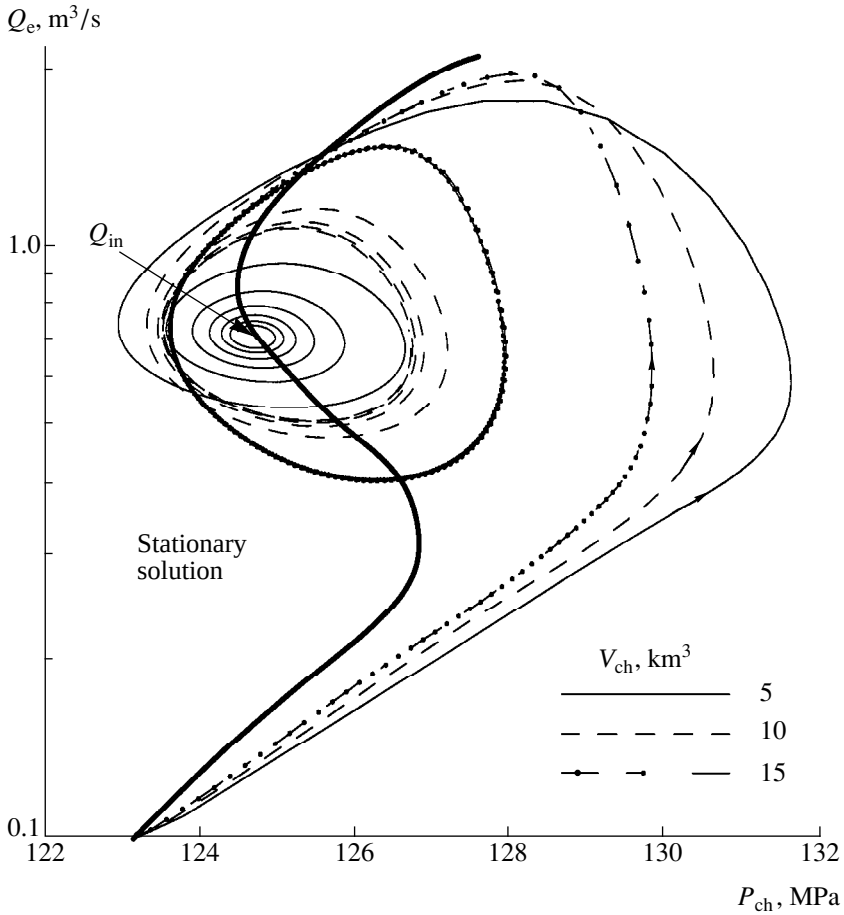

Fig. 1.

and β_{ch} = const. The steady-state solution is nonunique for certain values of pressure in the magmatic chamber; this is associated with the influence of crystallization. When the crystallization time is comparable with the time of magma elevation, the decreasing discharge rate results in increasing the crystal quantity and, consequently, in increasing the magma viscosity. For reducing resistance, it is essential to further decrease the discharge rate. The behavior of the unsteady solution depends substantially on the values of Q_{in} and τ. When Q_{in} corresponds to the upper or lower regimes, the eruption comes to the stationary state as time elapses. The greater the value of τ, the longer the time of approaching the stationary regime. The eruption is also stabilized in the case when Q_{in} corresponds to the average regime and τ is less than the critical value. For large τ, undamped periodic oscillations of the magma discharge rate occur. Their amplitude and period are τ-dependent. The different asymptotic behavior of the solution is connected with the change in the boundary condition: small τ values correspond to a given magma discharge rate from the magmatic chamber, while the stationary solution corresponding to a fixed discharge rate is unique. Large τ values correspond to a fixed pressure in the magmatic chamber, when the stationary solution is many-valued. The transition between stationary regimes provides undamped discharge-rate oscillations.

Shown in Fig. 2 are the functions $Q_e(t)$, $\beta_e(t)$, and $P_{ch}(t)$. The oscillation periods are 375, 495, and 675 days for the magma-chamber volumes equal to 5, 10, and 15 km^3, respectively. For the Soufriere Hills volcano, the two-year activity cycle was isolated [10]. The maxima and minima of $P_{ch}(t)$ and $Q_e(t)$ do not coincide because of specific boundary conditions.

The time dependence of Q_e for V_{ch} = 15 km^3 and $\beta_{ch} = \beta_0(1 + \varepsilon^* \sin(\omega t))$ with $\varepsilon = 0.05$ and a period of 40 days is shown in Fig. 3. The reason for such a change of the β_{ch} value may be the convective instability of the lower heated magma layer in the magmatic chamber, which causes the floating up of individual hot portions of magma and their elevation through the volcano conduit. The dashed line shows the time dependence of the discharge rate for $\beta_{ch} = \beta_0$. When the magma discharge rate is small, crystallization occurs in the volcano conduit and the mean crystal concentration in the conduit depends weakly on its value in the magmatic chamber. For a high discharge rate, the crystalli-

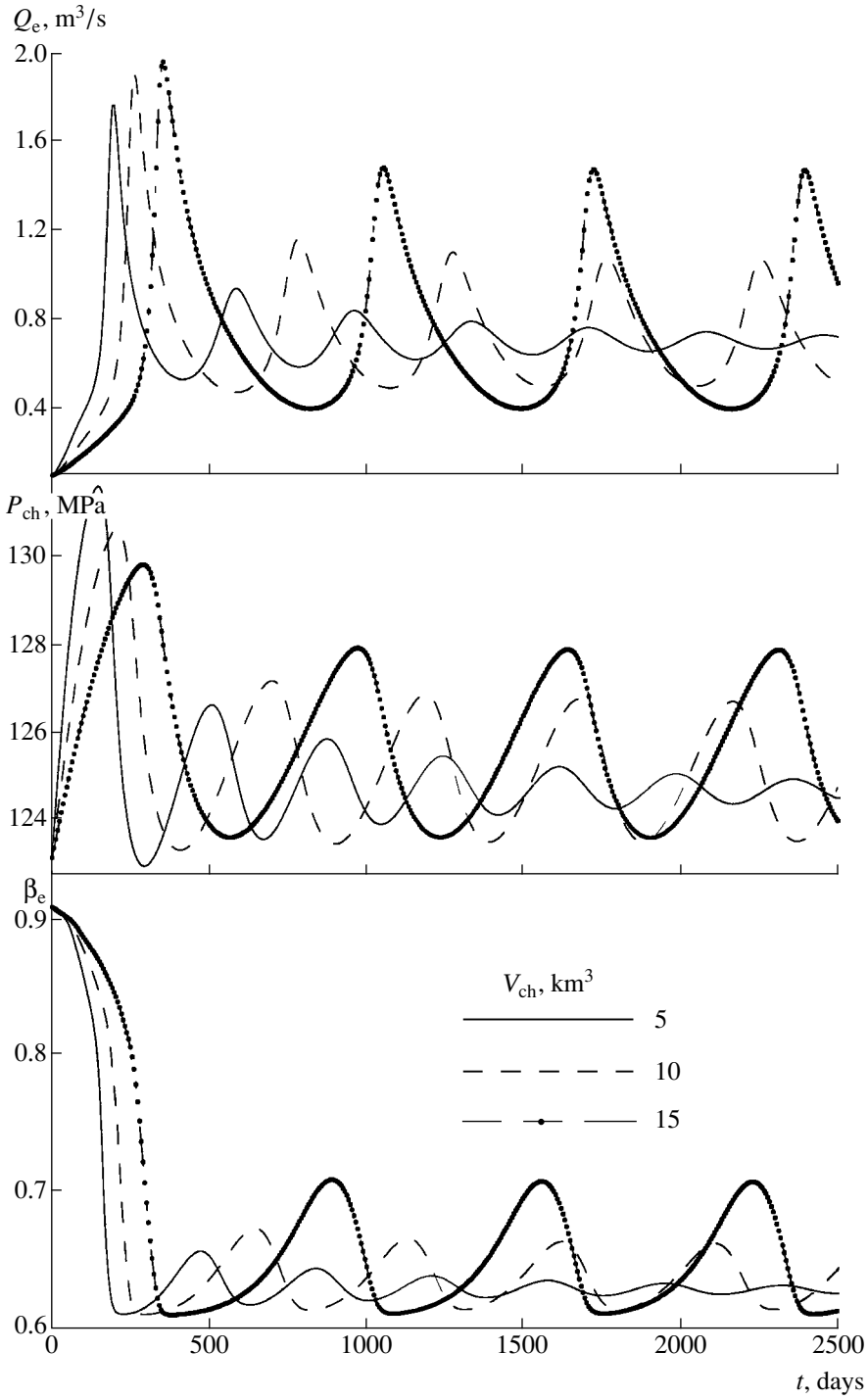

Fig. 2.

zation in the conduit is weak and the mean crystal concentration and, consequently, the magma viscosity are determined by their values in the magmatic chamber. This results in oscillations of Q_e with frequency β_{ch}. Cycles 6–7 weeks in duration were recorded for eruption of the Soufriere Hills volcano in the course of the overall activity increase in the vicinity of the maximum of the two-year cycle [11].

The constructed unsteady model for a volcanic eruption with allowance for magma crystallization and gas filtration through the magma provides an example of an object with distributed parameters possessing both limiting steady-state and periodic solutions. The calculations performed provide a method of explaining cyclic variations of the magma discharge rate in the course of an eruption and estimating the

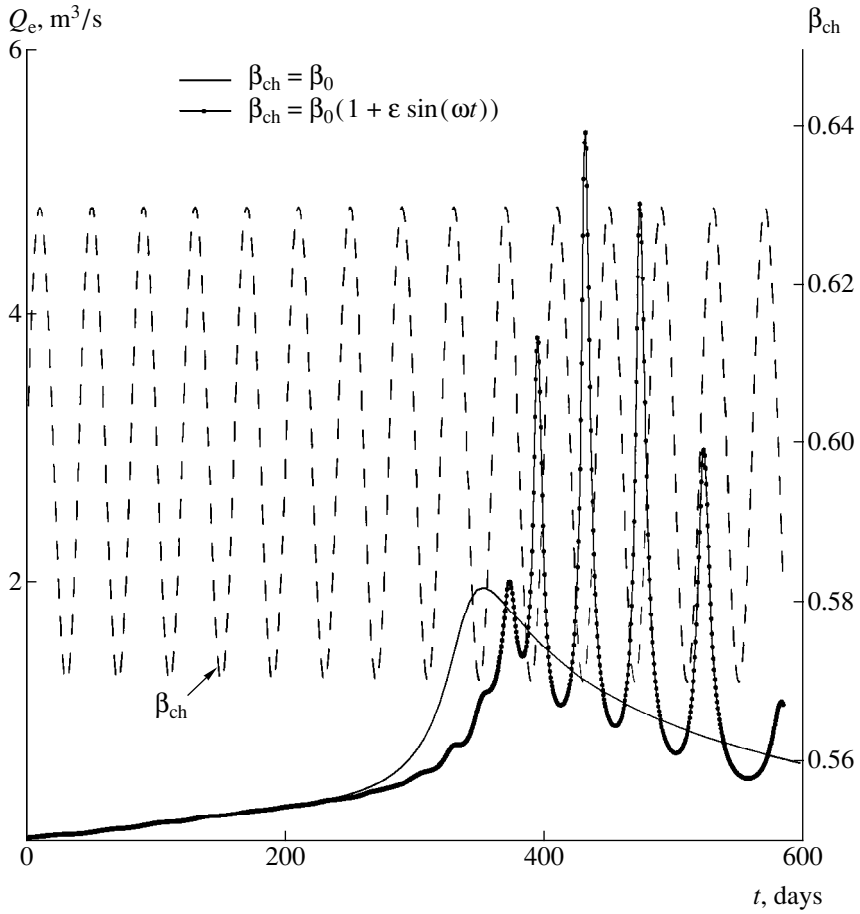

Fig. 3.

magma chamber dimension, which defies direct measurements.

ACKNOWLEDGMENTS

This work was supported by the Russian Foundation for Basic Research, project no. 99-01-01042, and NERC (GR3/11683, Great Britain).

REFERENCES

1. A. A. Barmin and O. É. Mel'nik, Izv. Akad. Nauk, Mekh. Zhidk. Gaza, No. 2, 49 (1993).
2. A. A. Barmin and O. É. Mel'nik, Izv. Akad. Nauk SSSR, Mekh. Zhidk. Gaza, No. 5, 35 (1990).
3. O. É. Mel'nik, Izv. Akad. Nauk, Mekh. Zhidk. Gaza, No. 4, 78 (1996).
4. S. Nakada and Y. Motomura, J. Volcanol. Geotherm. Res. **89**, 173 (1999).
5. K. V. Cashman, Contrib. Mineral. Petrol. **109**, 431 (1992).
6. O. E. Melnik and R. S. J. Sparks, Nature **402**, 37 (1999).
7. K. U. Hess and D. B. Dingwell, Am. Mineral. **81**, 1297 (1996).
8. R. I. Nigmagulin, in *Dynamics of Multiphase Media* (Nauka, Moscow, 1992), p. 360.
9. M. Hort, J. Petrol. **39**, 1063 (1998).
10. R. S. J. Sparks, S. R. Young, J. Barclay, *et al.*, Geophys. Res. Lett. **25**, 3421 (1998).
11. B. Voight, R. S. J. Sparks, A. D. Miller, *et al.*, B.W.I. Sci. **283**, 1138 (1999).

Translated by V. Tsarev

Doklady Physics, Vol. 46, No. 4, 2001, pp. 276–279. Translated from Doklady Akademii Nauk, Vol. 377, No. 5, 2001, pp. 634–637.

MECHANICS

Description of Intermittent Turbulent Flows by Solutions to the Navier–Stokes Equations

V. G. Priymak

Presented by Academician A.A. Samarskiĭ September 26, 2000

Received September 29, 2000

The classical problem of the laminar-to-turbulent transition in a viscous incompressible flow occurring in a pipe of a circular cross section is considered. It is well known that two types of equilibrium flows, statistically homogeneous along the pipe axis, can be observed far from the inlet and outlet sections of a pipe: time-independent (Poiseuille) and time-dependent (turbulent). These flows are well described by time-independent and statistically steady-state solutions to the three-dimensional Navier–Stokes equations, respectively [1, 2]. At the same time, there is experimental evidence [3, 4] that, at the Reynolds numbers $\mathrm{Re} = U_b \times 2R/\nu = 2200$, where U_b, R, and ν are, respectively, the cross-sectional average of fluid velocity, the pipe radius, and the kinematic viscosity, there is another equilibrium self-sustained flow regime in which turbulent puffs, surrounded by almost laminar flow regions and preserving their lengths, drift downstream. Nevertheless, until recently, the very existence of equilibrium puffs and, consequently, of the flow regimes characterized by intermittence at arbitrarily large distances from the pipe inlet was open to question.

In part, this is so because the pipes used in the experiments are not very long and the leading edge of a turbulent puff is highly diffuse. The last circumstance substantially lowers the accuracy of laboratory measurements. Fortunately, the equilibrium puffs are good candidates for direct numerical simulation based on the Navier–Stokes equations with periodic boundary conditions imposed on the flow velocity along the pipe axis (provided that the period X is sufficiently large). Papers [5, 6] describe two attempts at such a simulation at $\mathrm{Re} = 2200$, where $X = 36R$ and $X = 32\pi R$, respectively. The initial conditions used in both cases were specially fitted in the form of structures localized in space. Although the results of these calculations closely resemble the turbulent puffs observed in laboratory experiments, a fairly short computing time in [5], which is equal to $T \approx 120R/U_b$, does not provide an answer to the question of whether the equilibrium puffs exist. As for the investigation carried out in [6], it presents the values of convective rates at leading and trailing edges of turbulent puffs which differ from each other and are equal to $U_{LE} = 1.56U_b$ and $U_{TE} = 0.73U_b$, respectively. This means that either the calculated turbulent flow structure is not equilibrium (and, far from the pipe inlet, the neighboring puffs merge and form a purely turbulent flow) or the computing time ($T \approx 60R/U_b$) is also not sufficiently long.

The author of [7] tried to describe the intermittent flows by solutions of the Navier–Stokes equations with spatial period $X \approx 2\pi R$, which is much shorter than in the above papers. Undamped self-sustained oscillations were calculated at $\mathrm{Re} \geq 2250$. For $2000 < \mathrm{Re} \leq 2200$, they survive for a long time ($T \approx 3000R/U_b$). Then, the perturbations damp rapidly and the flow becomes laminar. The time-dependent solutions to the Navier–Stokes equations obtained in [7] describe flow regimes that are not intermittent, because, as the author points out, velocity oscillations are always chaotic in such flows and a noticeable flow simplification does not occur. On the contrary, the intermittent flows observed in the experiments exhibit essential simplification within a certain part of the pipe, where they become practically laminar. We have repeated some results of [7] by carrying out our calculations according to the algorithm described in [8] at $X = 2\pi R$. Similarly to [7], we established that all time-dependent flow regimes with period $X = 2\pi R$ (both undamped and long-lived and arising at small values of Re) are not intermittent; i.e., they do not consist of turbulent puffs alternating with almost laminar flow regions. This result is quite natural, because, according to experimental data (see, for example, [3]), the lengths of the turbulent puffs are on the order or larger than $40R$. Therefore, description of such a flow structure by solutions of spatial period $X = 2\pi R$ is obviously unrealistic (see also [9]).

To clarify the question of whether the equilibrium puffs exist in reality and, if so, what space–time structure they have, we have carried out a special series of calculations in the range of the transitional Reynolds numbers $1800 \leq \mathrm{Re} \leq 4000$. Due to the application of

Institute of Mathematical Modeling,
Russian Academy of Sciences,
Miusskaya pl. 4a, Moscow, 125047 Russia

1028-3358/01/4604-0276$21.00

an accurate and efficient numerical algorithm [8], we could perform the calculations over very long time intervals for each value of the Reynolds number [$T \approx (2500–4000)R/U_b$ at Re about 2200] using a Hitachi SR8000 parallel supercomputer at the Tokyo University. An exclusively long time of simulation entirely ensures us that the obtained flow regimes are equilibrium and self-sustained. Moreover, according to the calculations, stabilization of flow characteristics (for example, after a change of Re) is rather slow and, at Re ≈2200, takes a time on the order of $(500–1000)R/U_b$. This value is larger by a factor of 5–10 than the total lengths of time intervals used in [5, 6] for integration of the Navier–Stokes equations for the same Reynolds number.

All our calculations were carried out within the framework of the so-called long-wave approximation. This means that numerical solutions to the Navier–Stokes equations were sought as those having a considerable period $X = 16\pi R$ of velocity variation along the pipe axis. As was shown in [9], the value of $16\pi R$ is approximately twice the minimum period that allows adequate description of the long-wave motions characteristic of transitional Reynolds numbers); the calculations were carried out with a resolution of $(Q + 1) \times (2N + 1) \times (2M + 1) = 33 \times 41 \times 321$ points along the radial (r), azimuthal (φ), and longitudinal (x) coordinates, respectively. Below, we present the flow parameters corresponding to Re = 2200. They are $\mathrm{Re}_\tau = u_\tau \times 2R/\nu \approx 153$ (where $u_\tau = \sqrt{\bar{\tau}_w/\rho}$, $\bar{\tau}_w$ is the average tangential wall stress and ρ is the fluid density); the period $X^+ = Xu_\tau/\nu \approx 3846$; the minimum resolved wavelengths $\lambda_\varphi^+ = \pi \times 2Ru_\tau/N\nu \approx 24$ and $\lambda_x^+ = Xu_\tau/M\nu \approx 24$ in φ (at $r = R$) and x, respectively; the maximum and minimum distances in r $\Delta r_{\max}^+ = \Delta r_{\max} u_\tau/\nu \approx 3.75$ and $\Delta r_{\min}^+ = \Delta r_{\min} u_\tau/\nu \approx 0.09$ between the collocation points; the calculation time $T \approx 2405R/U_b \approx 167R/u_\tau$; and the drag coefficient $C_f = -\langle \nabla p \rangle_{r\varphi xt} D/2\rho U_b^2 \approx 9.68 \times 10^{-3}$, where $D = 2R$ and $\langle \nabla p \rangle_{r\varphi xt}$ is the time- and space-averaged pressure gradient. It should also be emphasized that the initial conditions used for integration of the Navier–Stokes equations were not *a priori* close to the desired intermittent flow regime.

The numerical simulation is carried out for 11 values of the Reynolds number (see Fig. 1). As initial conditions for the first calculation performed at Re = 4000, we use the superposition of the Poiseuille flow and of the least damping axisymmetric and three-dimensional eigenfunctions, which correspond to certain longitudinal and azimuthal wave numbers (see also [8]). The arrow in Fig. 1 connects the initial and final states of the process of transition to turbulence, where the open circle ($t = 0$) and filled circle *1* correspond, respectively, to the perturbed laminar flow and to the steady-state turbulent regime forming at Re = 4000. At smaller Reynolds numbers Re, turbulent, intermittent, and laminar flow regimes (filled circles numbered from *2* to *11*) are obtained successively; i.e., the statistically steady-state velocity field corresponding to the final stage of the ith calculation represents the initial data for the $(i + 1)$th calculation ($i = 1, 2, \ldots$).

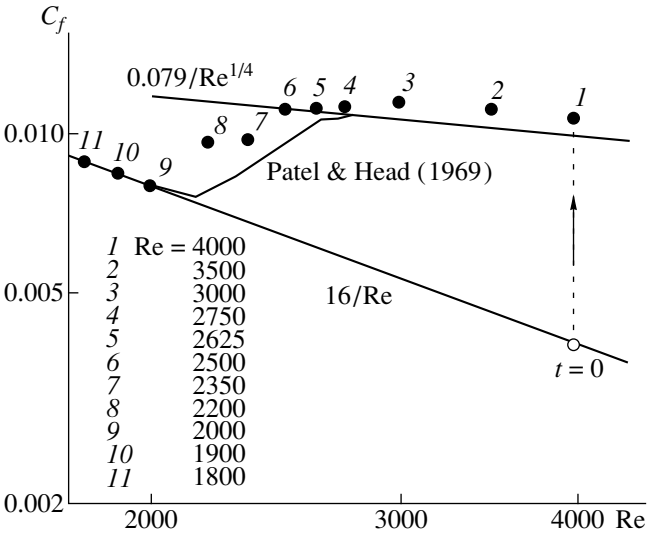

Fig. 1. Dependence of the drag coefficient on the Reynolds number. Dots (*1*)–(*6*), (*7*) and (*8*), and (*9*)–(*11*) correspond to purely turbulent flows, the regimes with alternating equilibrium puffs and laminar flow regions, and laminar Poiseuille flows, respectively.

Flows *1–6* can be considered purely turbulent, because the corresponding drag coefficients C_f agree well with the Blasius drag law $C_f = 0.079\mathrm{Re}^{-1/4}$ and these flows have no laminar inclusions. The last finding is illustrated in Fig. 2, where we show typical distributions of the longitudinal velocity component along the pipe axis ($r = 0$) for four Reynolds numbers: Re = (a) 2200, (b) 2350, (c) 2500, and (d) 4000. One can see that for Re = 4000 and 2500, the longitudinal velocity component exhibits no characteristic decrease in a certain (locally turbulent) region of the pipe axis. Conversely, at Re = 2200 and 2350 (Figs. 2a, 2b), a decrease in the longitudinal velocity component, which represents a property of all turbulent puffs, is clearly discernible and similar to that observed in laboratory experiments. Dotted lines plotted here pertain to laminar Poiseuille flows. Additional support of this fact is presented in Fig. 3, which shows, at Re = 2200, a fragment of the typical time variation of the longitudinal velocity component at a certain point of the pipe axis. The total time of integration of the Navier–Stokes equations is much longer than that shown in Fig. 2: after the statistically steady state has been reached, the calculation continued for a time $T \approx 2000R/U_b$. Such extraordinarily time consuming calculations allow us to assert that the intermittent flows simulated at Re = 2200

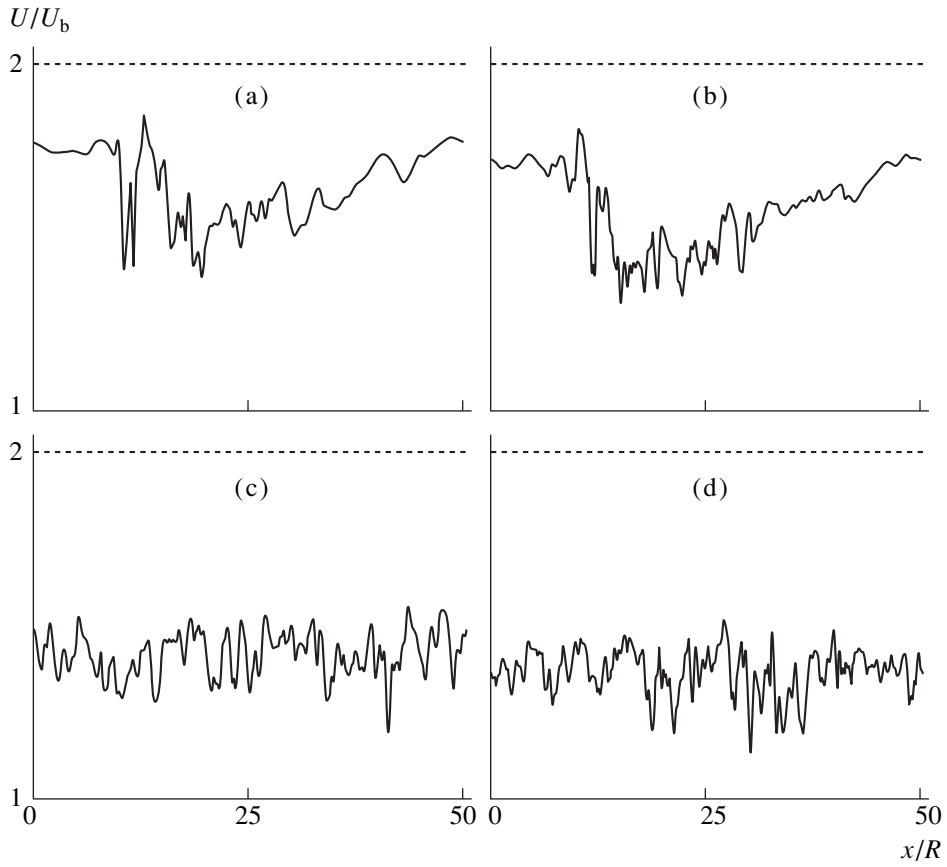

Fig. 2. Typical distributions of the longitudinal velocity component along the pipe axis.

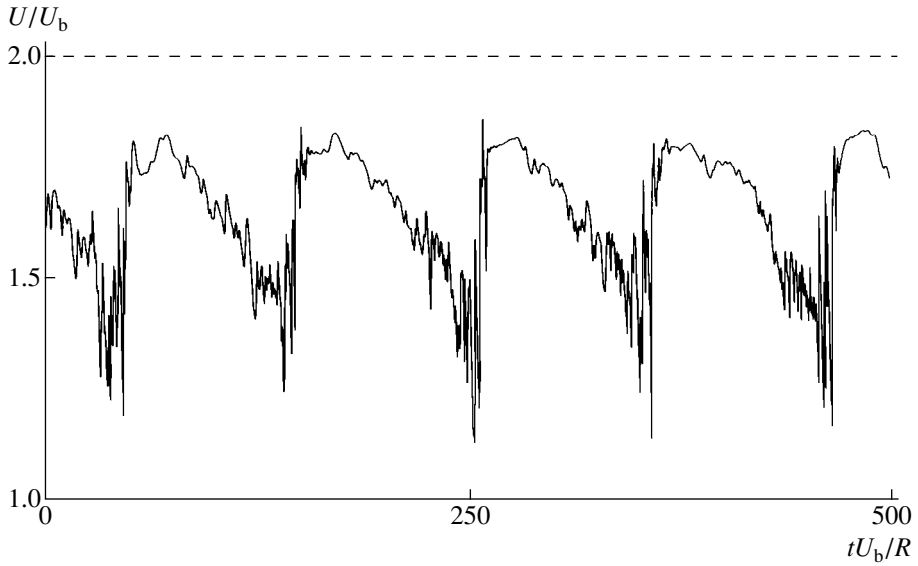

Fig. 3. Typical time variation of the longitudinal velocity component at a point on the pipe axis (Re = 2200).

and 2350 contain equilibrium self-sustained turbulent puffs.

From the above discussion we can make the following conclusions: (1) The equilibrium puffs do exist. (2) They can be described by long-wavelength solutions to the three-dimensional time-dependent Navier–Stokes equations at $2200 \le \mathrm{Re} \le 2350$. (3) In the present work, we performed systematic numerical simulation

of viscous incompressible flows formed in a pipe of a circular cross section in the entire range of transitional Reynolds numbers, including purely turbulent flows ($2500 \le Re \le 4000$), equilibrium self-sustained flows with alternating laminar and turbulent regions ($Re = 2200, 2350$), and purely laminar flows ($Re \le 2000$). (4) Flow-velocity fields recorded on magnetooptical carriers allow the distributions of certain quantities to be calculated at various distances from the leading and trailing edges of a turbulent puff. These quantities are the average velocity, the velocity components, the pressure, the Reynolds stresses, and all terms of the equation describing transport of kinetic turbulent energy. Study of the details of space–time and wave structures of equilibrium puffs is also prospective.

ACKNOWLEDGMENTS

I thank T. Miyazaki for his help in my work.

This study was supported in part by the Russian Foundation for Basic Research, project no. 99-01-00838.

REFERENCES

1. V. G. Priymak, Dokl. Akad. Nauk SSSR **316**, 71 (1991) [Sov. Phys. Dokl. **36**, 28 (1991)].
2. J. G. M. Eggels, F. Unger, M. H. Weiss, *et al.*, J. Fluid Mech. **268**, 175 (1994).
3. I. J. Wygnanski and F. H. Champagne, J. Fluid Mech. **59**, 281 (1973).
4. I. Wygnanski, M. Sokolov, and D. Friedman, J. Fluid Mech. **69**, 283 (1975).
5. A. Leonard and W. C. Reynolds, Lect. Notes Phys. **320**, 113 (1985).
6. H. Shan, B. Ma, Z. Zhang, and F. T. M. Nieuwstadt, J. Fluid Mech. **387**, 39 (1999).
7. N. V. Nikitin, Izv. Akad. Nauk, Mekh. Zhidk. Gaza, No. 6, 14 (1994).
8. V. G. Priymak and T. Miyazaki, J. Comput. Phys. **142**, 370 (1998).
9. V. G. Priymak and T. Miyazaki, Phys. Fluids **6**, 3454 (1994).
10. V. C. Patel and M. R. Head, J. Fluid Mech. **38**, 181 (1969).

Translated by Yu. Verevochkin

Doklady Physics, Vol. 46, No. 4, 2001, pp. 280–285. Translated from Doklady Akademii Nauk, Vol. 377, No. 6, 2001, pp. 758–763.

MECHANICS

Variational Inverse Boundary Value Problems of Aerohydrodynamics

A. M. Elizarov and D. A. Fokin

Presented by Academician G.G. Chernyĭ November 13, 2000

Received November 22, 2000

1. INTRODUCTION

In this paper, we use the term "variational inverse boundary value problems" (VIBV problems) to denote a class of boundary value problems with unknown boundaries, for which both solutions to a partial differential equation and domain D of its definition are desired quantities. In this case, domain D has an extremum property and one boundary condition is imposed on boundary ∂D. The extremum property of D manifests itself in a maximization (minimization) condition imposed on a given functional J (usually, under additional constraints). As to their formulation, the above problems belong to optimum-design problems (see, e.g., [1]). However, the solvability of these problems can be significantly affected by the presence (or absence) of additional constraints. Therefore, it is necessary to specify what functionals need to be considered and what additional constraints have to be imposed. It is difficult to answer these questions as based on general considerations. At the same time, theories of modeling natural phenomena (for example, gas flows or fluid flows) often involve VIBV problems. Classical aerohydrodynamics is one of such theories.

2. VIBV PROBLEMS IN AEROHYDRODYNAMICS

The problems mentioned above arise in one of the methods for optimizing aerodynamic profiles. In the two-dimensional case, the method consists in designing profiles that have optimum characteristics (a maximum lift coefficient or best aerodynamic characteristic, a minimum drag, etc.). In the case of an ideal-fluid flow or a subsonic gas flow, such problems are reduced, mathematically, to VIBV problems for analytical functions. For example, in [2], it was proved that among smooth arcs with a given length and a bounded curvature, the maximum velocity circulation Γ (hence, the maximum lift force Y) in an ideal incompressible fluid flow without separation is attained for a circular arc. A series of important results concerning the VIBV problems in aerohydrodynamics was obtained in the theory of jet and cavity flows, when solving the optimization problems with depression curves in the filtration theory, and in designing optimum aerodynamic profiles for supersonic and hypersonic flows (a review of these results and references can be found in [3–6]).

In the VIBV problems for all analytical functions which have been investigated to date, we can study whether the problem is well-posed provided that the set of desired domains can be given as a set of images for a canonical domain (in particular, the exterior of the unit circle $E^- = \{\zeta: |\zeta| > 1\}$) in a specific class of conformal and quasi-conformal mappings described by a control function P. After passage to the canonical domain, the problem functional can be presented in the form $J = J(P)$. In aerohydrodynamical VIBV problems, the procedure described above is implemented in the following manner.

We specify a class **L** of closed piecewise smooth profiles with a given perimeter L (Fig. 1) as a set of images of a unit circle under the conformal mappings $z = z_P(\zeta)$, $\zeta \in E^-$. These mappings are normalized in accordance with the conditions $z_P(\infty) = \infty$ and $z_P(1) = 0$ and are determined by the control function $P(\gamma)$, $\gamma \in [0, 2\pi]$, where γ is the polar angle for the circle points $\zeta = \exp(i\gamma)$. We assume that these profiles are impenetrable (with the possible exception of isolated singularities) and that an ideal fluid flows around them. The flow velocity v_∞ at infinity is horizontal, with $w = w(z)$ being the flow complex-valued potential. Let the func-

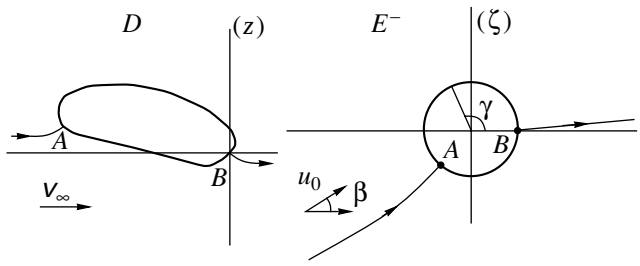

Fig. 1. Class of profiles being optimized.

Chebotarev Scientific Research Institute of Mathematics and Mechanics, Kazan State University, ul. Universitetskaya 17, Kazan, 420008 Russia

1028-3358/01/4604-0280$21.00 © 2001 MAIK "Nauka/Interperiodica"

tion $P(\gamma)$ satisfy the Hölder condition with a certain index (this condition is sufficient for the existence of improper integrals) and determine the limiting values on the circle of the real part of the function:

$$\chi(\zeta) = \chi_0(\zeta) - \chi_1(\zeta), \quad \chi_0(\zeta) = \ln\left[v_\infty^{-1}\frac{dw}{dz}(\zeta)\right].$$

This function is the difference between the Mitchell–Joukowski function $\chi_0(\zeta)$ and a proper function $\chi_1(\zeta)$, which is chosen to eliminate the singularities determined by the zeros and poles of the complex-conjugate velocity $\frac{dw}{dz}$. It is advisable to take $\chi_1(\zeta) = \ln\left(u_0^{-1}\frac{dw}{d\zeta}\right)$, where $w = w(\zeta)$ is the complex-valued potential for the flow around a circle and u_0 is the incident-flow velocity in plane ζ. In this case, $\left.\frac{dw}{d\zeta}\right|_\infty = u_0\exp(-i\beta)$, where β is the so-called theoretical angle of attack, which determines the angular deviation of the profile from the direction ensuring a circulation-free flow around this profile. Hence, $\chi(\infty) = i\beta$ and we have

$$\chi(\zeta) = \ln\frac{u_0}{v_\infty} - \ln\frac{dz}{d\zeta} - (2\pi)^{-1}\int_0^{2\pi} P(\gamma)\frac{e^{i\gamma}+\zeta}{e^{i\gamma}-\zeta}d\gamma + i\beta, \qquad (1)$$
$$P(\gamma) = \Re\chi(e^{i\gamma}), \quad \gamma \in [0, 2\pi].$$

Here, the density $P(\gamma)$ for the Schwartz integral satisfies the condition

$$\int_0^{2\pi} P(\gamma)d\gamma = 0. \qquad (2)$$

(Hereinafter, $\Re$ denotes the real part of a complex-valued function.) It follows from (1) that

$$\frac{dz}{d\zeta} = u_0 v_\infty^{-1}\exp[-\chi(\zeta)]. \qquad (3)$$

Because the profiles belonging to class **L** are assumed to be closed [i.e., the functions $z_P(\gamma)$ are one-valued], function $P(\gamma)$ must satisfy solvability conditions for the inverse boundary value problems in aerohydrodynamics, namely, the conditions for the closure of profile L (see [5, Ch. 2]):

$$\int_0^{2\pi} P(\gamma)\cos\gamma d\gamma = \int_0^{2\pi} P(\gamma)\sin\gamma d\gamma = 0. \qquad (4)$$

Finally, the class **L** of the profiles under consideration is defined by the conformal mappings $z = z_P(\zeta)$ determined from (3), while the control function $P(\gamma)$ satisfies constraints (2) and (4) in addition to those described above. Parameter u_0 specifies the linear scale in the physical plane and (since parameter L is given for profiles belonging to class **L**) is related to function $P(\gamma)$ by the equality following from (3):

$$u_0 = \frac{Lv_\infty}{J(P)}, \quad J(P) = \int_0^{2\pi}\exp[-P(\gamma)]d\gamma.$$

In this case, we assume that the flow trailing point is the original of the point $\zeta = 1$. The theoretical angle of attack $\beta \in (0, \pi/2]$ is an optimization parameter.

We consider the following variational problem.

Problem A. *It is required to find the impenetrable profile* (*belonging to the class* **L**) *which maximizes the lift force* (*or, which is the same, the velocity circulation*) *in an ideal flow without separation around the desired profile, with the velocity* v_∞ *given at infinity and the flow branching point being on the desired profile.*

As is known from the theory of inverse boundary value problems in aerohydrodynamics [5, 7], the solution to Problem A is unambiguously determined from (1) provided that the velocity $v = v(s)$ on the desired profile is given as a function of the arc length s of this profile. In this case, function $P(\gamma)$ and angle β are unambiguously determined by the distribution $v = v(s)$. To solve Problem A with regard to the equality

$$\Gamma = J_1(v) \equiv \int_0^L v(s)ds,$$

we have to maximize the functional $J_1(v)$ in the corresponding class of the functions $v(s)$. This class is defined by hydrodynamic reasonability conditions (the absence of boundary-layer separation, the limitation for the maximum velocity on the profile, etc.). As a result, informative variational problems appear [5] in which so-called plane-segment profiles, having an interval with a constant velocity, are extrema. In this case, solvability conditions (2) and (4) cannot be expressed in terms of function $v(s)$. Hence, they have to be satisfied either by the fitting of free parameters introduced in the class of profiles $v(s)$ or by employing the method of quasi-solutions to the inverse boundary value problems in aerohydrodynamics [5]. This method affects the extremum profile $v(s)$ in the minimum degree (in terms of the norm of the functional space used). However, it is most important that the value Γ of the velocity circulation (i.e., the extremum value of functional J_1) remains constant, although the angle β certainly varies.

Another way of solving Problem A is based on the following relation of the control function $P(\gamma)$ and the optimization parameter β to the circulation Γ:

$$\Gamma = \frac{4\pi L v_\infty \sin\beta}{J(P)}. \qquad (5)$$

This relation is a consequence of the Joukowski theorem on lift force and of formulas (1). Hence, in order to maximize Γ, we must minimize the functional

$J_0(P, \beta) = \dfrac{J(P)}{\sin\beta}$ under constraints (2) and (4) imposed on the control function $P(\gamma)$. The optimization parameter β is not related to function P; hence, the optimum value of β is, evidently, $\beta = \beta^* = \pi/2$. This corresponds to the flow around the profile in which the branching and trailing points coincide. Such a conclusion is completely consistent with the well-known fact that, in the case of ideal flow around a circle, with the stagnation point on the circumference, the maximum velocity circulation is attained when the trailing and branching points coincide. Our further analysis is based on the following statement.

Lemma 1. *Let the function $P(\gamma)$ belong to $L_2[0, 2\pi]$ and satisfy constraints* (2) *and* (4). *Then, for the strictly convex functional $J(P)$,*

$$\inf_{P(\gamma) \in L_2} J(P) = 2\pi$$

and this value is attained for the unique function $P(\gamma) = P_*(\gamma) \equiv 0$.

It follows from Lemma 1 that the desired optimum profile is determined by the mapping $z(\zeta) = \dfrac{L(\zeta - 1)}{2\pi}$ and is a circle with radius $\dfrac{L}{2\pi}$. The trailing and branching points in an ideal-fluid flow around this profile coincide. The absolute maximum Λ^* for the dimensionless circulation $\Lambda = \dfrac{\Gamma}{L_\infty v} = \dfrac{4\pi\sin\beta}{J(P)} = \dfrac{4\pi}{J_0(P, \beta)}$ is $\Lambda^* = 2$. It is worth noting that $\Lambda = \dfrac{C_y}{4}$, where C_y is the lift coefficient calculated according to the profile semiperimeter.

The above procedure for solving VIBV problems in aerohydrodynamics certainly uses the fact that the control function $P(\gamma)$ is not related to the control parameters (in the simplest case, to the parameter β) through constraints. The relation between function $P(\gamma)$ and the control parameters appears in the process of optimization and is caused by additional constraints. Under physical constraints (the condition for flow without separation with allowance for the flow viscosity in the boundary-layer approximation and the compressibility of the medium, etc.), we fail to prove the uniqueness for the extrema even for strictly convex functionals J. This situation becomes even more complicated if either the profile drag coefficient or the lift-drag ratio (even when both are written out in their explicit form) is chosen as a characteristic to be optimized. As a result, the optimized solutions significantly differ from a circle and can be evaluated only numerically. However, under certain simplifying assumptions (in particular, for the simplest set of empirical constants in the criteria for flow without separation), strictly convex functionals can be obtained and their extrema can be constructed [10–12].

3. A CIRCLE AS AN EXTREMAL SOLUTION

As follows from Lemma 1, in an ideal flow without separation around a profile belonging to the class of smooth closed impenetrable profiles with a fixed perimeter, the maximum lift force Y corresponds to a circle. If point singularities (sources and drains) appear on a profile, relationship (5) will include an additional factor with parameters defining the positions of the originals for these singularities on the circle. These parameters are not related in any way to the control function $P(\gamma)$. Hence, Lemma 1 allows us to state that only a circle can be the optimum solution in these cases. Moreover, because there are no relations between the control function $P(\gamma)$ and the controlling parameters, the initial variational problem is reduced to the minimization problem for a function of several variables under nonlinear constraints (i.e., equalities) [13].

Thus, a circle is an extremum in many of the variational inverse boundary value problems, as well as in the classical isoperimetric problems. Although such a profile does not fulfill the practical requirements of aircraft design, this circular solution is derived analytically under the least constraints following from the mathematical flow model. Therefore, the solution yields the least upper bound for the lift force Y in an ideal incompressible-fluid flow. It is natural to put forth the following question. Are there variational problems in the framework of the model of an ideal flow whose extrema differ from circles? The following problem is a natural generalization of Problem A.

Problem B. *It is required to find the profile in the class* **L** *which maximizes the quantity Y under the condition that the maximum value $v_{\max}$ of the relative flow velocity $\dfrac{v}{v_\infty}$ does not exceed the given value $v_* > 1$.*

It is worth noting that the additional constraint for Problem B takes the form

$$f_\beta(\gamma) \equiv P(\gamma) + \ln[2|\sin(\gamma - \beta) + \sin\beta|] \le \ln v_*, \quad \gamma \in [0, 2\pi]. \tag{6}$$

We now estimate the range of the controlling parameter β using the following statement of F.G. Avkhadiev (see [5, Ch. 53]).

Lemma 2. *Let* $\mathbf{F}(\mathbf{a})$ *be a set of functions analytic in E^-,*

$$F_a(\zeta) = \frac{a}{\zeta} + \sum_{k=2}^{\infty} a_k \zeta^{-k},$$

with a given coefficient $a \neq 0$ and the boundary condition $f_a(\gamma) = \Re F_a(e^{i\gamma})$ be an integrable function. Then, the equality

$$\inf_{F_a \in \mathbf{F}(\mathbf{a})} \sup_{\gamma \in [0, 2\pi]} f_a(\gamma) = \frac{|a|}{2}$$

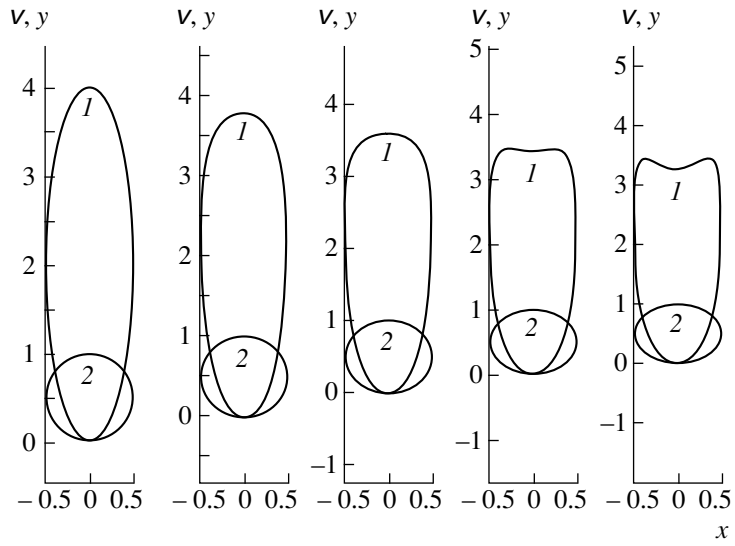

Fig. 2. Optimum profiles for $\beta = \pi/2$ and various v_*.

is valid in the class $\mathbf{F}(\mathbf{a})$ *with the infimum not attainable in* $\mathbf{F}(\mathbf{a})$; *i.e., for an arbitrary function* $f_a(\gamma)$, *we have*

$$\sup_{\gamma \in [0, 2\pi]} f_a(\gamma) > \frac{|a|}{2}. \tag{7}$$

Let

$$F_a(\zeta) = \chi(\zeta) + \ln\left[(1 - \zeta^{-1})\left(1 + \frac{e^{2i\beta}}{\zeta}\right)\right].$$

It is evident that $F_a(\zeta) \in \mathbf{F}(\mathbf{a})$ for $a = 2ie^{i\beta}\sin\beta$ and $f_a(\gamma) \equiv f_\beta(\gamma) = \Re F_a(e^{i\gamma})$. It follows from (7) that inequality $\sin\beta < \ln v_*$ is necessarily valid.

We now formulate the basic statement to be proved.

Theorem 1. *If* $v_* > 1$, *Problem* B *is undoubtedly solvable with* $\sin\beta^* < \ln v_*$ *and* $\Lambda^* < 2\ln v_*$. *In addition, if* $1 < v_* < 4$, *the extremal differs from a circle. If* $v_* \geq 4$, *the unique extremal is a circle. Moreover,* $\Lambda^* \geq v_* - 2$ *and* $\beta^* \geq \arcsin(v_*/2 - 1)$ *if* $2 < v_* \leq 4$, *while* $\Lambda^* = 2$ *and* $\beta^* = \pi/2$ *if* $v_* \geq 4$, *where* Λ^* *and* β^* *are the absolute maximum of* Λ *and the extremum value of* β, *respectively.*

In the particular case of Problem B when the quantity β is given (we referred to this case as Problem B'), the strictly convex functional $J(P)$ must be minimized under constraints (2), (4), and (6), with $\beta = \beta^*$ given.

The following theorem also holds.

Theorem 2. *The inequality* $\sin\beta^* < \ln v_*$ *is a necessary condition for Problem* B' *to be solvable. If* $v_* > 2$ *and* $\sin\beta^* \leq \frac{v_*}{2} - 1$, *the unique extremal is a circle. If* $v_* > 1$ *and* $\max\left\{0, \frac{v_*}{2} - 1\right\} < \sin\beta^* < \ln v_*$, *the extremal differs from a circle.*

In Fig. 2, we present examples of the optimum profiles evaluated numerically at $\beta = 90°$ (when the branching and trailing points coincide) for various values of v_* in the two-parametric set of the functions $P(\gamma) = a\cos 2\gamma + b\sin 2\gamma$ satisfying conditions (2) and (4), where a and b are certain parameters. All the velocity distributions (*1*) and profiles (*2*) are symmetric with respect to the vertical. The first example is a circle with $v_* = 4$. The thickness of these profiles significantly decreases with decreasing v_*, and a nearly straight section appears in the velocity distributions. The calculation results for the maximum lift coefficient $C_{y\max}$ as a function of v_* for various β showed that the values $C_{y\max}$ decrease within admissible ranges by smaller than 8% when the value v_* decreases. Moreover, for each β, there is a minimum value of the maximum velocity on the profile.

The solution given above determines the lower estimate for the dependence $C_{y\max} = C_{y\max}(v_*)$ in a narrowed class of the functions $P(\gamma)$. To exactly solve the problem for fixed β, we performed a numerical optimization for the class of the functions $P(\gamma) = \sum_{k=2}^{k=N} (a_k\cos 2\gamma + b_k\sin 2\gamma)$ by varying the coefficients a_k and b_k. One of the results of this numerical optimization for $\beta = 10°$, $v_* = 1.4$, and $N = 20$ is presented in Fig. 3. This is a symmetric profile (*2*) with a nearly straight section (*1*) in the velocity distribution on the profile upper surface.

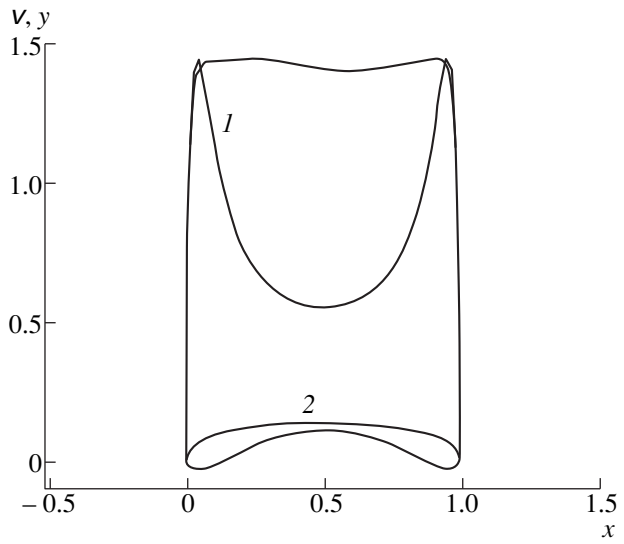

Fig. 3. Numerically optimized profile with a blunted trailing edge for $\beta = 10°$, $C_y = 1.16$, and $\alpha = 0.25°$.

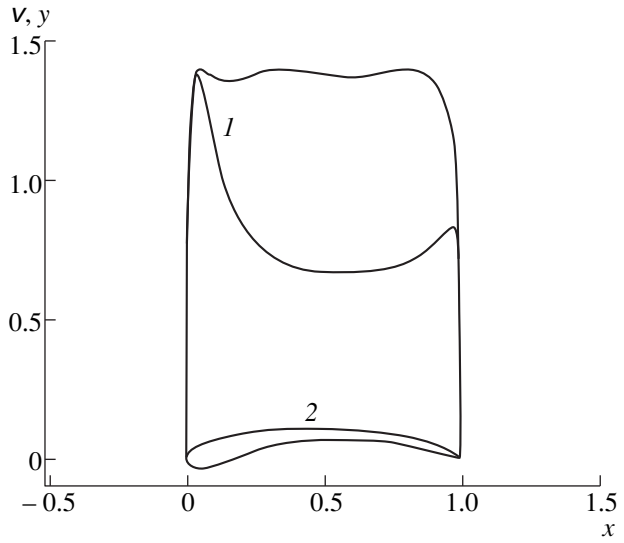

Fig. 4. Numerically optimized profile with a sharp trailing edge for $\beta = 10°$, $C_y = 1.15$, and $\alpha = –1.88°$.

The value $C_y = 1.16$ is attained at the angle of attack $\alpha = 0.25°$.

Actual profiles usually have a cusped trailing edge. In Fig. 4, we present the optimized shape (*2*) for the profile with a cusped trailing edge (with an interior angle of 36°). In this case, the coefficient C_y attains its maximum at $v_* = 1.4$ for $\beta = 10°$. The profile obtained for the calculated angle of attack $\alpha = –1.88°$ has $C_y = 1.15$. This value is fairly close to that evaluated previously for optimized profiles with blunted trailing edges. The velocity distribution (*1*) on the upper surface of the profile obtained has a nearly straight section, but high velocity gradients in the neighborhood of the trailing edge testify to the presence of a detached flow.

We now consider the case when an ideal flow around a desired profile has its branching points inside the flow. In this case, we have (see, for example, [9])

$$\beta = 0, \quad \Gamma > 4\pi u_0, \quad \frac{dw}{d\zeta} = \frac{u_0(\zeta + ir)(\zeta + i/r)}{\zeta^2},$$

where $\zeta_* = -ir$ is the original of the branching point and $r > 1$ is a parameter. We again introduce the function $P(\gamma)$ and use relationships (2)–(4). The equality

$$\Gamma = \frac{2\pi L v_\infty (r^2 + 1)}{rJ(P)}$$

is an analogue of (5). Because functional $J(P)$ has a lower bound, the upper bound of Γ goes to infinity with increasing r in the case of fluid flow around an arbitrary profile. Therefore, in this situation, Problem A loses its meaning.

In the case of Problem B, the inequality

$$f_r(\gamma) \equiv P(\gamma) + \ln(r^2 + 2r\sin\gamma + 1) - 2\ln r \le \ln\frac{v_*}{r},$$

$$\gamma \in [0, 2\pi]$$

is an analogue of condition (6). After fixing quantity r, we arrive at an analogue for Problem B'. The following theorem on the solvability of these problems sums up the above considerations.

Theorem 3. *If an ideal flow around a profile belonging to class* **L** *has its branching points inside the flow, then the following statements are true.*

(1) *Problem* B *is solvable only for* $v_* > e$, *with* $\Lambda^* \le r_* + r_*^{-1}$. *For* $e < v_* < 4$, *the extremum differs from a circle.*

(2) *The inequalities* $1 < r \le r_*$ *and* $v_* > e$ *are necessary conditions for Problem* B' *to be solvable. The solution is unique and is a circle, with* $\Lambda^* = r + r^{-1}$ *if* $1 < r \le r_1$ *and* $v_* > 4$. *In the case of* $r_1 < r \le r_*$, *the extremal differs from a circle, with* $\Lambda^* \le r + r^{-1}$.

Here, $r_1 = \frac{1}{2}(v_* - 2 + \sqrt{v_*^2 - 4v_*})$ *and* r_* *is a single root of the equation* $r\ln\frac{v_*}{r} = 1$.

ACKNOWLEDGMENTS

This work was supported by the Russian Foundation for Basic Research, project no. 99-01-00173, and by the Humboldt Foundation.

REFERENCES

1. J. Haslinger and P. Neittaanmaki, *Finite Element Approximation for Optimal Shape Design: Theory and Application* (Wiley, New York, 1988).

2. M. A. Lavrent'ev, *Proceedings of Central Institute of Aerohydrodynamics*, Vol. 155: *About an Extremal Problem and Theory of Airplane Wing* (Tsentr. Aérogidrodin. Inst., Moscow, 1934).
3. A. L. Gonor and G. G. Chernyĭ, in *Theory of Optimum Aerodynamic Shapes*, Ed. by A. Miele (Academic, New York, 1965; Mir, Moscow, 1969), pp. 292–305; 379–395.
4. A. N. Kraĭko, *Variational Problems of Gas Dynamics* (Nauka, Moscow, 1979).
5. A. M. Elizarov, N. B. Il'inskiĭ, and A. V. Potashev, *Inverse Boundary-Value Problems of Aerohydrodynamics: Theory and Methods for Design and Optimization of Wing-Shape Profiles* (Fizmatlit, Moscow, 1994).
6. D. V. Maklakov, *Nonlinear Problems of Hydrodynamics of Potential Flows with Free Boundaries* (Yanus-K, Moscow, 1997).
7. A. M. Elizarov, N. B. Il'insky, and A. V. Potashev, *Mathematical Methods of Airfoils Design. Inverse Boundary Value Problems of Aerohydrodynamics* (Wiley, Berlin, 1997).
8. A. M. Elizarov, Izv. Vyssh. Uchebn. Zaved., Mat., No. 10, 71 (1988).
9. M. A. Lavrent'ev and B. V. Shabat, *Methods in Theory of Functions of Complex Variables* (Nauka, Moscow, 1987).
10. A. M. Elizarov and E. V. Fedorov, Prikl. Mat. Mekh. **54**, 571 (1990).
11. A. M. Elizarov, E. V. Fedorov, and D. A. Fokin, Zh. Vychisl. Mat. Mat. Fiz. **33**, 958 (1993).
12. D. A. Fokin, Izv. Akad. Nauk, Mekh. Zhidk. Gaza, No. 3, 177 (1998).
13. D. F. Abzalilov and N. B. Il'inskiĭ, Dokl. Akad. Nauk **354**, 43 (1997) [Phys. Dokl. **42**, 265 (1997)].

Translated by V. Chechin

Doklady Physics, Vol. 46, No. 4, 2001, pp. 286–290. Translated from Doklady Akademii Nauk, Vol. 377, No. 6, 2001, pp. 764–768.

MECHANICS

Stability of a Thin Round Plate in Radial Compression

Yu. V. Zakharov* and K. G. Okhotkin**

Presented by Academician K.S. Aleksandrov September 11, 2000

Received September 25, 2000

Problems on the behavior of constructions (shells, membranes, rod systems, etc.) under the action of loads rapidly varying in time-dependent and true impact loads are of crucial importance both theoretically and in practice; however, their exact solutions are extremely difficult to obtain. Very often, such problems are solved by approximate or numerical methods; it has been possible to solve only a few of them analytically.

In the previous authors' papers [1, 2], the problem on magnetization reversal of a magnetic sheath with asymmetric boundary conditions was shown to be similar to Euler's stability problem for an elastic rod. For magnetic systems, a sequence of stability-loss threshold fields for a ferromagnetic layer was found and analogy to the dynamic stability loss for elastic systems studied by Lavrent'ev and Ishlinskiĭ [3] was drawn.

The analogy found allows a number of analytic results for describing the stability of the magnetic and elastic systems to be obtained. Thus, for elastic systems, we found exact solutions to the nonlinear equation of strong bending for an elastic rod-cantilever under the action of a transverse concentrated load at the free end [4].

The theoretical results obtained permit analysis of more involved elastic systems in a new way, in particular, the problem on thin-plate bending.

Problems on elastic-system bending are conventionally solved for geometrically linear equations for deflections using complicated trial functions for stresses [10–12]. In this case, sophisticated approximate calculating methods (Bubnov–Galerkin method, perturbation theory, etc.) must be used [10–13].

In the present study, an approach is proposed involving consistent analysis of geometrically nonlinear equations of the Föppl–Karman type for elastic-system deflections under the action of external forces [5–7].

Using this approach, we shall obtain an analytically exact solution to a model problem on strong bending of an elastic round thin plate.

We consider a geometrically nonlinear case and construct a system of solutions by analogy with the results for nonlinear bending of a thin rod [4] assuming that the plate is initially planar and is fixed at the edge. Hooke's law is assumed to be satisfied.

For describing the plate deflection, we use the widely known static equations of plate equilibrium [5–7] in the form [8–10]

$$\begin{aligned} D\Delta\Delta u_z \pm \Delta_k\Phi &= q, \\ \Delta\Delta\Phi \mp Eh\Delta_k u_z &= 0, \end{aligned} \tag{1}$$

where the desired functions u_z are the components of the elastic-displacement vector for points of the middle plate surface in the normal direction and Φ is the stress function; $D = \dfrac{Eh^3}{12(1-\mu^2)}$ is the cylindrical rigidity of the plate, E is Young's modulus, μ is Poisson's ratio, h is the plate thickness; Δ is the Laplace operator in arbitrary surface curvilinear coordinates and Δ_k is a mixed-type operator. For an arbitrary surface with a metric g_{ij} and second-quadratic-form components b_{ij},

$$\Delta f(x^1, x^2) \equiv \frac{1}{\sqrt{\det g}}\frac{\partial}{\partial x^i}\left(\sqrt{\det g}\,g^{ij}\frac{\partial f}{\partial x^j}\right), \quad i, j = 1, 2, \tag{2}$$

$$\Delta_k f(x^1, x^2) \equiv \frac{1}{\sqrt{\det g}}\frac{\partial}{\partial x^i}\left(\frac{\sqrt{\det b}(-1)^{i+j}b^{ij}}{\sqrt{\det g}}\frac{\partial f}{\partial x^j}\right), \quad i, j = 1, 2. \tag{3}$$

To reveal the effects associated with the geometric nonlinearity of the problem, we use exact expressions for the surface curvature instead of the popular approximation, where deflections are assumed to be small as compared to the overall plate dimensions. In our case, the first equation of system (1) for an initially unbent plate in arbitrary surface orthogonal coordinates (α, β)

* *Kirenskiĭ Institute of Physics, Siberian Division, Russian Academy of Sciences, Akademgorodok, Krasnoyarsk, 660036 Russia*

** *Siberian State Technological University, Prospect Mira 82, Krasnoyarsk, 650049 Russia*

1028-3358/01/4604-0286$21.00

for an arbitrary external load takes the following exact form:

$$D\Delta(\kappa_\alpha + \kappa_\beta) \pm h\sum_{\alpha\beta}\sigma_{\alpha\beta}\chi_{\alpha\beta} = q. \quad (4)$$

Here, $\sigma_{\alpha\beta} = \begin{pmatrix} \sigma_\alpha & \tau \\ \tau & \sigma_\beta \end{pmatrix}$ is the stress tensor and $\chi_{\alpha\beta} = \begin{pmatrix} \kappa_\alpha & \chi \\ \chi & \kappa_\beta \end{pmatrix}$ is the matrix of the principal surface curvatures κ and torsion χ. The minus sign corresponds to the positive direction of the external-load vector q, and the vector $u_z = w$ corresponds to the elastic displacement of a surface point along the internal normal to the plate surface. The desired surface-bending function (deviation from the equilibrium) enters into this equation through the surface curvatures. The radial load is expressed in terms of the stresses σ. The transverse load q appears in the equation explicitly. In the general case, to this equation, one should add the equation for the stress function, i.e., the continuity equation for the plate middle surface. In cylindrical coordinates, Eq. (4) takes the form

$$D\Delta_r(\kappa_r + \kappa_\varphi) + h(\sigma_r\kappa_r + \sigma_\varphi\kappa_\varphi) = q. \quad (5)$$

The following designations are introduced: R is the plate radius, w is the deflection, and p is the constant radial load uniformly distributed along the length of the contour. Here, we assume that the contour points freely transfer in the radial direction. The external distributed transverse load is absent; i.e., $q = 0$. In our case, we have axisymmetric buckling when the median plate plane changes to a surface of revolution (Fig. 1).

We introduce the tangent slope in the radial direction at the moving point $\theta(r)$ as the desired function (Fig. 1). The Laplace operator obtained from (2) is of the form

$$\Delta_r = \frac{\cos\theta_r}{r}\frac{d}{dr}\left(r\cos\theta_r\frac{d}{dr}\right). \quad (6)$$

The function $\theta(r)$ appears in Eq. (5) through the curvatures

$$\kappa_r = \cos\theta\frac{d\theta}{dr}, \quad \kappa_\varphi = \frac{\sin\theta}{r}, \quad \kappa_\varphi + \kappa_r = \frac{1}{r}\frac{d}{dr}(r\sin\theta).$$

For Eq. (5), we obtain

$$D\frac{\cos\theta}{r}\frac{d}{dr}\left(r\cos\theta\frac{d}{dr}\left(\frac{1}{r}\frac{d}{dr}(r\sin\theta)\right)\right) + h\left(\sigma_r\cos\theta\frac{d\theta}{dr} + \sigma_\varphi\frac{\sin\theta}{r}\right) = 0. \quad (7)$$

The boundary conditions for a plate with its edges rigidly bound to the contour are of the form

$$\theta(R) = 0, \quad \theta(0) = 0, \quad \theta(r) < \infty. \quad (8)$$

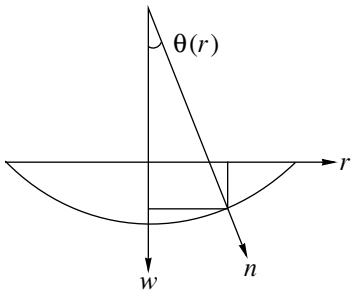

Fig. 1. Coordinate system.

From the equilibrium condition for a round plate, the radial σ_r stresses and the arc σ_φ stresses are related through the expression

$$\sigma_\varphi = \cos\theta\frac{d}{dr}\left(\frac{r\sigma_r}{\cos\theta}\right). \quad (9)$$

Using (9), we eliminate stress σ_φ in Eq. (7). Next, in our case of nonlinear deflection, we employ the expression for the radial stress $\sigma_r = p\cos^2\theta$ and perform the appropriate integration [the integration constant vanishes due to the boundedness condition for $\theta(r)$]. Then, we obtain the nonlinear second-order equation for $\theta(r)$:

$$\frac{d}{dr}\left(\frac{1}{r}\frac{d}{dr}(r\sin\theta)\right) + \frac{hp}{D}\sin\theta = 0. \quad (10)$$

The Bessel functions of the first kind with subscript 1 are the solutions to this equation, since the Bessel functions of the second kind J_1 are unbound at zero. We have

$$\sin\theta(r) = kJ_1(\lambda r), \quad (11)$$

where k is the integration constant and $\lambda = \sqrt{\frac{hp}{D}}$. The condition $\theta(R) = 0$ results in $J_1(\lambda R) = 0$; from this equation, we have $\lambda = \tau_n/R$, where τ_n is the nth zero of the Bessel function $J_1(r)$. Knowing the dependence $\theta(r)$, we express the plate profile $w(r)$ and curvilinear length $l(r)$ explicitly in terms of quadratures:

$$w(r) = \int_R^r \tan\theta(r)dr, \quad l(r) = \int_0^r \sec\theta(r)dr,$$

where the conditions $w(R) = 0$ and $l(0) = 0$ are taken

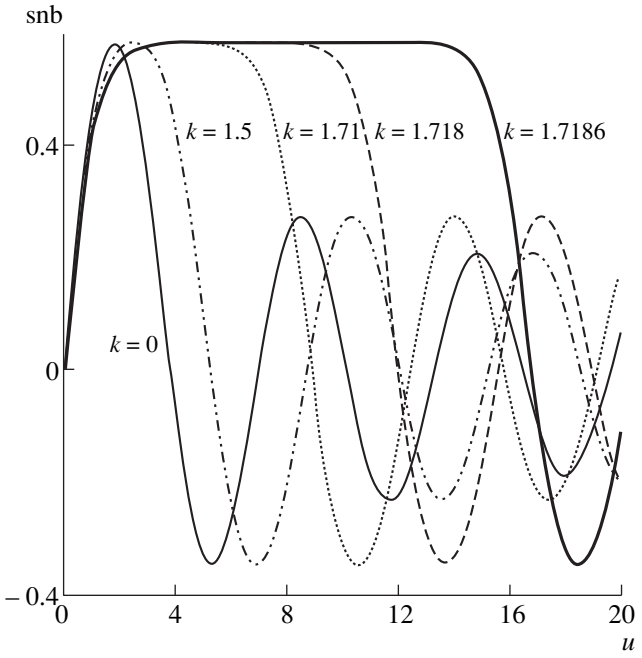

Fig. 2. "Elliptic Bessel sine" for various values of the modulus k. It is seen that the first "half-period" of the function tends to infinity when $k \longrightarrow k_{\max}$, the other periods being essentially unchanged.

into account. Using (11), we have

$$w(r) = -\int_r^R \frac{k_n J_1(\tau_n r/R)dr}{\sqrt{1-k_n^2 J_1^2(\tau_n r/R)}},$$
$$l(r) = \int_0^r \frac{dr}{\sqrt{1-k_n^2 J_1^2(\tau_n r/R)}}. \quad (12)$$

The form of the expressions obtained (12) is similar to the structure of the elliptic integrals in the Lagrange normal form. Therefore, it is worthwhile introducing a new system of special functions, i.e., integrals and their inversions, by analogy with elliptic integrals and Jacobi functions.

We introduce a new special function, "the elliptic Bessel integral":

$$\mathrm{Fb}(k, \varphi) = \int_0^\varphi \frac{d\varphi}{\sqrt{1-k^2 J_1^2(\varphi)}}. \quad (13)$$

Here, the main dissimilarity from the elliptic integral of the first kind is in the replacement of sine in the integrand by the Bessel function with subscript 1. The modulus values k must fall in the range between 0 and $\frac{1}{\mathrm{Max} J_1} = 1.7186\ldots$, where $\mathrm{Max} J_1 = 0.5818\ldots$ is the maximum value of the Bessel function; otherwise, the function $\mathrm{Fb}(k, \varphi)$ takes complex values for a real argument.

An "elliptic Bessel amplitude" is the inversion of the elliptic Bessel integral:

$$u = \mathrm{Fb}(k, \varphi), \quad \varphi = \mathrm{amb}(u, k). \quad (14)$$

This function also depends on the modulus k, and the Jacobian elliptic amplitude is its analogue.

By analogy with the elliptic Jacobi sine, we introduce an "elliptic Bessel sine" $\mathrm{snb}(u, k) = J_1(\mathrm{amb}(u, k))$. This function has zeros at the points $u = \mathrm{Fb}(k, \tau_n)$. The integral $\mathrm{Fb}(k, \tau_n)$ is the analogue of the complete elliptic integral of the first kind $\mathrm{K}(k) = \mathrm{F}(k, \pi/2)$ and plays the role of a nonuniform "half-period", similar to the function $2\mathrm{K}(k)$ playing the role of the uniform half-period in the theory of the Jacobi elliptic functions. The plot of the function $\mathrm{snb}(u, k)$ is shown in Fig. 2 for various k-values.

It is seen that the function $\mathrm{snb}(u, k)$ makes possible the modeling, by a single function, of linear and strongly nonlinear (in the region of the first maximum), properties of various systems with axial symmetry. An additional function can also be introduced:

$$\mathrm{dnb}(u, k) = \sqrt{1-k^2 \mathrm{snb}^2(u, k)}.$$

We represent the solutions to the problem found above with the aid of the functions introduced. The expressions for a curvilinear arc and polar radius are as follows:

$$l(r) = \frac{1}{\lambda}\mathrm{Fb}(k, \lambda r), \quad r(l) = \frac{1}{\lambda}\mathrm{amb}(\lambda l, k). \quad (15)$$

The expression for the tangent slope (11) changes to the following:

$$\sin\theta(l) = kJ_1(\mathrm{amb}(\lambda l, k)) = k\,\mathrm{snb}(\lambda l, k),$$
$$\cos\theta(l) = \sqrt{1-\sin^2\theta(l)} = \mathrm{dnb}(\lambda l, k), \quad (16)$$
$$\theta(l) = \arcsin[k\,\mathrm{snb}(\lambda l, k)].$$

The resulting expressions are structurally identical to those represented in terms of the elliptic functions for the tangent slope in the problem on the strong bending of a rod reported in [4] and for the angle of the nonlinear-pendulum deflection.

By L, we denote the total curvilinear length of the plate or "semidiameter," which is measured along the arc length on the plate surface. The boundary condition for the plate fixed at the edge, $\theta(L) = 0$, gives $\sin\theta(L) = k\,\mathrm{snb}(\lambda L, k) = 0$. From this relation, using properties of the function $\mathrm{snb}(u, k)$, we obtain the eigenvalue spectrum

$$\lambda = \frac{1}{L}\mathrm{Fb}(k, \tau_n). \quad (17)$$

The plate-end coordinate can be found from the known λ-value: $R = \frac{\tau_n}{\lambda}$. Using (17), we find the load thresholds:

$$p = \frac{\lambda^2 D}{h} = \frac{D\mathrm{Fb}^2(k, \tau_n)}{hL^2}.$$

By introducing the first critical load, i.e., the Eulerian force $p_1 = \frac{D\mathrm{Fb}^2(0, \tau_1)}{hL^2} = \frac{D\tau_1^2}{hL^2}$, the previous expression can be rewritten as

$$\frac{p}{p_1} = \left[\frac{\mathrm{Fb}(k, \tau_n)}{\tau_1}\right]^2. \quad (18)$$

Expression (18) gives, implicitly, the external-load-dependence of modulus $k(\lambda)$. For the external load $p < p_1$, the unique value $k = 0$ corresponds to every p-value. For the load value within the interval $p_1 < p < p_2$, there is one nonzero value of k for every p-value; for $p_2 < p < p_3$, there are already two values of k and two profile forms (they are the static mode and the first dynamic mode, according to Lavrent'ev–Ishlinskiĭ terminology [3]); etc.

Of course, as the load smoothly increases above the first threshold ($p > p_1$), only one profile form corresponding to the static mode will be realized. The first dynamic mode can be reached only upon pulsed (impact) loading [3], when the pulse rise time is less than the system relaxation time. Nonlinear properties of the system begin to show up clearly for k-values near $k_{\max}$.

Now, we find the plate profiles in the section made along the principal axis. An expression for the plate deflection can be written parametrically in terms of quadratures, where a curvilinear arc acts as a parameter:

$$w(l) = k\int_l^L \mathrm{snb}\left[\frac{\mathrm{Fb}(k, \tau_n)l}{L}, k\right]dl,$$
$$r(l) = \frac{L}{\mathrm{Fb}(k, \tau_n)}\mathrm{amb}\left[\frac{\mathrm{Fb}(k, \tau_n)l}{L}, k\right]. \quad (19)$$

These equations describe the shape of a strongly arched plate ($0 \le l \le L$) under the action of a static load ($n = 1$) and dynamic loads ($n > 1$). The modulus k ranges from 0 to 1.7186; it specifies the overall plate-profile curvature and is determined by the values of the external acting force p. For every threshold, dependence $k(p)$ is determined by its own equation (18) for the corresponding n-value. The system of solutions (19) and expressions for strong bending of a rod given in [4] have a similar structure.

Expressions (18), (19) are also true for a plate with a fixed edge if the identical substitution $\tau_n \longrightarrow \alpha_n$ is used in these expressions. Here, α_n is a set of roots of the transcendental equation $J_0(\alpha) - \frac{(1-\mu)J_1(\alpha)}{\alpha} = 0$.

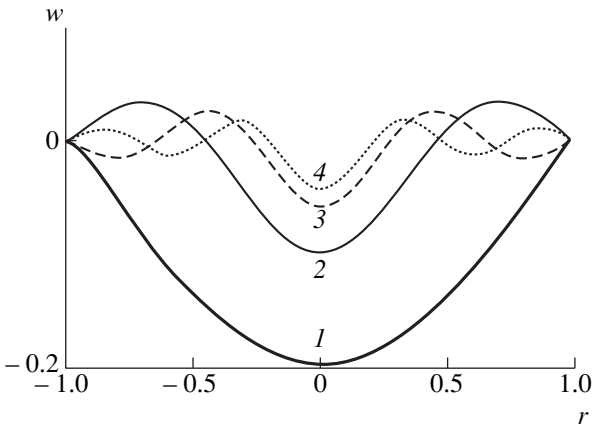

Fig. 3. The profiles of a plate fixed at the edge under an external load determined by modulus k. (*1*) Static mode ($n = 1$); dynamic modes: (*2*) for $n = 2$; (*3*) for $n = 3$; (*4*) for $n = 4$; all curves are given for the modulus value $k = 0.5$.

The plate profiles (dependence $w(r)$) are shown in Fig. 3. The length L is the unit of measurement in these plots.

Thus, when solving the general geometrically nonlinear equation for a round plate compressed by a radial load, it was shown that the solutions found are an extension of the solution of the problem on the strong bending of a rod to a two-dimensional surface.

The exact solution to the geometrically nonlinear equation for a round plate compressed by a radial load is not expressed in terms of known analytic functions. For description of the exact solution, we introduced a system of special functions: elliptic Bessel integrals and elliptic Bessel functions, which, for cylindrical symmetry, are the analogues of the elliptic integrals and Jacobi elliptic functions.

The system of functions introduced describes the essentially nonlinear properties of a system in a bounded region and describes the system as linear outside of this region; this system can be used to analyze processes in which a strong action takes place within a bounded region.

ACKNOWLEDGMENTS

The authors are grateful to K.S. Aleksandrov and R.G. Khlebopros for attention given to this work and comprehensive discussions and to S.G. Ovchinnikov, R.S. Iskhakov, A.M. Baranov, V.G. Sukhovol'skiĭ, and Yu.I. Man'kov for useful discussions and their interest in this study. This work was supported by the Russian Foundation for Basic Research, project no. 99-01-00766.

REFERENCES

1. Yu. V. Zakharov, Dokl. Akad. Nauk **344**, 328 (1995) [Phys. Dokl. **40**, 464 (1995)].
2. Yu. V. Zakharov and I. V. Uvaev, in *Proceedings of Moscow International Symposium on Magnetism, 1999*, Pt. 2, p. 44.
3. M. A. Lavrent'ev and A. Yu. Ishlinskiĭ, Dokl. Akad. Nauk SSSR **64**, 779 (1949).
4. Yu. V. Zakharov and A. A. Zakharenko, Vychisl. Tekhnol. **4** (1), 48 (1999).
5. A. Föppl, *Forlesungen über technische Mechanik*, Bd. 5: *Die wichtigsten Lehren der högeren Elastizilatstheorie* (B.G. Teubner, Leipzig, 1907).
6. Th. Karman, *Festigkeitsprobleme in Maschinenbau*, in *Enzyklopädie der mathematischen Wissenschaften*, Bd. 4: *Mechanik* (B.G. Teubner, Leipzig, 1910), Teilband 4, Hft. 3, Art. 27, Punkt 8, Ebene Platten, pp. 311-385.
7. Ph. Ciarlet and P. Rabier, *Les équations de Von Kármán* (Springer-Verlag, Berlin, 1980; Mir, Moscow, 1983).
8. V. Z. Vlasov, *General Theory of Shells and Its Application in Technique* (Gostekhizdat, Moscow, 1949).
9. V. G. Rekach and S. N. Krivoshapko, *Computation of Shells with Complicated Geometry* (UDN, Moscow, 1988).
10. A. S. Vol'mir, *Stability of Deformable Systems* (Nauka, Moscow, 1967).
11. Yu. N. Rabotnov, *Mechanics of Deformable Solids* (Nauka, Moscow, 1979).
12. L. D. Landau and E. M. Lifshitz, *Course of Theoretical Physics*, Vol. 7: *Theory of Elasticity* (Nauka, Moscow, 1987; Pergamon, New York, 1986).
13. Yu. V. Panov and V. N. Feodos'ev, Prikl. Mat. Mekh. **12**, 389 (1948); **13**, 116 (1949).

Translated by V. Tsarev

Doklady Physics, Vol. 46, No. 4, 2001, pp. 291–293. Translated from Doklady Akademii Nauk, Vol. 377, No. 6, 2001, pp. 769–771.

MECHANICS

Energy Estimates for Phase Transitions in a Ball Subjected to a Spherically Converging Compression Wave

Academician N. F. Morozov, I. A. Brigadnov, D. A. Indeĭtsev, Yu. V. Petrov, and A. B. Freĭdin

Received December 5, 2000

We propose a model for describing the deformation processes initiated by phase transitions in a ball subjected to a spherically converging intense compression wave. The effect of the formation of a cavity at the ball's center is explained.

1. FORMULATION OF THE PROBLEM AND BASIC HYPOTHESES

Let a continuous homogeneous isotropic ball with radius R be subjected to a spherically symmetric radial-compression shock load applied to its surface [1].

The equilibrium equation for a continuum takes the form

$$\rho\ddot{u} - \nabla \cdot \sigma = 0,$$

where ∇ is the Helmholtz differential operator, σ is the Cauchy stress tensor, ρ is the mass density, u is the displacement vector, and the points over a letter mean differentiation with respect to time.

At an initial moment, the ball is at rest; i.e., $u(0, r) = \dot{u}(0, r) \equiv 0$ for $r \in [0, R]$. For $t > 0$, the ball is subjected to normal spherically symmetric surface forces; i.e., $n \cdot \sigma(t, R) \cdot n = F(t)$, where n is the outward normal and the function $F(t)$ determines the time dependence of the shock pulse. In this case, the displacement at the ball's center remains bounded.

The medium, subjected to intense shock actions, is described by an unknown defining tensor relationship $\sigma = S\{\nabla u\}$, which allows for phase transitions. Here, the braces indicate an operator dependence. Hence, we will propose an approximate (using the conservation of energy) approach based on approximating the actual wave process by base functions that are determined from a solution to the simplified boundary-value problem with initial conditions under the following assumptions.

Institute of Problems in Machine Science, Russian Academy of Sciences, Bol'shoĭ pr. 61, St. Petersburg, 199178 Russia

(1) All quantities depend only on the radius, the displacements are radial, and the Cauchy stress tensor remains spherical up to the ultimate stress; i.e., $\sigma = -pI$, where p is the hydrostatic pressure and I is the unit tensor.

(2) By virtue of the low compressibility of iron, the strain in the ball is described by the small-strain tensor $\varepsilon = \frac{1}{2}(\nabla u + (\nabla u)^T)$.

(3) The medium is described by Hooke's linear law $p = -k_0 \mathrm{Tr}(\varepsilon)$, where k_0 is the bulk modulus.

As a result, the base functions are found from a solution to the classical problem on the propagation of an acoustic wave through the ball. According to the number of terms taken into account in the expansion of the wave solution, different models of actual physical processes can be developed.

(1) Keeping only the first term (compression wave), we can account for the origination of a cavity at the ball's center as the formation of a gaseous core surrounded by a liquid layer and, farther, by a solid crust.

(2) The allowance for the second term (rarefaction wave) makes it possible to explain the origination of the cavity by the cavitation at the center of the liquid molten core formed under the action of the compression wave.

(3) The allowance for the next terms is worthwhile for a fairly long pulsed loading.

The adequacy of these models can be verified by physical experiments.

2. ESTIMATION OF THE SIZES FOR THE SUBLIMATION CORE AND LIQUID LAYER

The first model deals with the processes during the first passage of the compression wave:

$$p(t, r) = \frac{R}{r} F\left(t - \frac{R}{c} + \frac{r}{c}\right) \text{ for } t \in \left(0, \frac{R}{c}\right).$$

1028-3358/01/4604-0291$21.00

Here, $c = \sqrt{\frac{k_0}{\rho}}$ is the front velocity [2]. We assume that at the moment when the compression wave converges at the ball center, the potential energy is instantaneously converted into internal energy in the central region of the ball. This may result in fusion and sublimation (dry evaporation) of the medium.

The amounts of energy needed to melt or sublimate a mass m are equal to $Q^{(i)} = mc_{\mathrm{p}}^{(i)}$, $i = 1, 2$, where $c_{\mathrm{p}}^{(1)}$ and $c_{\mathrm{p}}^{(2)}$ are the heats of melting and sublimation, respectively. Hence, according to the hypotheses accepted, both the sublimation core radius $r_a = aR$ and outer liquid-layer radius $r_b = bR$ are determined from the set of nonlinear equations

$$\begin{aligned}\int_0^a F^2\left(\frac{Rx}{c}\right)dx &= \frac{2}{3}\rho k_0 c_{\mathrm{p}}^{(2)} a^3,\\ \int_a^b F^2\left(\frac{Rx}{c}\right)dx &= \frac{2}{3}\rho k_0 c_{\mathrm{p}}^{(1)}(b^3 - a^3).\end{aligned} \tag{1}$$

The function $F(t)$ is rapidly decreasing [1]. Hence, it is easy to prove that the set of equations (1) always has a pair of real roots $0 \le a \le b$. The following cases are realized depending on the arrangement of the roots.

(1) If $a = b = 0$, the whole ball remains solid.

(2) If $0 = a < b < 1$, a liquid core surrounded by a solid crust forms.

(3) If $0 < a < b < 1$, a gaseous core surrounded by a liquid layer and, farther, by a solid crust forms.

(4) If $0 < a < 1 \le b$, a gaseous core surrounded by a liquid layer up to the ball surface forms.

(5) If $a \ge 1$, the whole ball passes into a gaseous state; i.e., it evaporates.

It is worth noting that set (1) always has the trivial solution $a = b = 0$, while the two last variants lead to full destruction of the ball.

3. PROCESSES IN THE SOLID CRUST AFTER PHASE TRANSITIONS

We assume that the pressure p_a in the sublimate is equalized along the radius nearly instantly. It can be estimated from the condition that the sublimation energy $Q^{(2)} = \rho V_a c_{\mathrm{p}}^{(2)}$ is equal to the potential energy $p_a V_a$ of compressed gas, where V_a is the sublimation core volume. The liquid layer transfers the sublimate pressure to the inner surface of the solid crust according to the Pascal law. Thus, the following estimates are valid:

$$p_a = \rho c_{\mathrm{p}}^{(2)}, \quad p_b = \eta^2 p_a, \quad \eta = \frac{a}{b}. \tag{2}$$

Under the action of pressure, the solid crust begins to expand and the stress tensor ceases to be spherically symmetric; the latter can lead to irreversible shear strains. Both the sublimate condensation on the liquid-layer inner surface and the thickening of the solid crust, which is due to the recrystallization of the liquid layer, take place simultaneously inside the sphere. As a result, the pressure under the rising crust drops and the crust growth stops. After cooling the ball, its external radius can rise up to $R_* = R + u_r(R)$.

The irreversible strains inside the solid crust are estimated by solving the problem of expanding a spherical layer through internal pressure. In this case, the stress–strain relation is taken in the deviator form [3]:

$$\varepsilon^D = \frac{\sigma_s}{2\mu\alpha} H\left(\frac{|\sigma^D|}{\sigma_{\mathrm{s}}} - 1\right)\left(\frac{|\sigma^D|}{\sigma_{\mathrm{s}}} - 1\right)\frac{\sigma^D}{|\sigma^D|}. \tag{3}$$

Here, μ is the shear modulus; $\alpha > 0$ and $\sigma_{\mathrm{s}} > 0$ are the dynamic coefficient of strengthening and the yield stress, respectively; and $H(x)$ is the Heaviside function.

The radial displacement $u_r(r) = \frac{C}{r^2}$ is found from the condition of plastic incompressibility: $\mathrm{Tr}(\varepsilon) = u_r' + \frac{2u_r}{r} = 0$. Here, the constant C is determined from the boundary condition on the inner surface of the solid crust: $\sigma_{rr}(r_b) = -p_b$.

Thus, the following estimate is valid for the relative increment of the outer radius of the solid crust:

$$\delta_R = \frac{u_r(R)}{R} = \frac{b^3\sigma_{\mathrm{s}}}{2\sqrt{6}\mu\alpha} H(s-1)(s-1). \tag{4}$$

Here, $s = \max\left\{\frac{|\sigma^D|}{\sigma_{\mathrm{s}}}\right\} = \left(\frac{3}{2}\right)^{1/2}\eta^2\left(\frac{p_a}{\sigma_{\mathrm{s}}}\right)$ is the relative tangential stress on the inner surface of the solid crust. For $s \le 1$, the outer radius of the ball does not increase because $\delta_R = 0$. Within the framework of the model under consideration, it is easy to verify that, for $\eta \le \eta_* = \left(\frac{2}{3}\right)^{1/4}\left(\frac{\sigma_{\mathrm{s}}}{p_a}\right)^{1/2}$, the cavity cannot form. In this case, the second model has to be employed.

The relative radius of the spherical cavity is found from the law of mass conservation by the formula

$$\delta_* = \frac{r_*}{R} = \left[(1+\delta_R)^3 - 1 - \left(\frac{\rho}{\rho_*} - 1\right)b^3\right]^{1/3}, \tag{5}$$

where ρ_* is the density of the recrystallization layer for the liquid phase.

4. NUMERICAL RESULTS

We analyzed the expressions obtained using, as an example, an iron ball with radius $R = 0.05$ mm. We

set [4] that $k_0 \approx 108$, $\mu \approx 84$, $\sigma_s \approx 1$ GPa, $\alpha \approx 0.1$ rel. units, $\rho \approx 7.6 \times 10^3$ kg/m^3, $c_p^{(1)} \approx 1.3 \times 10^4$ J/mol, $c_p^{(2)} \approx 3.5 \times 10^5$ J/mol, and $m_0 \approx 6 \times 10^{-2}$ kg/mol (molar mass of iron). We considered the simplest approximation to the shock pulse: $F(t) = F_0 \exp^{-t/\lambda}$, where $\lambda = 0.15$ μs [1].

Figure 1 shows the relative values for (*1*) the sublimation core radius a, (*2*) outer radius b of the liquid layer, and (*3*) radius δ_* of the spherical cavity (under the assumption that $\rho_* = \rho$) as functions of the amplitude F_0 of the shock pulse.

For the typical value $F_0 = 40$ GPa [1], the relative values for the sublimation core radius and the outer radius of the liquid layer, $a \approx 0.14$ and $b \approx 0.53$, correspond to the third state of the above-mentioned states of the ball. In this case the sublimate pressure $p_a \approx 44.3$ GPa. The relative increment of the outer radius is $\delta_R \approx 0.01$. Under the assumption that $\rho_* = \rho$, the relative radius of the spherical cavity is, hence, $\delta_* \approx 0.32$; this estimate is well consistent with experimental data [1].

The liquid-phase recrystallization takes place at pressure p_a and temperature T_a. According to the perfect gas law, the latter is estimated as

$$T_a = p_a \frac{3m_0}{2\rho R_0} = \frac{3c_p^{(2)} m_0}{2R_0} \approx 3.75 \times 10^3 \text{ K},$$

where $R_0 = 8.31$ J/(K mol) is the gas constant.

The following improvements of the model proposed are possible:

(1) more accurate estimation of the strain potential energy at the moment when the shock wave converges at the center;

(2) allowance for both temperature and pressure effects on the heats of melting and sublimation, as well as for temperature variations, under adiabatic compression;

(3) more accurate estimation of pressure in the sublimate;

(4) allowance for the processes of sublimate condensation and melt recrystallization under solid-crust expansion, which is reduced to solving the Stefan problem combined with the problem on viscoplastic flow;

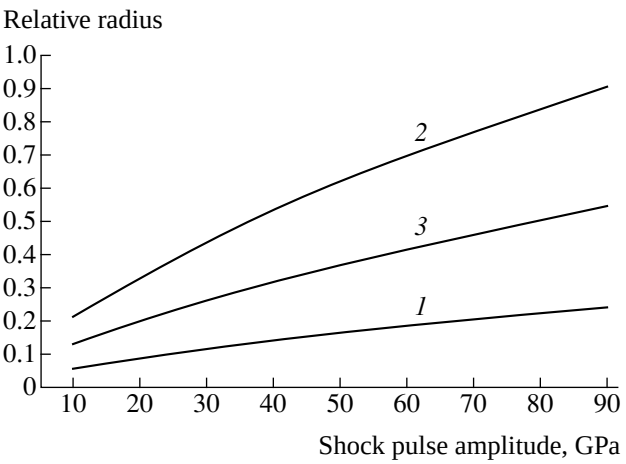

Relative values of (*1*) the sublimation core radius a, (*2*) outer radius b of the liquid layer, and (*3*) radius δ_* of the spherical cavity as functions of the shock pulse amplitude.

(5) allowance for both temperature and pressure effects on the phase composition in the recrystallization layer, as well as for the medium loosening.

ACKNOWLEDGMENTS

This work was supported by the Russian Foundation for Basic Research, projects no. 98-01-01054 and no. 00-15-99273, and the Ministry of Higher Educational Institutions of the Russian Federation, project no. 8-4.3-66.

REFERENCES

1. *Metals and Minerals Research in Spherical Shock-Wave Recovery Experiments*, Ed. by B. I. Litvinov (ONTI RFNC VNIITF, Snezhinsk, 1996).
2. L. I. Slepyan, *Nonstationary Elastic Waves* (Sudostroenie, Leningrad, 1972).
3. V. D. Klyushnikov, *Mathematical Theory of Plasticity* (Mosk. Gos. Univ., Moscow, 1979).
4. *Physical Quantities. Handbook*, Ed. by I. S. Grigor'ev and E. Z. Melïkhov (Énergoatomizdat, Moscow, 1991).

Translated by V. Chechin

Doklady Physics, Vol. 46, No. 4, 2001, pp. 294–297. Translated from Doklady Akademii Nauk, Vol. 377, No. 6, 2001, pp. 772–775.

MECHANICS

Formation of the Deterministic Fatigue Curve in a Stochastic Model of a Fiber Bundle

D. A. Onishchenko

Presented by Academician V.V. Kozlov October 16, 2000

Received October 24, 2000

The model of a fiber bundle is one of the basic structural systems in studying the strength problem of discrete media in its probabilistic formulation [1, 2]. The term "fiber bundle" is applied in strength mechanics to differentiate this system from that considered within the mathematical theory of reliability of the parallel connection model: the failures of elements in the latter are independent (in the probabilistic meaning), whereas the events of fiber failure in the bundle are dependent due to the redistribution of stresses.

Beginning with the classical work [3], in which the case of linearly elastic fibers was considered assuming the uniform redistribution of a statically applied load, the model of the fiber bundle was intensively studied under various modifications. The cases of the localized redistribution of load were studied, as well as problems on the long-term strength and models with nonlinear diagrams of the fiber tension (see, e.g., [4–7] and references therein).

In this report, we consider the case where a cyclically varying tensile load is applied to the bundle. Fatigue failure [1, 8, 9] induced by such actions occurs under loads sufficiently less than those needed for static failure. In engineering, this results in the necessity of considering the cyclic actions (e.g., vibrations in technique or wave action on naval buildings) as one of the calculated cases. As applied to the model of the fiber bundle, the problem consists in determining the fatigue endurance of the bundle (measured as the number of loading cycles after which the failure occurs) on the assumption that the fiber fatigue properties are known.

Exhibiting a significant statistic variability [1, 8, 10], the endurance requires a probabilistic description. The model studied in this report is close in some aspects to those proposed earlier [11, 13]; however, we consider a more general formulation. The main result is as follows: asymptotically, a deterministic fatigue curve forms in a stochastic bundle, the lifetime of which turns out to be shorter than the mean lifetime of individual fibers.

1. Let the bundle consisting of n nominally identical fibers be subjected to the action of a cyclic tensile load with amplitude S. It is assumed that fibers can be destroyed as a result of cumulative fatigue damage and that the load is always uniformly distributed among nondestroyed fibers. In particular, the initial load on each fiber is $s = \frac{S}{n}$. Let us designate by $N(s)$ the lifetime of an individual fiber for a constant amplitude s of the accepted load and consider this value as random, with the distribution function $F_N(t; s)$ being identical for all fibers.

After the failure of the "weakest" fiber in the bundle, the stresses in the remaining fibers increase from the value $\frac{S}{n}$ up to the value $\frac{S}{n-1}$; after the failure of the next fiber, they increase up to the value $\frac{S}{n-2}$, etc. Thus, the load acting upon the fiber in the bundle is not constant (in the sense of its amplitude) and represents a so-called multilevel loading [1] of the kind $\{l_1; q_1\} + \{l_2; q_2\} + \ldots$, where l_i is the duration of the block (level) and q_i is the load magnitude. Therefore, the information presented by the function F_N alone is insufficient for determination of the sequential instants of the fiber failure in a bundle and additional hypotheses are required for the cumulative damage and for the corresponding criterion of the fiber failure under multilevel loading conditions, naturally, within the framework of the probabilistic approach.

Let us specify the model of fatigue endurance of the bundle with allowance for the considerations presented above. We suggest that the fatigue properties of fibers are described by a probabilistic fatigue curve (the other notation is the *S–N* curve or the Wöhler diagram) of the form

$$N(s) = \frac{r}{\varphi(s)}, \tag{1}$$

where $\varphi(s)$ is a monotonically increasing load function and r is an arbitrary characteristic of the fatigue

Institute of Problems of Mechanics,
Russian Academy of Sciences,
pr. Vernadskogo 101, Moscow, 117526 Russia

1028-3358/01/4604-0294$21.00

strength, which represents a random value with distribution function $F_r(x)$. Using such an approach [1], an individual *S–N* curve is assigned to each fiber depending on the particular realization of the random value *r*. Usually, it is assumed [1, 11, 13] that φ is a power-law function and, therefore,

$$N(s) = \frac{r}{s^u}, \quad u \geq 1; \tag{2}$$

however, this is unessential at the given stage of analysis. On account of (1),

$$F_N(t; s) = F_r(\varphi(s)t).$$

We restrict our consideration to the case when the values of r_i [and, therefore, $N_i(s)$ $(i = 1, 2, \ldots, n)$] corresponding to different fibers are independent. It is obvious that the failure of fibers in the bundle occurs in order of increasing r_i values, as the larger fiber lifetime corresponds to the larger value of *r*, according to formula (1). For the sake of convenience, we renumber the fibers in order of increasing fatigue strength characteristics: $r_{(1)} \leq r_{(2)} \leq \ldots \leq r_{(n)}$ (such a sequence is termed a variational series, and its *i*th term is termed the *i*th order statistics) [14].

As a criterion of the fiber failure under multilevel loading, we employ its probabilistic modification corresponding to the model of a linear summation of damage, which is widely used in engineering applications [1, 9, 10] and is known as the Palmgren–Miner rule. We designate the load acting upon the nondestroyed fibers of the bundle within the *i*th loading level (when exactly f_i fibers are destroyed) by $s_i = \frac{S}{n-i}$ $(i = 0, 1, \ldots, n-1)$ and the duration of the *i*th level by k_i. Then, one can assert that the fiber with number *m*, $m = 1, 2, \ldots, n$ is destroyed under the multilevel (*m*-level) loading $\{s_0; k_0\} + \ldots + \{s_{m-1}; k_{m-1}\}$; in this case, the values of k_i are sequentially found from the condition that the corresponding total damage in the *i*th fiber is equal to the critical value 1:

$$\mu_0^{(m)} + \ldots + \mu_{m-1}^{(m)} \equiv \frac{k_0}{N_{(m)}(s_0)} + \ldots + \frac{k_{m-1}}{N_{(m)}(s_{m-1})} = 1.$$

Here, $\mu_i^{(m)}$ is the damage accumulated during the *i*th loading level in the *m*th fiber and the values $N_{(m)}(s_i)$ are defined by relation (1) for the corresponding values of $r_{(m)}$.

Summing the durations of all *n* loading levels, we find the required (random) lifetime of bundle $T_n(s) = k_0 + \ldots + k_{n-1}$:

$$T_n(s) = \sum_{i=1}^{n} N_{(i)}(s)\left[\frac{\varphi(s)}{\varphi\left(\frac{n}{n-i+1}s\right)} - \frac{\varphi(s)}{\varphi\left(\frac{n}{n-i}s\right)}\right], \tag{3}$$

where $s = \frac{S}{n}$ is the specific load [for $i = n$, we set $\varphi(\infty) = \infty$].

Thus, the lifetime of the bundle of *n* fibers under the action of a cyclic load with specific value *s* is a linear combination of the order statistics $N_{(i)}(s)$ defined under the same load *s*. The latter statement is essential, since it means that in the model under study, the information on the tests for fibers with a constant load amplitude is sufficient for determination of the bundle lifetime.

The coefficients in relation (3) are simplified in the case of the power-law function $\varphi(s) = s^u$, and this relation takes the form

$$T_n(s) = \sum_{i=1}^{n} c_i N_{(i)}(s), \quad c_i = \left(1 - \frac{i-1}{n}\right)^u - \left(1 - \frac{i}{n}\right)^u, \tag{4}$$

where the coefficients c_i are independent of the load.

The combined distribution of the order statistics is known only formally [14], since it is set by an *n*-dimensional integral over the nontrivial domain. Therefore, it is impossible to make any general conclusions on the distribution or numerical characteristics of the bundle lifetime for relatively small values of *n*.

2. Now, we will show that for $\varphi(s) = s^u$ $(u \geq 1)$, our model allows one to study the behavior of the random value $T_n(s)$ for $n \longrightarrow \infty$. First, we consider the case $u = 1$ consistent with the linear function φ, where we introduce the additional designation $T_n^{(0)}$ for the bundle lifetime. For this case, the analysis can be done without utilizing the theory of order statistics. Actually, for $u = 1$, we obtain that $c_i = \frac{1}{n}$ for all *i*. Therefore,

$$T_n^{(0)}(s) = \frac{1}{n}\sum_{i=1}^{n} N_{(i)}(s), \tag{5}$$

where $N_{(i)}(s)$ are the order statistics. However, $N_{(i)}$ is understood (further on, we consider *s* a fixed value and drop it in the designations) simply as a set of realizations of the fiber lifetimes N_i, $i = 1, 2, \ldots, n$; not arranging them in increasing order, the sum remains unchanged. Consequently, expression (5) can be treated as a standard estimate of the mean value of a certain random quantity (fiber lifetime in this case) with a preassigned distribution. According to the central limit theorem [15], the quantity T_n $(= T_n^{(0)})$ has an asymptotically normal distribution with mean value $T = \mathrm{M}[N]$ and variance $\sigma_n^2 = \frac{\mathrm{D}[N]}{n}$, where M[*N*] and D[*N*] are the respective values for the lifetime of isolated fibers (we assume that the values are finite). The asymptotic normality means that for all *a*, *b* $(a < b)$,

$$\lim_{n\to\infty} P\{T + a\sigma_n < T_n < T + b\sigma_n\} = \Phi_0(b) - \Phi_0(a), \tag{6}$$

where $P\{\cdot\}$ is the event probability and Φ_0 is the normal distribution (with zero mean value and unit variance). Property (6) for considerably large n allows one to approximate the distribution function for the bundle lifetime T_n by a normal law.

3. Consider now the general case $u > 1$. In the theory of order statistics [14], the following conclusion is proved. Let the coefficients c_i in the linear statistics T_n (4) be written in the form

$$c_i = \frac{1}{n}J\left(\frac{i}{n}\right), \quad i = 1, 2, \ldots, n, \tag{7}$$

where the function $J(z)$ is continuous on the segment [0, 1] and the following condition is fulfilled:

$$\beta^2(J, F_N) \equiv 2\iint\limits_{\{x<y\}} J[F_N(x)]J[F_N(y)] \times F_N(x)(1-F_N(y))dxdy > 0.$$

Then, the quantity T_n is asymptotically normal and relation (6) is valid for it where

$$T = \int\limits_{-\infty}^{+\infty} xJ[F_N(x)]dF_N(x), \quad \lim_{n\to\infty} n\sigma_n^2 = \beta^2(J, F_N). \tag{8}$$

One cannot apply this assertion directly to the problem considered because relations (4) for c_i do not comply with the form of (7) (except for the case of $u = 1$ studied above). Nonetheless, one can show that the quantities c_i for $u > 1$ are representable by the sum of two components, $c_i = c_i^{(\mathrm{I})} + c_i^{(\mathrm{II})}$, the first of which has the form (7) with function $J(z) = u(1-z)^{u-1}$, and the second is written as $c_i^{(\mathrm{II})} = B_i n^{-u}$, where B_i are some bounded functions of the parameters i, n, and u: $|B_i| < B = \mathrm{const}$, $i = 1, 2, \ldots, n$ [for $u \geq 2$, this is illustrated by a direct expansion of expressions (4) for c_i in a Taylor series]. Then, the lifetime of the bundle T_n (3) is written as a sum:

$$T_n = T_n^{(\mathrm{I})} + T_n^{(\mathrm{II})} = \sum_{i=1}^{n} c_i^{(\mathrm{I})} N_{(i)} + \sum_{i=1}^{n} c_i^{(\mathrm{II})} N_{(i)}.$$

The second term, owing to the estimate $\left|T_n^{(\mathrm{II})}\right| \leq \frac{B}{n^{u-1}} T_n^{(0)}$, tends to zero for $n \longrightarrow \infty$ (since $u > 1$), and the first one, according to the above assertion on the behavior of linear statistics, has an asymptotically normal distribution with the mean value $T^{(\mathrm{I})}$ calculated by formula (8):

$$T^{(\mathrm{I})} = \int\limits_0^{+\infty} [1 - F_N(t)]^u dt. \tag{9}$$

Thus, it is proved that the lifetime of the bundle really becomes a deterministic quantity (with the value $T^{(\mathrm{I})}$) as the bundle size increases, since its variance tends to zero with increasing n. In addition, noting that

$$\mathrm{M}[N] = \int\limits_0^{+\infty} [1 - F_N(t)]dt,$$

we come to the conclusion that the bundle lifetime is always less than the lifetime of the fibers making up this bundle (excluding the case $u = 1$, where these values are the same).

4. Consider a simple example. Let the family of fatigue curves for the fibers be written in the form of power-law dependence (2) and the parameter r of the fatigue strength of the fibers be defined by the Weibull distribution, which is often employed in various strength models [1, 2, 9]:

$$F_r(x) = 1 - \exp\left[-\left(\frac{x}{r_0}\right)^{\rho}\right], \tag{10}$$

where r_0, ρ are some parameters. Then, it follows from (2) that the distribution of the quantity N—the lifetime of isolated fibers—is also the Weibull distribution

$$F_N(t; s) = 1 - \exp\left[-\left(\frac{s^u}{r_0}t\right)^{\rho}\right]$$

with the mean value

$$\mathrm{M}[N] = \frac{r_0}{s^u}\Gamma\left(1 + \frac{1}{\rho}\right).$$

It is simple to verify that the asymptotic value of lifetime of the bundle T (9) takes the form

$$T = K_b \mathrm{M}[N], \quad K_b = u^{-1/\rho},$$

where the quantity K_b can be interpreted as the coefficient of realization of the mean fiber lifetime in the bundle.

Experimental data (see, e.g., [1, 12]) give evidence that the exponent in fatigue curve equation (2) usually satisfies the condition $u \geq 4$ and that the parameter ρ in the Weibull distribution (10) ranges from 1 to 5. Under these conditions, the coefficient K_b takes a value ranging from 0.25 to 0.75.

5. The linear dependence of expression (3) for the bundle lifetime on the lifetimes of the isolated fibers is due to the application of the rule of linear summation of damage in multilevel loading. Such a linearity is known [1, 9, 10] to poorly confirm sharp changes in the load level in experiments, especially when the load decreases. In the bundle model considered above, even for a relatively small number of fibers, the loading level changes insignificantly, increasing from level to level. This gives grounds to consider the use of the indicated

rule in the bundle model quite feasible not only from the methodical but also from the practical standpoint.

The effect of the bundle lifetime reduction may turn out even more essential if one additionally takes into account the existence of the limiting static tensile strength of fibers and/or considers the model with a nonuniform redistribution of the load. The latter, in particular, relates to models of the strength of fiber composites in which the load accepted by the destroyed fibers is transferred only to the closest neighboring fibers.

It is of interest to note that in the problem on the static tensile strength of the fiber bundle, the effect of lowering the bundle specific strength relative to the mean strength of individual fibers also takes place. This is true both for the linear [2, 3] and nonlinear [7] stress–strain diagrams for the fiber, though the mathematical model substantially differs from that considered in this report.

ACKNOWLEDGMENTS

This work was supported by the Russian Foundation for Basic Research, project no. 00-15-96066.

REFERENCES

1. V. V. Bolotin, *Prediction of Machine and Construction Resources* (Mashinostroenie, Moscow, 1984).
2. A. M. Freudenthal, in *Fracture*, Ed. by H. Leibowitz (Academic, New York, 1968; Mir, Moscow, 1975), Vol. 2.
3. H. E. Daniels, Proc. R. Soc. London, Ser. A **183**, 405 (1945).
4. B. D. Coleman and D. W. Marquardt, J. Appl. Phys. **29**, 1091 (1958).
5. L. N. McCartney and R. L. Smith, J. Appl. Mech. **50**, 601 (1983).
6. C.-C. Kuo and S. L. Phoenix, J. Appl. Probab. **24**, 137 (1987).
7. D. A. Onishchenko, in *Proceedings of the IX Conference on Strength and Plasticity* (Inst. Problem Mekhaniki Ross. Akad. Nauk, Moscow, 1996), Vol. 3, p. 150.
8. M. Ronay, in *Fracture*, Ed. by H. Leibowitz (Academic, New York, 1971; Mir, Moscow, 1976), Vol. 3.
9. J. R. Schaff and B. D. Davidson, J. Compos. Mater. **31** (2), 128 (1997).
10. K. Sobczyk, Adv. Appl. Probab. **19**, 652 (1987).
11. B. Stahl and J. F. Geyer, J. Struct. Eng. **110**, 2307 (1984).
12. E. Castillo, A. F. Cantelli, V. Esslinger, and B. Thurlimann, in *Proceedings of the IABSE* (IABSE Periodica, Zürich, 1985), P-82/85, No. 1.
13. A. Kumar and D. I. Karsan, J. Struct. Eng. **116**, 719 (1990).
14. H. A. David, *Order Statistics* (Wiley, New York, 1981; Nauka, Moscow, 1979).
15. B. V. Gnedenko, *Course of Probability Theory* (Nauka, Moscow, 1988).

Translated by T. Galkina